Transport of Metabolites in Chloroplasts

Dissertation zur Erlangung des Doktorgrades

der Fakultät für Biologie

der Ludwig-Maximilians-Universität München

vorgelegt von

Annette Constanze Schock

München, 7. Mai 2014

Dissertation eingereicht am: 07.05.2014

Tag der mündlichen Prüfung:15.07.2014

Erstgutachter: Prof. Dr. J. Soll

Zweitgutachter: Prof. Dr. P. Geigenberger

Table of Contents

Abbreviations I

Summary IV

Zusammenfassung V

1 Introduction 1

2 Material and Methods 9

2.1 Material 9

2.2 Methods 14

2.2.1 Plant physiological methods 14

2.2.2 Microbiological methods 19

2.2.3 Molecular biology methods 21

2.2.4 Biochemical methods 25

2.2.5 Metabolite analysis 33

2.2.6 Computational methods 34

3 Results 35

3.1 PRAT2 in the inner chloroplast envelope 35

3.1.1 Analysis of double mutants for *PRAT2.1* and *PRAT2.2* in *Arabidopsis thaliana* 36

3.1.2 Phenotypic analysis of *prat2* double mutant plants 38

3.1.3 POR expression in *prat2* double mutant plants 39

3.1.4 Analysis of POR activity in *prat2-dm* plants 42

3.1.5 Analysis of SAM and tocopherol levels in *prat2-dm* mutant plants 43

3.1.6 Metabolite analysis in *prat2-dm* mutant plants 45

3.1.7 Analysis of sulphur-containing metabolites in *prat2-dm* mutant plants 50

3.1.8 Transport activity studies in *Saccharomyces cerevisiae* 52

3.2 IEP57 in the inner chloroplast envelope 53

3.2.1 Biochemical characterization of IEP57 54
3.2.2 IEP57 *in planta* 56
3.2.3 Mutation of IEP57 in *Arabidopsis thaliana* 59
3.2.4 Rescue of IEP57 mutant phenotypes 63
3.2.5 IEP57 and the non-mevalonate pathway 69
3.3 OEP40 in the outer chloroplast envelope 73
3.3.1 Biochemical characterization of OEP40 73
3.3.2 Mutation of OEP40 in *Arabidopsis thaliana* 78
3.3.3 Analysis of floral induction in *oep40* mutant plants 83
4 Discussion 88
4.1 PRAT2 in the inner chloroplast envelope 88
4.2 IEP57 in the inner chloroplast envelope 95
4.3 OEP40 in the outer chloroplast envelope 103
References 110
Figures 119
Tables 121
Appendix 122
Curriculum vitae 125
Eidesstattliche Erklärung 126
Danksagung 127

Abbreviations

AA	amino acid
AGI	*Arabidopsis* Genome Initiative
AP	alkaline phosphatase
At	*Arabidopsis thaliana*
ATP	adenosine triphosphate
BCA	bichinonic acid
BCAA	branched chain amino acid
Bp	base pairs
BSA	bovine serum albumin
CD	circular dichroism
cDNA	complementary deoxyribonucleic acid
CLN	cauline leave number
Col-0	*Arabidopsis thaliana* ecotype: Columbia
cTP	chloroplast transit peptide
Dex	dexamethasone
DMAPP	dimethylallyl diphosphate
DNA	deoxyribonucleic acid
DNase	deoxyribonuclease
dNTP	deoxy nucleoside triphosphate
DTB	days to bolting
DTF	days to flowering
DTT	dithiothreitol
DUF	domain of unknown function
E. coli	*Escherichia coli*
EDTA	ethylenediaminetetraacetic acid
FCH	fold change
f_{dil}	dilution factor
GFP	green fluorescent protein

his-tag	histidine tag
HPL	hydroperoxid lyase
IE	inner chloroplast envelope
IEP57	inner envelope protein of 57 kDa
IPTG	isopropyl β-D-1-thiogalactopyranoside
IPP	isopentenyl diphosphate
kDa	kiloDalton
LB medium	lysogeny broth
LB	left border
LR	linear recombination
M	molar
mA	milliampere
MEcPP	2-C-methyl-D-erythritol-2,4-cyclodiphosphate
MgMT	Mg protoporphyrine IX methyltransferase (*At-CHLM*, At4g25080)
Mg PPX	magnesium protoporphyrine IX
Mg PPX MoMe	magnesium protoporphyrine IX monomethylester
mRNA	messenger ribonucleic acid
MS medium	Murashige and Skoog medium
MTA	S-methyl-5'-thioadenosin
MVA	mevalonate
MW	molecular weight
OEP40	outer envelope protein of 40 kDa
OD	optical density
OE	outer chloroplast envelope
OEX	overexpression
PAGE	polyacrylamide gel electrophoresis
PCR	polymerase chain reaction
P_i	inorganic phosphate
POR	NADPH:protochlorophyllide oxidoreductase
PP IX	protoporphyrine IX

PRAT	preprotein and amino acid transport
Ps	*Pisum sativum,* pea
PVDF	polyvinylidene difluoride
qRT-PCR	quantitative real time RT-PCR
RB	right border
RCF	relative centrifugal force
RER	reticulata-related
RLN	rosette leaf number
RNA	ribonucleic acid
RNAi	RNA interference
RNAse	ribonuclease
ROS	reactive oxygen species
Rpm	revolutions per minute
RT	room temperature
RT-PCR	reverse transcription polymerase chain reaction
SAM	S-adenosylmethionine
SAM	shoot apical meristem
SD	standard deviation
SDS	sodium dodecyl sulfate
T-DNA	transfer DNA
TLN	total leaf number
TMD	transmembrane domain
tRNA	transfer RNA
V	volt
VDAC	voltage dependent anion channel
x g	times the force of gravity

Summary

In eukaryotic cells, the separation of enclosed compartments by intracellular membranes requires a permanent and regulated exchange of ions and metabolites between these specialized organelles and the surrounding cytosol. The organelle, which defines the plant cell, is the chloroplast, a metabolically highly active compartment harboring many essential biosynthetic pathways important for the plant cell and for plant development. Due to its endosymbiotic origin, the chloroplast is surrounded by two membranes, the outer and the inner chloroplast envelopes, across which ion and metabolite transport has to be mediated. Across the inner chloroplast envelope, this is mainly accomplished by specific carriers. The outer envelope has long thought to be an unselective sieve, across which solutes pass by diffusion. However, this has been disproved by the identification of outer envelope proteins (OEPs), which mediate selective transport also across the outer chloroplast envelope.

In this study, the previously characterized inner chloroplast envelope proteins PRAT2.1 and PRAT2.2 were integrated into the metabolic status of the model plant *Arabidopsis thaliana* in order to assign them with a physiological role. Analysis of *prat2* double mutant plants under different light conditions lead to the suggestion that the observed phenotype is due to imbalances in thiol group-containing metabolites.

The second part of this study addressed the previously identified envelope proteins IEP57 and OEP40. Both proteins were characterized biochemically and analyses of mutants in the model plant *Arabidopsis thaliana* were conducted to investigate their physiological roles. IEP57, an essential, plant-specific protein annotated as a potential solute transporter, was found to be a member of the reticulata-related protein family. Investigation of biosynthetic pathways affected in other reticulate mutants and analysis of a possible involvement in the plastid non-mevalonate pathways using feeding studies, however, did not lead to the identification of a specific function for IEP57. For OEP40, channel activity was detected *in vitro* and could be linked to an early flowering phenotype under low temperature conditions suggesting that OEP40 is involved in the transport of a metabolite, which also plays a role in flowering time control.

Zusammenfassung

Die Abgrenzung abgeschlossener Kompartimente in eukaryotischen Zellen durch intrazelluläre Membranen erfordert einen regulierten, dauerhaften Austausch von Ionen und Stoffwechselprodukten zwischen den spezialisierten Organellen und ihrer zytosolischen Umgebung. Der Chloroplast stellt als Organell, welches die Pflanzenzelle definiert, ein metabolisch hochaktives Kompartiment dar, in welchem viele, für die Zelle und die Pflanzenentwicklung wichtige, biosynthetische Prozesse ablaufen. Aufgrund seines endosymbiotischen Ursprungs ist der Chloroplast von zwei Membranen umgeben, der äußeren und der inneren Chloroplastenhüllmembran. Über diese müssen Ionen und Stoffwechselprodukte kontrolliert transportiert werden. Über die innere Chloroplastenhüllmembran geschieht dies vorwiegend durch spezialisierte Carrierproteine. Die äußere Chloroplastenhüllmembran wurde lange für ein nicht-selektives Sieb gehalten, welches gelöste Stoffe allein durch Diffusion passieren. Dies konnte jedoch durch die Entdeckung von OEPs (engl.: outer envelope proteins) widerlegt werden, da sie einen selektiven Transport über die äußere Chloroplastenhüllmembran vermitteln.

In dieser Arbeit wurden die bereits beschriebenen Proteine PRAT2.1 und PRAT2.2 aus der inneren Chloroplastenhüllmembran in den metabolischen Zustand des Modellorganismus *Arabidopsis thaliana* integriert, um ihnen eine physiologische Funktion zuweisen zu können. Die Untersuchung von *prat2* Doppelmutanten unter verschiedenen Lichtbedingungen führte zu der Annahme, dass der beobachtete Phänotyp auf ein Ungleichgewicht von Thiol-haltigen Metaboliten zurückzuführen ist.

Der zweite Teil dieser Arbeit befasste sich mit den bereits identifizierten Hüllmembranproteinen IEP57 und OEP40. Beide Proteine wurden biochemisch charakterisiert und entsprechende Mutanten des Modellorganismus *Arabidopsis thaliana* wurden untersucht, um ihre physiologische Rolle zu ermitteln. IEP57, ein essentielles, pflanzenspezifisches Protein, welches als potentieller Transporter beschrieben wurde, konnte als Mitglied der reticulata-related (RER) Proteinfamilie identifiziert werden. Die Untersuchung von synthetischen Stoffwechselwegen, welche in anderen Reticulatamutanten betroffen sind sowie die Untersuchung einer möglichen Rolle in der plastidären Synthese von Isoprenoidvorstufen durch Fütterungsversuche führten jedoch nicht zur Bestimmung

einer spezifischen Funktion von IEP57. Für OEP40 konnte Kanalaktivität nachgewiesen werden, welche mit dem beobachteten frühblühenden Phänotyp unter Niedrigtemperatur-bedingungen in Verbindung gebracht werden konnte. Dies weist auf eine mögliche Rolle von OEP40 im Transport eines Metaboliten hin, welcher auch eine Rolle bei der Kontrolle der Blühinduktion spielt.

1 Introduction

In eukaryotic cells, intracellular membrane systems do not only increase the surface where many essential biochemical processes can take place, but also separate enclosed compartments from the cytosol, thereby creating functionally specialized organelles. Because the lipid bilayers surrounding these organelles are impermeable to most solutes and molecules, the membranes need to be equipped with transport systems responsible for the transport of metabolites and ions, as well as for the import and insertion of proteins specific for the respective organelle. Two of the most important organelles in plant cells, mitochondria and chloroplasts, are both surrounded by two membranes due to their evolutionary origin from Gram-negative like bacteria. First, mitochondria developed from the uptake of an ancestral α-proteobacterium into a prokaryotic host cell (Embley and Martin, 2006) approximately two billion years ago (Gross and Bhattacharya, 2009). About 500 million years later, chloroplasts originated from an ancestor of today's cyanobacteria, which was enclosed by an eukaryote already containing mitochondria (Gould et al, 2008). Consequently, both mitochondria and chloroplasts show similarities to their bacterial ancestors. Both organelles retain a functional genome, but throughout the endosymbiotic process, parts of the organellar genome were either lost entirely or transferred to the host cell nucleus. As a result, these endosymbiotically acquired genes code for proteins which have to be either reimported into the organelles or have evolved to be targeted to and to function in other parts of the cell. Otherwise, mitochondria and chloroplasts have recruited proteins originating from the eukaryotic host. The reduced gene-coding capacity is not sufficient to support the needs of the biosynthetically highly active organelle.

The organelle that defines the plant cell is the chloroplast. It harbors the machinery, which is responsible for the light-powered reactions of photosynthesis, a process in which CO_2 is converted to carbohydrates under the release of oxygen and on which essentially all life depends. In addition, the chloroplast also performs a number of vital metabolic functions such as fatty-, nucleic- and amino acid synthesis, synthesis of tetrapyrroles and isoprenoids, synthesis of polyphenols and lignins as well as sulfate and nitrate assimilation. To allow the integration of these metabolic processes with those of other cellular compartments, a constant and regulated exchange of ions and metabolic intermediates has to be carried out

between the chloroplast and the cytosol. This regulated network was essential to install the endosymbiont permanently inside the host and to make the chloroplast one of the metabolic powerhouses of the plant cell. Like its Gram-negative bacterial ancestor, the chloroplast is surrounded by two membranes called the outer and the inner chloroplast envelopes, which are separated by an intermembrane space, an analogue to the periplasm in bacteria (Bölter and Soll, 2001). The two envelope membranes differ in terms of their structure, function and biochemical properties (Block et al., 2007), but were also shown to collaborate in protein translocation for example (Jarvis and Soll, 2001). Integrated into these membranes are the transport proteins required for the exchange of metabolic precursors, intermediates and end products.

Solute transport across the chloroplast envelope

Across the inner chloroplast envelope, solute exchange is generally performed by specific carrier proteins, which usually consist of α-helical membrane domains and transport hydrophilic solutes. Inner envelope metabolite translocators frequently act as antiporters (Figure 1), a mechanism that is common to other subcellular compartments and very well suited to interconnect metabolic pathways between the organelles (Weber and Fischer, 2007 and references therein). The inner chloroplast envelope has long been considered to be the actual permeability barrier between the chloroplast stroma and the cytosol. In contrast, the outer chloroplast envelope was thought to be a rather unselective mesh, containing porin-like channels that delimit the movement of solutes only by size. This assumption was supported by the unselective diffusion by which the voltage dependent anion channel (VDAC), a β-barrel porin in the outer membrane of mitochondria transports ions and metabolites (Zeth and Thein, 2010). The selectivity in this case is solely mediated by the carriers of the inner mitochondrial membrane. However, studies on the subcellular localization of VDAC proteins could assign their existence only to mitochondria (Clausen et al, 2004). In addition it was shown that the oversimplification of unselective transport does not necessarily hold true for the outer envelope of the chloroplast. Here, transport capacity and selectivity could be assigned to several channel proteins. They specifically regulate the transport of small molecules and are termed OEPs, for outer envelope proteins (Duy et al., 2007, Figure 1). Since chloroplasts and mitochondria originated from two independent endosymbiotic events, it is possible that they contain different channels and

porin types in their membranes. The more complex situation in chloroplasts possibly results from the conversion of the endosymbiont into a biosynthetically highly active organelle that had to meet the needs of newly developing metabolic networks. It is assumed that the outer envelope of chloroplasts and the outer membrane of mitochondria are derived from the outer membrane of their Gram-negative bacterial ancestors. Therefore, the outer membranes of the organelles are equipped with channels and porins from prokaryotic origin. Contributions by the eukaryotic host cell and by a possible Chlamydia-like Gram-negative cosymbiont (Tyra et al., 2007, Moustafa et al., 2008) are also thought to be possible. Even though more comprehensive data is needed to enable the reconstruction of the composition and origin of plastid-targeted proteins, it could be shown that apart from the cyanobacterial endosymbiont, proteobacteria and Chlamydiae constitute significant sources of genes derived from horizontal gene transfer that encode for plastid-targeted proteins (Qiu et al., 2013).

In Gram-negative bacteria, the outer membrane forms a selective protection barrier to the bacterium's surrounding and contains a variety of porins which allow the passive entering of hydrophilic molecules. These porins form water-filled open channels by amphipathic transmembrane β-strands and are found exclusively in the outer but not in the plasma membrane. In general, the β-barrel porins are characterized by an even number of β-strands (14, 16 or 18) whereas for VDAC, a 19 β-strand structure with a however similar architecture has been observed (for a review, see Zeth and Thein, 2010). Porins can be classified into different groups according to their properties. Classical porins (a) form rather unselective water-filled channels that allow diffusion of solutes up to 600 kDa, whereas slow porins (b) allow the diffusion of larger solutes. Specific channels (c) can selectively bind solutes thereby making diffusion more specific and efficient. TonB-dependent receptor channels (d) bind their respective ligands which induces the gating of the channel via an interaction with the TonB protein in the periplasmic space (for a detailed overview see Duy et al, 2007 and references therein).

Metabolite transport across the chloroplast envelope by OEPs

Due to the endosymbiotic relationship between Gram-negative bacteria and chloroplasts, a large number of different solute channels could also be assumed for the outer chloroplast envelope. Sequence analyses predict the presence of many β-barrel membrane proteins which could fulfill metabolite transport function (Schleiff et al, 2003). The channel forming OEPs in the outer chloroplast envelope have been named according to their location and their molecular weight (Figure 1). They were all isolated from protein bands of separated outer envelope preparations from *Pisum sativum* (pea) and therefore correspond to abundant components of this membrane. The high abundance of OEPs in the outer chloroplast envelope from pea and the differential expression of their orthologues in *Arabidopsis thaliana* strongly support the idea of a selective, regulated metabolite transport across the outer envelope of the chloroplast. The results of organellar proteome analyses assign a much larger number of yet unknown membrane transport proteins to chloroplasts and all other plant organelles as well.

Usually, OEPs do not contain a classic chloroplast transit peptide (cTP) which distinguishes them from other plastid localized, nuclear encoded proteins. For OEPs, the existence of targeting signals and the exact membrane insertion mechanisms still have to be elucidated. Recent studies showed that OEP24 and OEP37 can be integrated *in vitro* in isolated mitochondria, can partially complement the growth phenotype of yeast cells lacking porin (VDAC in higher eukaryotes), this membrane's general metabolite transporter and are assembled into mitochondria when expressed in yeast cells (Ulrich et al, 2012). OEPs are deeply integral to the membrane like other pores, have a neutral to basic isoelectric point and do mostly display a β-barrel structure in resemblance to the porins in the outer membrane of their Gram-negative ancestors as it is the case for OEP21, OEP24 and OEP37 (Duy et al., 2007). OEP16 on the other hand displays an α-helical structure (Zook et al., 2013) and therefore might represent a descendant from either the endosymbionts or the host cells plasma membrane or from other bacterial cosymbiontical sources. It is assumed, that OEP16 was introduced postendosymbiotically into the early plastid.

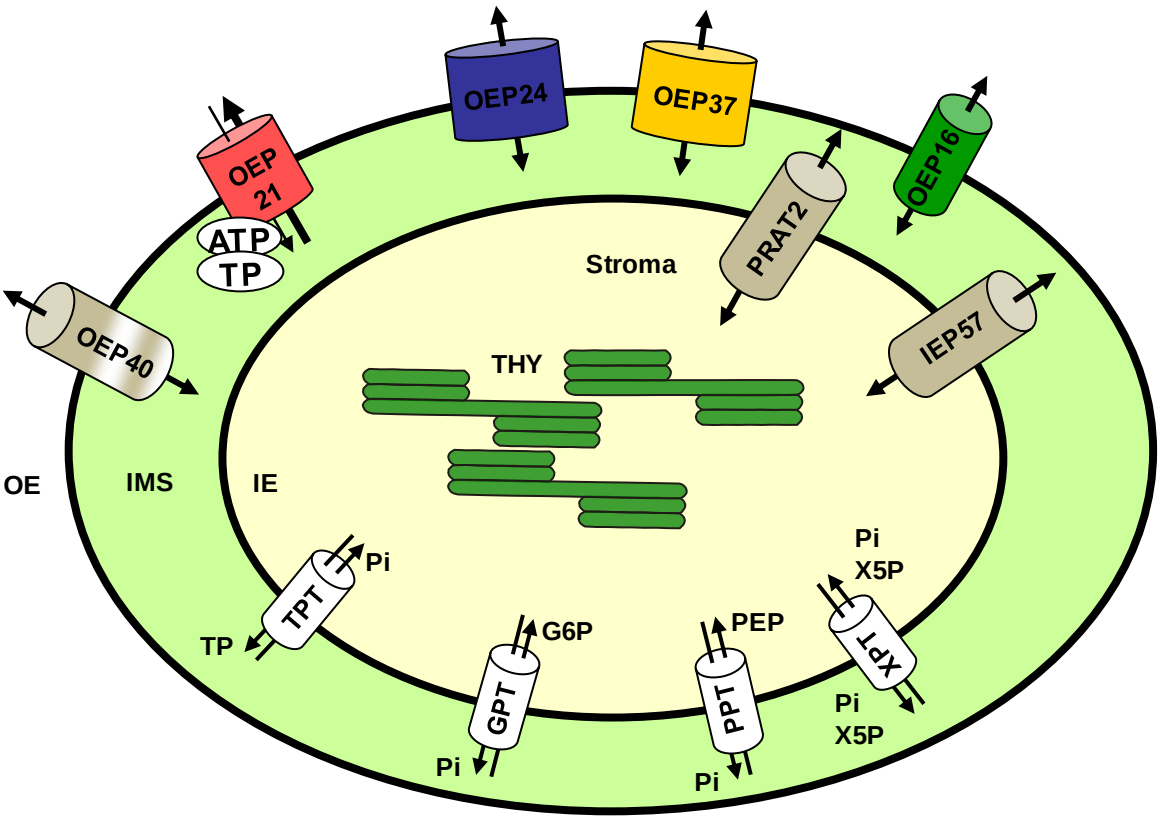

Figure 1: Solute transport across the chloroplast envelopes

Schematic depiction of a chloroplast with the outer (OE) and inner envelope (IE) separated by the intermembrane space (IMS), and the chloroplast stroma containing the thylakoid membrane system (THY). The outer envelope proteins (OEPs, upper half of the chloroplast) described so far are depicted in red (OEP21), blue (OEP24), yellow (OEP37) and green (OEP16). Numbers indicate their molecular weight in kDa when isolated from pea (Duy et al., 2007). The plastid phosphate (Pi) translocators of the inner chloroplast envelope acting as antiporters are depicted in white (lower half of the chloroplast): the triose phosphate (TP)/phosphate translocator (TPT), the glucose-6-phospate (G6P9/phosphate translocator (GPT), the phosphoenolpyruvate (PEP)/phosphate translocator (PPT) and the xylulose-5-phosphate (X5P)/phosphate translocator (XPT) (Knappe et al., 2003a, b). The envelope proteins investigated in this study are depicted in grey (upper half of the chloroplast): PRAT2, a plastid member of the family of preprotein and amino acid transport (PRAT), the inner envelope protein of 57 kDa (IEP57) and the outer envelope protein of 40 kDa (OEP40).

The OEPs identified and characterized so far (Figure 1) can be distinguished due to their properties similar to the outer membrane proteins in Gram-negative bacteria:

With **OEP24**, the outer envelope contains a rather unselective channel, whose properties closely resemble those of classical bacterial porins. OEP24 from pea was shown to form a high-conductive pore about 3 nm in diameter and to be slightly cation-selective transporting triphosphates, sugars and charged amino acids in a reconstituted *in-vitro*

system. Hydropathy analysis and circular dichroism (CD) measurements confirmed the expected β-barrel conformation, suggesting 12 membrane-spanning β-strands (Pohlmeyer et al., 1998, Schleiff et al., 2003). No sequence similarities to bacterial porins could be observed but Ps-OEP24 was shown to functionally replace VDAC in yeast (Röhl et al., 1999). The two isoforms present in *Arabidopsis* show tissue specific expression in early pollen and late seed development (Duy et al., 2007). Taken together, these data suggest that OEP24 *in vivo* forms an unselective pore with a specific function defined by its expression pattern.

OEP21 was described to be a substrate- and ATP-regulated channel in the outer envelope. OEP21 from pea was shown to form an intrinsically rectifying anion channel, which is permeable to inorganic phosphate and phosphorylated carbohydrates and regulated by ATP and triosephosphates from the side of the intermembrane space (Bölter et al., 1999). CD measurements, protease resistance experiments and computer-assisted modeling confirmed the expected β-barrel structure, suggesting an OEP21 monomer of 8 membrane-spanning β-strands (Hemmler et al., 2006). Ps-OEP21 displays an asymmetric topology with different diameters for vestibule and pore region and contains two ATP binding sites responsible for a fine-tuning of the channel. Of the two isoforms in *Arabidopsis*, one contains both binding sites whereas the other contains only one. Taken together, these data suggest that regulation of transport of metabolites across the chloroplast membranes can already be regulated at the level of the outer envelope.

OEP37 was demonstrated to form a rectifying high-conductance channel selective for cations, which shows different diameters for the channel's vestibule and the pore region like OEP21 (Götze et al., 2006). Most likely, OEP37 forms a β-barrel pore composed of 12 membrane-spanning β-strands (Schleiff et al., 2003). A long loop, connecting strand 5 and 6 facing the intermembrane space might be responsible for substrate specificity or recognition, as observed in outer membrane channels of Gram-negative bacteria where the loop faces the outside. The knock-out of the ubiquitously expressed, single-copy gene in *Arabidopsis* shows that OEP37 is not essential for plant development even though expression is elevated in germinating seedlings and late embryogenesis. The substrate specificity and metabolite transport capacity of this channel still needs to be further elucidated but planar lipid bilayer measurements showed sensitivity for the precursor of the TIC32 protein and synthetic peptides (Götze et al., 2006).

In contrast to the other OEPs which are composed of β-strands, **OEP16** displays an α-helical structure (Zook et al., 2013) and forms a slightly cation-selective, high-conductance channel highly specific for amino acids and amines *in vitro* (Pohlmeyer et al., 1997). The pore diameter was calculated to approximately 1 nm but the channel is still not permeable to uncharged sugar molecules. Therefore, OEP16 displays the highest specificity of the identified OEPs so far. According to CD measurements, OEP16 consists of four α-helical transmembrane domains and the functional channel is probably formed by di- or oligomers, in which the first two helices of one monomer form the pore. As described for channels and porins of the outer membrane of Gram-negative bacteria, OEP16 contains a long loop connecting helix one and two, which could be responsible for substrate specificity or recognition. Pea contains two and *Arabidopsis* three isoforms of OEP16. It has been shown, that OEP16.1 and OEP16.2 in both species display an alternating expression pattern with OEP16.1 being expressed in early embryo development and first leaves and OEP16.2 dominating in late seed developmental stages. The knockout of OEP16 leads to a metabolic imbalance of amino acids in seed tissue, which substantiates the function of OEP16 in amino acid transport across the outer chloroplast envelope (Pudelski et al., 2012).

OEP16 is part of a protein family whose members address both needs of the plant cell that arose from compartmentalization, the import of preproteins and the exchange of solutes across organellar membranes. The preprotein and amino acid transporter (PRAT) family of proteins has first been described by Rassow et al. (1999) and consists of 17 members in the model organism *Arabidopsis,* which localize to either mitochondria or chloroplasts. Common features of the PRAT proteins are the absence of a cleavable transit peptide and the composition of four membrane-spanning α-helices as described for OEP16 (Murcha et al., 2007, Pudelski et al., 2010). Although varying in their N- and C-termini, the sequences of the PRAT family proteins show similarities in the region of the second and third transmembrane helix with a more or less conserved consensus motif (Rassow et al., 1999, Murcha et al., 2007). The proteins in this family are similar rather on a functional than on sequence level. The family members can be phylogenetically divided into 8 groups: The plant orthologues for the TIM17, TIM23 and TIM22 proteins localize to the mitochondria and form the protein translocase of the inner membrane. The plastid OEP16 channels transport amino acids across the outer chloroplast membranes (see description above). The chloroplast

TIM17 homologues PRAT1.1 and PRAT1.2 localize to the inner envelope and are speculated to be involved in an alternative protein import pathway (Murcha et al., 2007). PRAT3 and PRAT4 are defined as distinct subfamilies, localize to mitochondria but have not been characterized further so far. The PRAT2.1 and PRAT2.2 proteins form a separate subgroup, due to their dual targeting to chloroplasts and mitochondria as well as the presence of a sterile alpha motif, called SAM domain, in their C-terminus (for an overview see Pudelski et al., 2010).

Aims of this study

Aims of this study were the assignment of a functional role to the previously biochemically characterized PRAT2 proteins of the inner chloroplast envelope (Doctoral thesis S. Kraus, 2010). This was investigated by analyzing the metabolic situation in two *prat2* double mutant lines grown under different light conditions and by functional assays in yeast cells. Further, two previously isolated chloroplast envelope proteins, IEP57 and OEP40 (Doctoral thesis I. Jeshen, 2012) had to be characterized biochemically in more detail. In addition, their functional role in the model plant *Arabidopsis thaliana* had to be addressed by studying loss of function mutants for both proteins. IEP57 had to be integrated into the metabolic network of the plant cell in order to assign a substrate to its putative transport function. For OEP40, the role as a classical β-barrel protein providing selective transport capacity to the chloroplast outer envelope was analyzed. In general, the metabolic events inside the chloroplast had to be connected to the metabolic network of the plant cell through the action of the respective transport proteins. In the long term, integration of these processes will be important for plant development and productivity.

2 Material and Methods

2.1 Material

Chemicals

All chemicals used in this work were obtained from Amersham Biosciences (part of GE Healthcare, Chalfont St. Giles, Great Britain), AppliChem GmbH (part of ITW - Illinois Tool Works Inc., Chicago, IL, USA), Biomol GmbH (Hamburg, Germany), Duchefa (Haarlem, The Netherlands), Fluka (part of Sigma-Aldrich, St. Louis, MO, USA), Invitrogen (part of LifeTechnologies, Carlsbad, CA, USA), Merck KGaA (Darmstadt, Germany), MoBiTec GmbH (Göttingen, Germany), Riedel-de-Haën (part of Sigma-Aldrich, St. Louis, MO, USA), Roche (Basel, Switzerland), Roth (Karlsruhe, Germany), Serva Electrophoresis GmbH (Heidelberg, Germany), Sigma-Aldrich (St. Louis, MO, USA) and Thermo Fisher Scientific Inc. (Waltham, MA, USA).

Enzymes

Restriction enzymes were purchased from Fermentas (part of Thermo Fisher Scientific Inc., Waltham, MA, USA) and New England Biolabs GmbH (Ipswich, MA, USA). M-MLV reverse transcriptase was purchased from Promega (Fitchburg, WI, USA). Taq polymerase was obtained from Bioron GmbH (Ludwigshafen, Germany), Phusion polymerase from New England Biolabs (Ipswich, MA, USA) and Pfu polymerase from Fermentas (part of Thermo Fisher Scientific Inc., Waltham, MA, USA). T4 ligase was obtained from Fermentas (part of Thermo Fisher Scientific Inc., Waltham, MA, USA). RNAse free DNAse I was purchased from Roche (Basel, Switzerland) and RNAse from Amersham Biosciences (part of GE Healthcare, Chalfont St. Giles, Great Britain). Cellulase was obtained from Serva Electrophoresis GmbH (Heidelberg, Germany) and Macerozyme R10 from Yakult Pharmaceutical Industry CO., LTD. (Tokyo, Japan).

Oligonucleotides

Oligonucleotides were ordered from Metabion (Martinsried, Germany) and from MWG Operon (Eurofins Genomics, Ebersberg, Germany) in standard desalted quality.

Table 1: Oligonucleotides used in the work on PRAT2 in this study

Name	Sequence (5'-3' orientation)	Application
Act2/8 fw	GGTGATGGTGTGTCT	qRT-PCR
Act2/8 rv	ACTGAGCACAATGTTAC	
At_PRATC2.1_LC_fw	ATTGGTGAGCCAAGGA	
At_PRATC2.1_LC_rv	TCATGGCAATAGCAGCTAA	
At_PRATC2.2_LC_fw	GCCTATGAATGCAATCACC	
At_PRATC2.2_LC_rv	GAAGAAGGAGAGAGGCT	
At_PORA_LC_fw	GTTACGTCTCCGAGTCAG	
At_PORA_LC_rv	GCCAAAACACAACTACTAAATC	
At_PORB_LC_fw	TTCACAGGCGTTTCCA	
At_PORB_LC_rv	GTACCGAGAGGTGTCAT	
At_PORC_LC_fw	CGTTACCACGAGGAAACA	
At_PORC_LC_rv	AAATCTTGAGTTCATGCCA	
SALK 112126 RP2	CTGCTGGTTTTGCTGTTTTTC	genotyping of SALK mutant lines
SALK 112126 LP2	TATCATAAGTCTTGGCCCTGG	
SALK 136525 RP2	CCAGGAAACAACAATTCACAC	
SALK 136525 LP2	CAAAACAGAAGTTACCGGTGG	
SALK 149871 RP2	AATAACATGGTGTTGGCAACG	
SALK 149871 LP2	AAAGTTCCCATTAAACCACCG	
LBa1	TGGTTCACGTAGTGGGCCATCG	

Table 2: Oligonucleotides used in the work on IEP57 in this study

Name	Sequence (5'-3' orientation)	Application
Act2/8 fw	GGTGATGGTGTGTCT	qRT-PCR
Act2/8 rv	ACTGAGCACAATGTTAC	
At_IEP57_LC_fw	AGGGATTATCGAGGGC	
At_IEP57_LC_rv	AGATGGGACCGTCACA	
At_HPL_fw	ATGAGAGACGCTAATGTTT	qRT-PCR (wounding assay)
At_HPL_rv	CAATTTGAGTTTCAATTCGGAT	
35S_fw	GATGTGATATCTCCACTGACGTAAGG	genotyping of At-IEP57 OEX/popON lines
attB1 (gateway fw)	ACAAGTTTGTACAAAAAAGCAGGCT	genotyping of At-IEP57 popOFF lines
At_IEP57_RNAi_rv	TTTCCAATGTTTCCACCCCCTCC	genotyping of At-IEP57 OEX/popON/popOFF lines
At_IEP57_fw(cacc)	CACCATGTCACATATGGTGTTTCAGAGCG	Cloning of IEP-GFP fusion constructs (GATEWAY)
At_IEP57_rv(fl)-st	AGAGGCAGATGCAGCCACCTTC	
At_IEP57_rv(1TM+10)-st	TGTGTTTCCATAGGAACGACATGGAGC	
Ps_IEP57_fw(cacc)	CACCATGTCCTCTCACGCTCTGTTTCAAGC	
Ps_IEP57_rv(fl)-st	GTCGACATAGAATCCCTACAAAAAA	
Ps_IEP57_(1TM+10)-st	TGTGTTTCCATATGAACGACAAGGAGCAAGGG	

At_IEP57_fw(fl)_NcoI At_IEP57_rv(fl)_SalI+st At_IEP57_rv(fl)_SalI-st	CCATGGATGTCACATATGGTGTTTCA GTCGACTTAAGAGGCAGATGCAGCCA GTCGACAGAGGCAGATGCAGCCAC	Cloning of OEX constructs in pET21d
At_IEP57_fw (N42-278)_NcoI	CCATGGCTTCTTCGTCCTCGTTTCTTGTCG	Cloning of OEX constructs in pET21d and pPROEX
At_IEP57_rv (N42-278)XhoI_-st	CTCGAGCCATTCCTCTTTTAGTCTATTCTTACG	Cloning of OEX constructs in pET21d
At_IEP57_rv (N42-278)_PstI_+st	CTGCAGCTACCATTCCTCTTTTAGTCTATTCTTAC	Cloning of OEX constructs in pPROEX
At_IEP57_fw (42-278)_SalI At_IEP57_rv (42-278)_XbaI_+st	GTCGACGCTTCTTCGTCCTC TCTAGATTACCATTCCTCTTTTAG	Cloning of OEX constructs in pCOLDII
Ps_IEP57_fw (N44-278)_NcoI Ps_IEP57_fw (N44-278)_PstI_+st	TTCCATGGTTCGATCGTCGTCCGCCTCCC CTGCAGTCACTCTTGCTTTATCCTATCTTTTCGATTTTTAA	Cloning of OEX constructs in pPROEX

Table 3: Oligonucleotides used in the work on OEP40 in this study

Name	Sequence (5'-3' orientation)	Application
Act2/8 fw Act2/8 rv At_OEP40_LC_fw At_OEP40_LC_rv	GGTGATGGTGTGTCT ACTGAGCACAATGTTAC CGTTAGGGTTCCTACGG CTCAGCTACATTGCCCTC	qRT-PCR
35S_fw At_OEP40_RNAi_rv	GATGTGATATCTCCACTGACGTAAGG GATAGAGAAATCGCCGAATTGAGGT	genotyping of At-OEP40 OEX lines
At-OEP40-1_fw At-OEP40-1_rv At-OEP40-3_fw LB1 SAIL	GGGATAAACAAACAACCAGGC TATCCACCACCTCAATCGAAG TTTCGTGAAGAGCAAAAGCC GCCTTTTCAGAAATGGATAAATAGCCTTGCTTCC	genotyping of At-OEP40 T-DNA insertion lines
Ps-OEP40_PM1_M2_fw Ps-OEP40_PM2_M2_rv	CAAACCCAAATAATCACAGCAAAACTACCAATCACC GGTGATTGGTAGTTTTGCTGTGATTATTTGGGTTTG	site-dir. mutagenesis of Ps-OEP40 (Met19Ile)
At-OEP40_fl_fw(NcoI) At-OEP40_fl_+st_rv(XhoI) At-OEP40_fl_-st_rv(XhoI)	CCATGGATGAAGGCATCGATGAAGT CTCGAGTCAAGCAGCTCCTTTCAAAG CTCGAGAGCAGCTCCTTTCAAAGCTT	cloning of OEX constructs in pET21d

Plasmid vectors and constructs

Table 4: Plasmid vectors used in this study

Name	Application	Origin
pJET1.2	subcloning, sequencing	Thermo Fisher Scientific Inc. (Waltham, MA, USA)
pET21d	Heterologous overexpression of IEP57/OEP40 in *E. coli*	Novagen®/Merck KGaA, Darmstadt, Germany
pPROEX HTa	Heterologous overexpression of IEP57 in *E. coli*	Invitrogen™/Life Technologies (Carlsbad, CA, USA)
pCOLDII	Heterologous overexpression of IEP57 in *E.coli*	Clontech Laboratories Inc. (Mountain View, CA, USA)
pENTR/ D-TOPO	entry vector for LR recombination (GATEWAY)	Invitrogen™/Life Technologies (Carlsbad, CA, USA)
pH2GW7	binary GATEWAY overexpression vector	Plant Systems Biology (University of Gent, Belgium)
pK7FWG2	binary GATEWAY vector for the expression of GFP fusion proteins	Plant Systems Biology (University of Gent, Belgium)

Table 5: Contructs created in this study

Name	Application
At-IEP57_fl_+st_pJET1.2(NcoI/SalI)	subcloning, sequencing
At-IEP57_fl_-st_pJET1.2(NcoI/SalI)	
At-IEP57_fl_+st_pET21d(NcoI/SalI)	heterologous overexpression in *E. coli*
At-IEP57_fl_-st_pET21d(NcoI/SalI)	
At-IEP57_42-278_+st_pJET1.2(NcoI/PstI)	subcloning, sequencing
At-IEP57_42-278_-st_pJET1.2(NcoI/XhoI)	
At-IEP57_42-278_+st_pJET1.2(SalI/XbaI)	
At-IEP57_42-278_+st_pPROEX(NcoI/PstI)	heterologous overexpression in *E. coli*
At-IEP57_42-278_-st_pET21d(NcoI/XhoI)	
At-IEP57_42-278_+st_pCOLDII(SalI/XbaI)	
Ps-IEP57_44-278_+st_pJET1.2(XhoI/PstI)	subcloning, sequencing
Ps-IEP57_44-278_+st_pPROEX(XhoI/PstI)	heterologous overexpression in *E. coli*
At-IEP57_fl_-st_pENTR/D-TOPO	subcloning for LR recombination (GATEWAY), sequencing
Ps-IEP57_fl_-st_pENTR/D-TOPO	
At-IEP57_fl_-st_pK7FWG2	GFP fusion (GATEWAY)
Ps-IEP57_fl_-st_pK7FWG2	
At-IEP57_1-308_-st_pENTR/D-TOPO	subcloning for LR recombination (GATEWAY), sequencing
Ps-IEP57_1-311_-st_pENTR/D-TOPO	
At-IEP57_1-308_-st_pK7FWG2	GFP fusion (GATEWAY)
Ps-IEP57_1-311_-st_pK7FWG2	
At-OEP40_fl_+st_pJET1.2(NcoI/XhoI)	subcloning, sequencing
At-OEP40_fl_-st_pJET1.2(NcoI/XhoI)	
At-OEP40_fl_+st_pET21d(NcoI/XhoI)	heterologous overexpression in *E. coli*
At-OEP40_fl_-st_pET21d(NcoI/XhoI)	
Ps-OEP40_fl_-st_pET21d(NcoI/XhoI)_Met19Ile	

Molecular weight marker and DNA standard

For size determination of separated proteins on SDS gels, the peqGOLD protein marker I (PEQLAB Biotechnologie GmbH, Erlangen, Germany) was used. DNA of phage lambda (Fermentas GmbH, part of Thermo Fisher Scientific Inc., Waltham, MA, USA) digested with PstI was used for size determination of separated DNA fragments on agarose gels.

Antisera

Primary antibodies directed against Ps-IEP57 (synthetic peptide from the N-terminal of Ps-IEP57, AA 133 - 160) and At-OEP40 (mature, full length protein from *Arabidopsis*) were generated by Pineda Antikörperservice (Berlin, Germany) during this study. Overexpression and purification of At-OEP40 is described under 2.2.4. Antiserum recognizing MAGNESIUM CHELATASE (At-CHLM, At4g25080) was obtained from Uniplastomic (Biviers, France). Primary antibodies against Ps-OEP37, Ps-OEP40, At-POR B, At-PRAT2.1 and Ps-TIC110 were already available in the group.

Bacterial strains

Cloning in *E. coli* was performed using the strains DH5α, TOP10 and DB3.1 (Invitrogen, part of LifeTechnologies, Carlsbad, CA, USA). Heterologous overexpression of proteins was performed in *E. coli* BL21 (DE3) (Novagen®/Merck KGaA, Darmstadt, Germany). The *Agrobacterium tumefaciens* GV3101::pMK90RK strain (Koncz and Schell, 1986) used for stable transformation of *Arabidopsis* was obtained from Dr. J. Meurer (Dept. Biology I, Botany, LMU, Munich, Germany). The *Agrobacterium tumefaciens* AGL1 strain used for transient transformation of *Nicotiana benthamiana* (tobacco) was obtained from Dr. T. Ott (Dept. Biology I, Botany, LMU, Munich, Germany).

Plant material

All experiments were performed on *Arabidopsis thaliana* ecotype Columbia 0 (Col-0, Lehle seeds, Round Rock, TX, USA). The second T-DNA insertion line for *At-OEP40* (*noep40*-3) was obtained from NASC (Nottingham Arabidopsis stock centre, Nottingham, Great Britain). Peas (*Pisum sativum*) var. Arvica were obtained from Bayrische Futtersaatbau GmbH (Ismaning, Germany). Tobacco (*Nicotiana benthamiana*) plants were obtained from Dr. T. Ott (Dept. I Biology, Botany, LMU, Munich, Germany).

2.2 Methods

2.2.1 Plant physiological methods

Growth of *Arabidopsis thaliana*

Seeds of *Arabidopsis* were either sown on MS media (0.215 % MS plant salts 4.52 g/L, 0.1 % 2-(*N*-morpholino)ethanesulfonic acid (MES), 0.3 % gelrite/ 1-1.5 % agar (pH 5.8/KOH), (Murashige and Skoog, 1962), in some cases supplemented with 1 % (w/v) sucrose, or directly on soil (Stender substrate A210, Stender AG, Schermbeck, Germany). If necessary, seedlings were transferred onto soil after growing on sterile media for two to three weeks. Before sowing on sterile media, seeds were surface sterilized with 70 % ethanol (2 min), 6 % NaClO with 0.05 % Tween 20 (3-5 min) and subsequently washed in sterile ddH_2O three times. Bigger amounts of seeds were sterilized using chlorine gas in a closed recipient (desiccator) over night by mixing 20 ml NaClO with 1 ml concentrated HCl. Sterilized seeds were transferred onto media containing plates with autoclaved toothpicks. To synchronize germination, plates or pots were kept at 4 °C in the dark for one to three nights. Transformed plants and T-DNA insertion lines were selected on MS media containing the respective antibiotic or herbicide (25 µg/ml hygromycin, 100 µg/ml kanamycin, 50 µg/ml ammonium glufosinate, BASTA). In case of the popOFF2 and popON2 systems, protein loss or overexpression was induced by adding 10 µM dexamethasone to the MS media. In order to transfer large amounts of plants onto plates containing dexamethasone, *AtIEP57*/popOFF2 and *At-IEP57*/popON mutant plants were sown onto propyltex mesh fabric (210 µm, SEFAR, Heiden, Switzerland). In case of feeding studies with different metabolites and intermediates on plates, the respective substances were dissolved, sterile filtered and added in appropriate concentrations after the medium was autoclaved. Plant growth occurred in growth chambers with one of the following light regimes:

Table 6: Light regimes used for the growth of *Arabidopsis thaliana*

Regime	light	dark
Longday	16 hrs, 21 °C photon flux density of 100 µMol m^{-2} s^{-1}	8 hrs, 16 °C
Shortday	8 hrs, 21 °C photon flux density of 100 µMol m^{-2} s^{-1}	16 hrs, 16 °C
Ultra longday	22 hrs, 21 °C photon flux density of 100 µMol m^{-2} s^{-1}	2 hrs, 16 °C
Constant light	24 hrs, 21 °C photon flux density of 100 µMol m^{-2} s^{-1}	
Constant low light	24 hrs, 21 °C photon flux density of 10 µMol m^{-2} s^{-1}	
Longday, cold	16 hrs, 10 °C photon flux density of 100 µMol m^{-2} s^{-1}	8 hrs, 10 °C

Hydroponic growth of *Arabidopsis thaliana*

In order to analyze the phenotype of single plants growing on a minimal amount of liquid medium which can be supplemented with different substances of interest, Col-0 wild-type and *At-IEP57*/popOFF mutant plants were grown in a hydroponic culture system. This system was a combination of the Araponics growing system (Araponics SA, Liège, Belgium) and the method described by Conn et al. (2013, see figure x). For the seedholders, the lids of lightproof Eppendorf tubes (Safe-Lock Tubes 1.5 ml, amber, Eppendorf, Hamburg, Germany) were separated from the tubes and a 2 mm hole was punched in the middle with revolving punch pliers (Rennsteig Werkzeuge, Viernau, Germany). After autoclaving, the plain sides of the lids were placed on the adhesive side of tape in the airflow cabinet and the protruding ring was filled with 0.5 MS media without sucrose containing 0.75 % agar so that an agar plug with a dome arose from the protruding ring. The autoclaved tube bottoms were positioned in an Araponics growth container in a custom-made plastic inlay with 11 mm holes and filled with 1.6 ml of liquid 0.5 MS media without sucrose. After solidifying, the agar filled lids were placed on top and up to 3 surface-sterilized seeds were transferred onto the agar patch. The growth container was covered with its transparent lid and closed on the sides with cling film and tape to enhance humidity. The containers were placed at 4 °C in the

dark for 1-3 days and then transferred into a growth cabinet under longday conditions. After 7 days, the cling film was removed and the germinating plants were thinned down to one per lid. The medium containing tubes were exchanged for fresh ones every seven days. After 14 or 21 days of growth, plants were transferred onto tubes containing 0.5 MS media with 10 µM dexamethasone and/or the respective substance of interest. Metabolites or intermediates were dissolved, sterile filtered and added in appropriate concentrations to the autoclaved medium.

Wounding assay

In order to analyze the induction of the stress gene hydroperoxide lyase (HPL) by wounding in Col-0 wild-type and *At-IEP57*/popOFF lines, plants were grown on 0.5 MS + 1 % sucrose for ten days and then transferred onto plates with or without 10 µM dexamethasone. After 7 and 10 days, half of the plants induced with dexamethasone and half of the plants grown without dexamethasone were wounded using forceps with corrugated tips in order that all of the leaves of one plant were wounded. After a wounding time of 90 min, replicates of 5 plants each were harvested and immediately frozen in liquid nitrogen. Three replicates from unwounded and wounded plants grown with our without dexamethasone were produced. The harvested plant material was used for RNA isolation, cDNA production and qRT-PCR.

Phenotypic analysis of *oep40* mutant plants

To closely monitor the delay in bolting, growth and flowering time in *oep40* mutant plants compared to wild-type under low temperature conditions (see table 1), a detailed phenotypic analysis was conducted. A detailed list of all parameters recorded is given in table 2 (modified from Salomé et al., 2011 (table S1) and personal communication with Dr. V. Wahl, MPI of molecular plant physiology, Golm, Germany).

Table 7: Detailed description of parameters recorded for phenotypic analysis

Parameter	Description
DTB	Days to bolting: Days until the inflorescence had elongated to 0.5 cm
DTF	Days to flowering: Days until the first flower was opened
RLN	rosette leaf number at 15 cm main shoot length
CLN	cauline leaf number at 15 cm main shoot length
TLN	Total leaf number: sum of RLN and CLN

For phenotypic monitoring, a set of 27 plants from each, Col-0 wild-type as well as *oep40-1* and *oep40-3* mutant plants, was grown at 21 °C under longday conditions for 7 days and then switched to low temperature conditions at 10 °C. Plants were equally distributed on the three levels of the growth cabinet and monitored daily. An additional set of wild-type and mutant plants was kept at 21 °C for controlling purposes.

Stable transformation of *Arabidopsis thaliana*

Stable transformation of *Arabidopsis* was performed as described by Bechthold et al., 1993. Three days before transformation, a single colony of *Agrobacterium tumefaciens* harboring the desired binary vector was used to inoculate 10 ml of LB medium containing selective antibiotics. This starting culture was incubated at 180 rpm and 28 °C. After two days, 500 ml LB medium was inoculated 1:100 with the starting culture and incubated at 180 rpm and 28 °C for 24 hrs. The cells were harvested (6 000 x g, 10 min) and reconstituted in 400 ml infiltration medium (5 % (w/v) sucrose, 0.215 % MS, 0.05 % (v/v) Silwet L-77). One night before transformation, siliques were cut from the plants to be transformed and the plants were covered with plastic bags to allow a maximum opening of the stomatal cells. The flowering stalks were dipped into the infiltration medium and infiltrated under vacuum in a desiccator for 5 min. The plants were then left to recover horizontally on a humid paper towel covered by a plastic bag for 24 hrs before they were rinsed with H_2O and placed in an upright position. The T1 generation of seeds was harvested and transformants were selected on MS agar plates containing the respective selective antibiotic.

Transformation of *Nicotiana benthamiana* (tobacco)

Infiltration: Plants to be transformed were watered thoroughly and kept under cling film. A single colony of *Agrobacterium tumefaciens* AGL1 harboring the desired binary vector was used to inoculate 3 ml of LB media containing selective antibiotics and incubated at 180 rpm and 28 °C for 24 hrs. 30 ml LB media containing selective antibiotics was inoculated with the starting culture and incubated at 180 rpm and 28 °C for 4 hrs. The cells were harvested (4000 x g, 15 min, RT), resuspended in infiltration medium (10 mM MES, 10 mM $MgCl_2$, 200 µM acetosyringone) and subsequently incubated at 75 rpm and 28 °C for two hrs. The cells were harvested (4000 x g, 15 min, RT) and resuspended in 5 ml 5 % sucrose solution with 200 µM acetosyringone. The optical density (OD_{600}) was adjusted to 0.6 - 0.8 and the suspension was injected into tobacco leaves via the stomatal cells. The infiltrated plants were moistened, covered with cling film and incubated over night. After one to three days, pieces were cut from the infiltrated leaves to check for GFP fluorescence. Subsequently, mesophyll protoplasts were isolated and used for confocal laser scanning microscopy.

Isolation of mesophyll protoplasts: Before protoplast isolation, 10 ml of enzyme solution (1 % cellulase R10, 0.3 % Macerozym R10 in buffer F-PIN) was incubated at 55 °C for 10 min. After cooling down to room temperature, the enzyme solution was supplemented with 0.1 % BSA and sterile filtered (0.45 µM sterile filter, Whatman/Schleicher) directly onto 0.5-1 g leaf material from infiltrated plants. The leaf material was cut with a razor blade, the solution transferred to a 100 ml vacuum flask and then infiltrated for 20 sec. The solution was incubated in the dark at 40 rpm for 90 min and the protoplasts were then released at 80 rpm for one min. After filtration of the protoplast solution through a nylon net (100 µM) into a 15 ml COREX tube, the solution was overlaid with 2 ml F-PCN and centrifuged (70 x g, 10 min, 4 °C). Intact protoplasts were collected at the interface with a cut tip, washed with 10 ml W5 and collected at 50 x g and 4 °C for 10 min. After resuspending in 1 ml W5, the protoplasts were used for confocal laser scanning microscopy.

F-PIN (500 ml): macro MS (modified), 0.5 ml 1000x micro MS, 1 ml 500x PC vitamins, 20 mM MES, 55 g sucrose (ultrapure), adjust pH to 5.8 with KOH, adjust osmolarity with sucrose to 550 mOsm, filtrate (0.45 µM).

F-PCN (500 ml): macro MS (modified), 0.5 ml micro MS, 500x PC vitamine, 500 µl 6-benzylamino-purine, BAP, [1 mg/ml], 50 µl α-naphthaleneacetic acid, NAA [1 mg/ml], 20 mM MES, 40 glucose, adjust pH to 5.8 with KOH, adjust osmolarity with glucose to 550 mOsm, filtrate (0.45 µM).

2M NH_4 succinate (50 ml): 11.8 g succinic acid, 5.3 g NH_4Cl, 11 g KOH pellets, adjust pH to 5.8, filtrate (0.45 µM)

Macro MS (modified): 20 mM each: KNO_3, $CaCl_2$ x 2 H_2O, $MgSO_4$ x 7 H_2O, KH_2PO_4, 5 ml 2 M NH_4 succinate

1000x micro MS (100 ml): 83 mg KJ, 620 mg H_2BO_3, 2230 mg $MnSO_4$, 860 mg $ZnSO_4$, 25 mg Na_2MoO_4, 2.5 mg $CuSO_4$, 2.5 mg $CaCl_2$

500x PC vitamins (100 ml): 10 g myoinositol, 100 mg pyridoxine HCl, 50 mg thiamine HCl, 100 mg nicotinic acid), 1 g biotin, 100 mg Ca panthotenate

2.2.2 Microbiological methods

Media and growth of *Escherichia coli* and *Agrobacterium tumefaciens*

The *Escherichia coli* strains TOP10, BL21 and DB3.1 were cultivated in LB media (1 % tryptone, 0.5 % yeast extract, 1 % NaCl, if necessary 1.5 % agar) at 37 °C in either liquid culture or on agar plates both containing the respective antibiotic (ampicillin 100 µg/ml, kanamycin 50 µg/ml, spectinomycin 100 µg/ml) of the harbored vector. For stable transformation of *Arabidopsis*, *Agrobacterium tumefaciens* GV3101::pMKR90RK (Koncz and Schnell, 1986) was cultivated at 28 °C in liquid LB media or on LB plates supplemented with agar containing the appropriate antibiotics (kanamycin 50 µg/ml (resistance of strain GV3101), rifampicin 100 µg/ml (resistance of Ti-plasmid), spectinomycin 100 µg/ml (resistance of transformed vector)). For the transformation of *tobacco, Agrobacterium tumefaciens* AGL1 was cultivated at 28 °C in liquid LB media or on LB plates containing the appropriate antibiotics (carbenicillin 100 µg/ml (resistance of strain AGL1), spectinomycin 100 µg/ml (resistance of transformed vector)).

Production and transformation of competent bacterial cells

Chemically competent cells of *E. coli* were produced as described by Hanahan (1983). The transformation with plasmid DNA was performed using the heat shock method (Sambrook

et al., 1989). For the production of competent cells of *A. tumefaciens* GV3101 and AGL1, a single colony was used to inoculate 3 ml of LB media containing the respective antibiotics (see section above) and incubated at 180 rpm at 28 °C for 24 hrs. Subsequently, 50 ml LB media containing the respective antibiotics were inoculated with this starting culture and incubated at 180 rpm at 28 °C for another 24 hrs. The cells were then harvested (6000 x g, 10 min, 4 °C) and washed in 10 ml TE buffer (10 mM Tris/HCl, pH 8, 1 mM EDTA). The cells were again harvested (6000 x g, 10 min, 4 °C) and resuspended in 5 ml LB media. Aliquots of 200 µl were frozen in liquid nitrogen and kept at -80 °C. For transformation of competent agrobacteria, 0.1 – 0.5 µg plasmid DNA were added to one aliquot of competent cells and incubated on ice for 30 min followed by 5 min in liquid nitrogen and 5 min at 37 °C. After adding 800 µl of LB media, the cells were incubated at 180 rpm at 28 °C for 4 hrs and then harvested (4000 x g, 2 min, 4 °C). The pellet was resuspended in 100 µl LB media and incubated on LB plates containing the respective antibiotics (see section above) at 28 °C for 72 hrs.

Uptake studies in *Saccharomyces cerevisiae*

For functional characterization of the PRAT2 proteins, uptake studies with radiolabelled S-adenosylmethionine, methionine and cysteine were carried out in the heterologous yeast system. The complete coding sequences of PRAT2.1 and PRAT2.2 were present in the pNEV yeast vector with and without being fused to the signal peptide SUC2 at the beginning of this study (doctoral dissertation Sabrina Kraus, 2011). Transformation and preparation of yeast cells was carried out by PD Dr. Markus Geisler (Department of Biology, Plant Biology, Université Fribourg, Switzerland). For the uptake studies, a preculture of 10 ml SD medium (pH 5.5) with the appropriate selection of amino acids was inoculated with one colony of transformed yeast cells and grown at 30 °C at 200 rpm over night. At OD_{600} = 1, 50 µl of the preculture was used to inoculate 20 ml of SD medium (pH 5.5) with the appropriate selection of amino acids. The main culture was incubated at 30 °C at 200 rpm over night. Cells were grown to an OD_{600} of about 1.5 and kept at room temperature until further use. For uptake studies, the cells were collected in a 50 ml falcon tube and centrifuged at 1500 rpm for 5 min at 4 °C. The pelleted fraction was resuspended in 40 ml (RT) ultrapure H_2O and centrifuged at 1500 rpm for 5 min at 4 °C. Meanwhile, glass fiber filters (Glass fiber prefilters (APFB02500), Millipore Corporation, Billerica, MA, USA) were distributed on a vacuum pump

(1225 Sampling manifold (XX2702550), Millipore Corporation, Billerica, MA, USA) and washed twice with 2 ml of ultrapure water to ensure equal distribution of the vacuum on all sample cups. The pelleted fraction was then resuspended in 10 ml (RT) SD medium (pH 4.5) and 20 µl of radioactive mix was added to each sample. The suspension was mixed well and 4 aliquots of 500 µl were removed immediately and placed on the respective filters (time point 0). The filters were washed immediately with ultrapure H_2O twice, removed and dried on whatman paper. The yeast cells were incubated at room temperature under shaking for twenty min while a new set of glass fiber filters was installed in the vacuum pump and washed twice with ultrapure H_2O. After 20 min another 4 aliquots of 500 µl were placed on the respective filters (time point 20) and washed immediately with ultrapure H_2O. The filters were then removed and dried on whatman paper. When dried, all filters were placed into scintillation counter collection tubes and 5 ml of scintillation liquid was added. The samples were incubated under shaking for at least 2 hrs and analyzed with the appropriate program in a scintillation counter (2200CA Tri-Carb liquid scintillation analyzer, formerly Packard Bioscience, now Perkin-Elmer, Waltham MA, USA). The collected data was analyzed using the GraphPad Prism 4 software (GraphPad Software Inc., La Jolla, CA, USA). All yeast uptake studies were carried out under the guidance of PD Dr. Markus Geisler at the Department of Biology, Plant Biology, Université Fribourg, Switzerland.

2.2.3 Molecular biology methods

Polymerase Chain Reaction (PCR)

DNA fragments used for cloning and genotyping of *Arabidopsis* mutant lines were amplified by polymerase chain reaction (PCR) (Saiki et al., 1988). Phusion polymerase and *Pfu* polymerase were used for amplifying DNA fragments for cloning from wild-type cDNA obtained from *Arabidopsis* or *Pisum sativum* (pea) and for site-directed mutagenesis. *Taq* polymerase was used for genotyping. The applied PCR protocol was according to manufacturers' instructions.

Site-directed mutagenesis

Site-directed mutagenesis was performed using the QuikChange method as described by Nøhr and Kristiansen (2003). A pair of complementary primers harboring the desired mutation in their center was used to amplify entire vectors containing the DNA fragment to

be mutated. *Phusion* or *Pfu* polymerase was used according to manufacturers' recommendation. Unmutated, parental plasmids were digested with the restriction enzyme DpnI and the reaction was transformed into chemically competent *E. coli* TOP10 cells. Successful mutagenesis was checked by sequencing.

Cloning strategies

Agarose gel electrophoresis, restriction digests, DNA ligation and determination of DNA concentrations were performed following standard protocols (Sambrook et al., 1989) and according to manufacturers' instructions. PCR products were purified from agarose gels using the Nucleospin Extract II Kit (Macherey and Nagel, Düren, Germany). LR recombination in the GATEWAY system was also performed according to manufacturers' instructions.

Isolation of plasmid DNA from *Escherichia coli*

Preparation of plasmid DNA from transformed *E. coli* cells was performed according to Zhou et al. (1990) by alkaline lysis with SDS and NaOH from 3 ml overnight cultures. For high yield DNA plasmid preparation, the Nucleobond AX Plasmid Purification Midi (AX 100) kit (Macherey and Nagel, Düren, Germany) was used according to manufacturers' recommendations.

Isolation of genomic DNA from *Arabidopsis thaliana*

Genomic DNA from *Arabidopsis* was prepared using two to three rosette leaves which were ground with 450 µl of extraction buffer (200 mM Tris/HCl (pH 7.5), 250 mM NaCl, 25 mM EDTA, 0.5 % SDS, 100 µg/ml RNase) in a tissue lyser (Retsch/Qiagen, Hilden, Germany) for three min. The samples were incubated at 37 °C for 10 min and centrifuged (16 000 x g, 10 min, 4 °C). The DNA present in the supernatant was precipitated with 300 µl isopropanol for five min at room temperature and the samples were centrifuged (16 000 x g, 10 min, 4 °C). The pellet was washed with 70 % ice cold ethanol and after drying reconstituted in 50 µl 10 mM Tris/HCl (pH 8). For PCR genotyping, 5 µl of genomic DNA was used in a 25 µl reaction volume.

Determination of DNA and RNA concentrations

DNA and RNA concentrations were measured photometrically according to the Lambert-Beer principle. The absorption of a diluted sample at 260 nm and 320 nm was determined and the concentration was calculated using the following equations:

DNA: $c\ [\mu g/\mu l] = (E_{260}\text{-}E_{320}) \times 0.05 \times f_{dil}$

RNA: $c\ [\mu g/\mu l] = (E_{260}\text{-}E_{320}) \times 0.04 \times f_{dil}$

Characterization of *Arabidopsis* T-DNA insertion lines by PCR genotyping

To identify mutants with the T-DNA insertion present in both alleles (homozygous), a combination of T-DNA specific primers and gene-specific primers flanking the predicted T-DNA insertion site were used. Amplification using T-DNA specific primers (LB or RB) in combination with a gene-specific primer will only generate a PCR product in plants which are hetero- or homozygous. Using two gene-specific primers flanking the T-DNA insertion site will generate a PCR product only in wild-type and heterozygous plants, thereby allowing a clear differentiation between plants that are wild-type, hetero- or homozygous for the respective T-DNA insertion. To determine the specific T-DNA insertion site to analyze the unknown T-DNA borders, the DNA fragments amplified with the specific primer combinations were subsequently cloned into pJET1.2 and sequenced. Primers used for PCR genotyping are listed in Table 1, 2 and 3.

DNA sequencing

Sequencing of generated subclones, mutated vectors and products from PCR genotyping was performed by the sequencing service of the Genomics Service Unit (GSU), Genetics, Department I, Ludwig-Maximilians University, Munich, Germany.

Extraction of total RNA from *Arabidopsis thaliana*

Plant material for RNA isolation was either ground directly in liquid nitrogen or frozen in liquid nitrogen and kept at –80 °C until RNA preparation. An equivalent to 50 µl of plant material ground in liquid nitrogen was used for total RNA isolation with the RNeasy Plant Mini Kit (Qiagen, Hilden, Germany).

Reverse transcription

To generate cDNA, 0.5 - 1 µg of RNA was transcribed using MMLV reverse transcriptase. Reverse transcription was performed according to manufacturers' instructions in a reaction

volume of 10 µl containing 4 µM oligo-dT primer and 0.5 mM dNTP. After an incubation at 70 °C for 2 min, the reaction was cooled down on ice, 2 units of MMLV reverse transcriptase were added and the reaction was incubated at 42 °C for 90 min. 1 µl of the obtained cDNA was used for non-quantitative RT-PCR in a 25 µl reaction volume.

Quantitative real time RT-PCR

The obtained cDNA was diluted 1:20 in ddH_2O supplemented with 0.1 µg/µl tRNA and the reaction was carried out using the FastStart DNA Master SYBR-Green Plus Kit (Roche, Basel, Switzerland) according to manufacturers' recommendations. Detection and quantification of transcripts was performed with the LightCycler system (Roche Applied Science, Basel, Switzerland). A total of 45 cycles composed of 1 s at 95 °C (denaturation), 7 s at 49 °C (annealing), 19 s at 72 °C (elongation) and 5 s at 79 °C (detection) were realized (Philippar et al., 2004). Real time RT-PCR using oligonucleotides amplifying AtAct2 (At3g18780) and AtAct8 (At1g49240) was performed to normalize the gene specific mRNA content to 1000 actin molecules. The relative amount of RNA was calculated using the following equation: Relative amount of cDNA = $2^{[n(actin)-n(gene)]}$ with n being the threshold cycle of the respective PCR product. Primers used for qRT-PCR are listed in Table 1, 2 and 3.

Quantitative real time RT-PCR with the flowering gene primer platform

In order to screen the expression of various flowering genes in Col-0, *oep40-1* and *oep40-3* plants grown under low temperature conditions over a time course of 16 days, plant material was harvested at the end of the day period after 38, 42, 46, 50 and 54 days after sowing. For each time point, three replicates consisting of three plants each were prepared for all three lines. RNA was isolated as described above and precipitated for shipping to the group of Prof. Dr. Mark Stitt, Metabolic Networks, Max Planck Institute for Molecular Plant Physiology, Golm, Germany. There, the RNA was resolved in H_2O and adjusted to a concentration of 1 µg/µl. DNA digestion and cDNA synthesis were performed as described in Wahl et al., 2013 (Supplementary Material). qRT-PCR was performed on three biological replicates with four technical replicates each. Reference genes, reaction mix and qRT-PCR program were as listed in Wahl et al., 2013 (Supplementary Material). All steps were performed under the guidance of Dr. Armin Schlereth from the group of Prof. Dr. Mark Stitt at the Max Planck Institute for Molecular Plant Physiology, Golm, Germany.

2.2.4 Biochemical methods

Determination of protein concentrations

Protein concentrations were determined using the Bradford (Bradford, 1976) (Bio-Rad Protein Assay, Bio-Rad, Munich, Germany) or the bichinoninic acid (BCA) (Pierce BCA Protein Assay Kit, Thermo Scientific, Waltham, MA, USA).

Total protein extraction from *Arabidopsis thaliana*

Plant material was ground in liquid nitrogen and subsequently mixed with one sample volume of extraction buffer (50 mM Tris/HCl (pH 8), 50 mM EDTA, 2 % lithium dodecyl sulphate (LDS), 0.1 % phenylmethylsulfonyl fluoride (PMSF)). The samples were incubated on ice for 30 min and centrifuged (16 000 x g, 15 min, 4 °C) to dispose of insoluble components. An aliquot was taken from the protein containing supernatant for determination of the protein concentration using the BCA method. The generated protein solution was immediately supplemented with 0.15 % DTT and 50 mM EDTA and kept at -20 °C.

Total membrane protein extraction from *Arabidopsis thaliana*

Plant material was ground in liquid nitrogen and subsequently mixed with 400 - 600 µl of urea buffer (50 mM Tris/HCl (pH 8), 0.2 mM EDTA, 6 M urea). The samples were vortexed and rotated at room temperature for 10 min. After centrifugation (16 000 x g, 10 min, RT), the pelleted fractions were resuspended in 200 µl SDS buffer (50 mM Tris/HCl (pH 8), 0.2 mM EDTA, 1 % SDS) and rotated at room temperature for 10 min. After centrifugation (16 000 x g, 10 min, RT), the membrane protein containing supernatant was transferred to a new reaction tube and an aliquot was taken for determination of the protein concentration using the BCA method. Samples were then kept at -20 °C.

Preparation of outer and inner envelope vesicles from *Pisum sativum*

To isolate outer and inner envelope vesicles, pea seedlings grown for 9 – 12 days on sand under a 12/12 hrs light/dark regime were treated according to Waegemann et al., (1982).

SDS polyacrylamide gel electrophoresis (SDS-PAGE)

The separation of proteins under denaturing conditions according to their size was performed as described in Laemmli (1970). Acrylamide concentrations were varied according to the desired resolution from 10 to 15 % in the separating gel (acrylamide to N,N'-methylenebisacrylamide ratio: 30 : 0.8). Stacking gels and separating gels were

prepared with 0.5 M Tris/HCl, pH 6.8 and 0.5 M Tris/HCl, pH 8.8, respectively. Protein samples were supplemented with Laemmli buffer (250 mM Tris/HCl, pH 6.8, 40 % glycerine, 9 % SDS, 20 % β-mercaptoethanol, 0.1 % bromphenol blue) before being loaded on the gel. Proteins were focused in the stacking gel at 100 V and then separated at 150 – 175 V.

Staining of acrylamide gels

Coomassie Brilliant Blue staining: to visualize the separated protein samples, acrylamide gels were incubated in Coomassie staining solution (0.18 % Coomassie Brilliant Blue R250, 50 % methanol, 7 % acetic acid) for 15 - 30 min at RT under shaking. The background was destained (40 % methanol, 7 % acetic acid, 3 % glycerine) under shaking until protein bands were clearly visible. Destained gels were rinsed in ddH_2O and dried under vacuum.

Reversible imidazole/zinc staining: to transitionally visualize separated protein samples, acrylamide gels were rinsed with ddH_2O and incubated under shaking in 0.2 M imidazole for 10 min. Gels were transferred to 0.3 M $ZnCl_2$ and shaken against a dark background to follow the development of the transparent protein bands on a milky white background. After sufficient development, gels were rinsed with ddH_2O several times. At this point, requested protein bands were excised from the gels. For destaining, gels or excised bands were incubated in 2 % citric acid until the milky white background became completely clear. Gels or excised bands were then able to be used for downstream applications.

Electrotransfer of separated proteins

To make protein samples available for detection with specific antibodies, the separated proteins were transferred onto a PVDF membrane (Zefa Transfermembran Immobilon-P, 0.45 µm, Zefa-Laborservice GmbH, Harthausen, Germany) using a semi-dry blotting equipment as described in Kyhse-Andersen (1984). Three blot absorbent filter papers soaked in anode buffer I (300 mM Tris, 20 % methanol, pH 10.4) followed by two papers soaked in anode buffer II (25 mM Tris, 20 % methanol, pH 10.4) were placed onto the anode plate. The PVDF membrane was activated in methanol, soaked in anode buffer II and placed on top followed by the acrylamide gel and another three papers soaked in cathode buffer (25 mM Tris, 40 mM aminocapron acid, 20 % methanol, pH 7). The equipment was closed with the cathode plate and the transfer was carried out for 1.5 hrs at 0.8 mA per cm^2 membrane surface. After the transfer, lanes containing protein standard markers were cut from the membrane and visualized by amido black staining (0.1 % amido black in ddH_2O).

Immunodetection of proteins

To prevent the binding of the antisera to its non-protein bound part, the PVDF membrane was blocked three times with skimmed milk buffer (SMB, 1 -3 % skimmed milk powder, 100 mM Tris/HCl, pH 7.5, 150 mM NaCl). The identification of proteins was carried out with specific, polyclonal antibodies which were visualized by secondary antibodies coupled to alkaline phosphatase (goat anti-rabbit IgG (whole molecule)-AP conjugated (Sigma-Aldrich, St. Louis, MO USA). After blocking, the membrane was incubated with a dilution of the primary antibody for two hrs at RT or over night at 4 °C (1:250 – 1:2000 in TTBS (100 mM Tris-HCl (pH 7.5), 0.2 % Tween 20, 0.1 % BSA, 150 mM NaCl)). After three washings with SMB to remove unbound primary antibodies, the membrane was incubated with a dilution of the secondary antibody (1 : 8000 in TTBS) for one hour at RT. After three washings with SMB to remove unbound secondary antibodies, the membrane was rinsed twice with ddH_2O to remove residual SMB. The staining for alkaline phosphatase reaction was started by the addition of 0.3 mg/ml nitroblue tetrazolium (NBT) and 0.16 mg/ml 5-bromo-4-chloro-3-indolyl phosphate (BCIP) in 100 mM Tris/HCl, pH 9.5, 100 mM NaCl, 5 mM $MgCl_2$. After sufficient development, the reaction was stopped with 50 mM EDTA.

Generation of antisera

Antiserum against full length At-OEP40: for the generation of an antiserum against the full length OEP40 protein from *Arabidopsis*, the complete coding sequence was subcloned into the pET21d plasmid vector. For heterologous overexpression, the construct was transformed into chemically competent *E. coli* BL21 cells and grown in LB medium at 37 °C in the presence of 100 µg/ml ampicillin to an OD_{600} of 0.4 – 0.6. Overexpression was induced by the addition of 1 mM isopropyl β-D-1-thiogalactopyranoside (IPTG) and cells were grown at 37 °C for three hrs at 180 rpm (Figure 2, A). Cells were harvested at 6000 x g for 10 min at 4 °C and the pellet fraction was resuspended in resuspension buffer (50 mM Tris/HCl, pH 8, 200 mM NaCl, 5 mM β-mercaptoethanol). Cells were broken in a microfluidizer processor (Microfludics, Westwood, MA, USA) twice and subsequently genomic DNA was degradated using ultrasonification. Samples were centrifuged at 20 000 x g for 30 min at 4 °C and the resulting inclusion body pellet was resuspended in detergent buffer (20 mM Tris/HCl, pH 7.5, 200 mM NaCl, 1 % deoxycholic acid, 1 % Nonindet P-40, 5 mM β-mercaptoethanol). Samples were centrifuged at 12 000 x g for 10 min at 4 °C and the pellet fraction was resuspended in

triton buffer (20 mM Tris/HCl, pH 7.5, 0.5 % Triton X-100, 5 mM β-mercaptoethanol). After centrifugation at 12 000 x g for 10 min at 4 °C, washing with triton buffer was repeated. The pelleted fraction was then resuspended in tris buffer (200 mM Tris/HCl, pH 8, 10 mM DTT) and centrifuged at 12 000 x g for 10 min at 4 °C. After a second washing step with tris buffer, the pelleted fraction was resuspended in SDS buffer (50 mM Tris/HCl, pH 8, 100 mM NaCl, 1 % SDS) and rotated at RT for 1 h to solubilize the desired protein from the inclusion bodies. After centrifugation at 20 000 x g for 15 min at RT samples from pelleted fraction and supernatant were analyzed via SDS PAGE and coomassie staining and the desired protein could be found soluble in the supernatant fraction (Figure 2, B). Due to the lack of an affinity tag, the protein was further purified by electroelution from an acrylamide gel slice. 7 mg of total solubilized protein were separated via a preparative 12.5 % SDS PAGE (3 mm) and after coomassie staining of two peripheral gelstrips for comparison, the respective band region was cut from the gel. Small pieces of the excised gel piece were placed into a dialysis tubing (14 kDa) equilibrated in water and filled with SDS buffer. The recombinant protein was electroeluted at 16 mA over night in SDS buffer. The eluted protein sample (Figure 2, C) was sent for antibody production in rabbits (Pineda Antikörperservice, Berlin, Germany). When tested on a via SDS PAGE separated preparation of chloroplast envelopes of *Arabidopsis* (Figure 2, D), a distinct band corresponding to At-OEP40 at the expected size of around 45 kDa could be detected by immunoblotting with the antiserum from the 240 days bleeding in a 1:500 dilution whereas no distinct band was detectable in total protein extract (TPE) from 14-day-old wild-type seedlings (data not shown), which might be due to the protein's low abundance. When tested on total membrane protein extract (TMPE) from three-week-old plants (Figure 2, E), a distinct band corresponding to At-OEP40 at the expected size of around 45 kDa could be detected by immunoblotting with the antiserum from the 240 days bleeding in a 1:500 dilution (Figure 2, E), which is probably due to the fact, that TMPE has a much higher protein concentration than TPE containing detectable amounts of otherwise low abundant proteins.

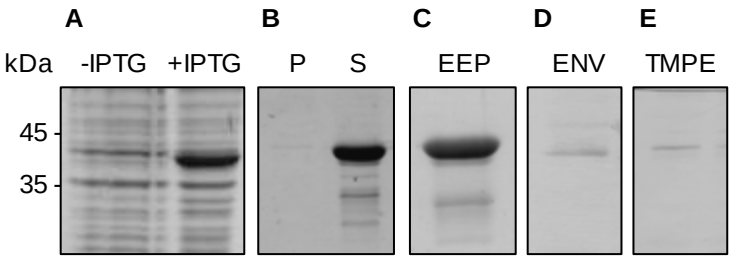

Figure 2: Purification of At-OEP40 for antibody production and α-At-OEP40 antibody test

A) Overexpression of At-OEP40 from pET21d in *E.coli* BL21, cell suspension seperated via SDS PAGE and coomassie stained before and after induction of the overexpression with 1 mM IPTG B) Solubilized At-OEP40 from cleaned inclusion bodies, insoluble protein containing pellet fraction (P) and soluble protein containing supernatant fraction (S) after treatment with 1 % SDS (0,5 µl of 5 ml samples), separated via SDS PAGE and coomassie stained. C) At-OEP40 after electroelution from an acrylamide gel, 2,5 µg of electroeluted protein (EEP), separated via SDS PAGE and coomassie stained. D) Envelope preparation from *Arabidopsis* Col-0 wild-type (ENV, 10 µg/lane) E) Total membrane protein extract from *Arabidopsis* Col-0 wild-type (TMPE, 10 µg/lane) D+E) Samples were separated via SDS PAGE and analyzed by immunoblotting with the produced antibody (α-At-OEP40, 240 d bleeding, animal 1, 1:500 in TTBS). Numbers indicate the molecular masses in kDa.

Antiserum against a peptide fragment of Ps-IEP57

In addition to the already existing antibody directed against an overexpressed part from the C-terminus of Ps-IEP57, a second antibody against the N-terminal part was ordered (Pineda Antikörperservice, Berlin, Germany.) to further characterize IEP57 biochemically and to elucidate the orientation of the N- and C-termini in the inner chloroplast envelope.

Hydrophobicity analysis

Four aliquots of outer envelope preparations from pea were ultracentrifuged at 256 000 x g for 10 min at 4 °C and the pelleted vesicles were resuspended 1 M NaCl in 10 mM Tris/HCl, pH 8, 0.1 M $NaCO_3$ in ddH_2O, pH 11.3, 4 M urea in 10 mM Tris/HCl, pH 8 and 1 % Triton X-100 in 10 mM Tris, pH 8, respectively. After incubation on ice (urea sample at RT) for 1 h with mixing every ten min, the samples were ultracentrifuged at 100 000 x g for 10 min at 4 °C. The pelleted fraction was resuspended in 10 mM Tris/HCl, pH 8 and both fractions were equally divided before separation via SDS PAGE. The samples were analyzed by immunoblotting using antisera against the desired protein as well as a control protein (Okamoto et al., 2001).

Proteolysis of inner envelope vesicles

For proteolysis treatment, inner envelope vesicles were precipitated at 100 000 x g for 15 min at 4 °C and resuspended in buffer pwII (330 mM sorbitol, 50 mM HEPES, pH 7.6, 0.5 mM $CaCl_2$). After determination of the total protein content, 2 µg of thermolysin in pwII; 1 µg trypsin in pwII; 0.1 µg of GluC in 10 mM NaPi buffer, pH 7; 1 µg ProC was added per 1 µg of protein and proteolysis was allowed to proceed for 0, 15, 30 and 45 min on ice in the dark. Inner envelope vesicles treated with 1 % Triton X-100 prior to protease treatment were used as a control. Reactions were stopped with 5 mM EDTA per protease; 1 µg/µg protease macroglobulin, 5 µg/µg protease trypsin inhibitor, 1 mM PMSF per 1 µg protease; 5 µg/1 µg protease macroglobulin; 10 mM PMSF per 1 µg protease, respectively. The samples were equally parted and separated via SDS PAGE. The resulting digestion patterns were analyzed using specific antibodies directed against Ps-IEP57 (N-terminus) and a control protein.

Overexpression and purification of Ps-OEP40 for electrophysiological measurements

The full length coding sequence of Ps-OEP40 without the stopcodon was subcloned into the pET21d plasmid vector. The methionine at position 19 was exchanged for an isoleucine using site-directed mutagenesis to obtain a single protein band. For heterologous overexpression, the construct was transformed into chemically competent *E. coli* BL21 cells and grown in LB medium at 37 °C in the presence of 100 µg/ml ampicillin to an OD_{600} of 0.4 – 0.6. Overexpression was induced by the addition of 1 mM isopropyl β-D-1-thiogalactopyranoside (IPTG) and cells were grown at 37 °C for three hrs at 180 rpm. Cells were harvested at 6000 x g for 10 min at 4 °C and the pellet fraction was resuspended in resuspension buffer (50 mM Tris/HCl, pH 8, 200 mM NaCl, 5 mM β-mercaptoethanol). Cells were broken in a microfluidizer processor (Microfludics, Westwood, MA, USA) twice and subsequently genomic DNA was degradated using ultrasonification. Samples were centrifuged at 20 000 x g for 30 min at 4 °C and the resulting inclusion body pellet was treated as described in (generation of antisera). After the second washing with triton buffer the pelleted fraction was resuspended in 15 ml urea buffer (50 mM Tris/HCl, pH 8, 100 mM NaCl, 6 M urea) and rotated for 1 hr at RT to solubilize the desired protein from the inclusion bodies. After centrifugation at 20 000 x g for 15 min at RT, samples from pelleted fraction and supernatant were analyzed via SDS PAGE and coomassie staining and the desired protein could be found

soluble in the supernatant fraction. The supernatant was supplemented with 5 mM imidazole and incubated with 250 µl of Ni-NTA-sepharose (GE Healthcare, Chalfont St. Giles, Great Britain) under rotation over night at RT. After centrifugation at 1 000 x g for 2 min at RT, all but 5 ml of the supernatant was removed and the pelleted Ni-NTA beads were resuspended and applied onto a 2.5 ml column (MoBiTec GmBH, Goettingen, Germany). The desired protein was eluted with 50 - 500 mM imidazole in urea buffer. The eluted fractions were analyzed via SDS PAGE and the fractions with 100, 200 and 500 mM imidazole were sent to the group of Prof. Dr. R. Wagner, Biophysics, University of Osnabrück for reconstitution and lipid bilayer measurements.

***In vitro translation* of Ps-OEP40 using reticulate lysate**

For the translation of Ps-OEP40 in a cell-free, eukaryotic system, the TNT® Coupled Reticulate Lysate System (Promega, Madison, WI, USA) was used according to manufacturers' instructions. Ps-OEP40 was transcribed from the full length coding sequence in the pET21d plasmid vector using T7 polymerase and translated with equal amounts of non-radiolabelled amino acid mixes lacking cysteine and methionine, respectively in the coupled system for 120 min at 30 °C. A second reaction not containing plasmid DNA was used in parallel as a control. Samples from both reactions were separated by SDS PAGE and immunoblotted to confirm the presence of the desired protein using a specific antibody directed against Ps-OEP40. Both reactions were subsequently centrifuged at 80 000 rpm for 15 min at 4 °C and the pelleted fractions were resuspended in 50 mM Tris/HCl pH 8, 100 mM NaCl. Samples from supernatants and pellet fractions were analyzed by immunoblotting and the desired protein could be found in the supernatant of the reaction containing plasmid DNA. Therefore, the supernatants from both reactions were sent to the group of Prof. Dr. R. Wagner, Biophysics, University of Osnabrück for reconstitution and lipid bilayer measurements.

***In vitro translation* of Ps-OEP40 using wheat germ lysate and subsequent purification**

In order to translate the Ps-OEP40 protein *in vitro* using wheat germ lysate, the full coding sequence of Ps-nEOP40 without the stop codon was transcribed from the pET21d plasmid vector. First, 5 µg of plasmid DNA were linearized using the restriction enzyme PstI and the reaction was cleaned using the Nucleospin Extract II Kit (Macherey and Nagel, Düren, Germany). 1 µg of the linearized, cleaned plasmid DNA was used for *in vitro* transcription in a

50 µl reaction volume with 20 % transcription buffer (5 x transcription buffer, Thermo Scientific, Waltham, MA, USA), 0.05 % BSA, 2 mM DTT, 0.25 mM CAP, 0.4 mM ACU, 1.25 µl RNAse inhibitor (RiboLock RNase Inhibitor, 40 U/µl, Thermo Scientific, Waltham, MA, USA) and 1.5 µl T7 polymerase (T7 RNA polymerase, 20 U/µl, Thermo Scientific, Waltham, MA, USA). The reaction was filled to 47 µl with H_2O and incubated at 37 °C for 15 min before adding 3 µl GTP. The complete reaction was then incubated at 37 °C for 2 hrs. Before translation, the obtained RNA was incubated at 65 °C for 3 min. 5 µl of the RNA were used in a 100 µl reaction volume with 50 % wheat germ lysate (from AG Schwenkert, Plant Biochemistry and Physiology, Department Biology I, Botany, Ludwig-Maximilians University, Munich), 6 µl amino acid mix lacking methionine, 6 µl amino acid mix lacking cysteine, 1 x buffer A+ (10 x: 140 mM HEPES, pH 7.6, 12.5 mM MgAc, 20 mM DTT, 480 mM KAc), 1 x buffer B (10 x: 12.5 mM ATP, 2.5 mM GTP, 4 mM spermidine, 0,25 mM HEPES, pH 7.6, 160 mM creatine phosphate, 4,5 mg/ml creatine phosphate kinase), H_2O ad 100 µl. The reaction was incubated at 25 °C for 2 hrs. To use wheat germ translated Ps-OEP40 for reconstitution and lipid bilayer measurements, 8 translation reactions were carried out as described above, two reactions each were pooled and supplemented with 500 µl lysis buffer (30 mM Tris/HCl, pH 7.9, 300 mM NaCl, 0.5 % SDS, 5 mM imidazole). The mix was incubated at 55 °C for 3 min while a mobicol minispin column (MoBiTec GmBH, Goettingen, Germany) was washed and filled with 200 µl Ni-NTA sepharose. The filled column was washed three times with H_2O (1000 x g, 30 sec, RT) and three times with lysis buffer. The heated mix was then added to the column and rotated for 1 h at RT. The flow-through was removed by centrifugation at 1000 x g for 30 sec at RT and the column subsequently washed six times with wash buffer (30 mM Tris/HCl, pH 7.9, 300 mM NaCl, 0.5 % SDS, 10 mM imidazole). To elute the desired protein, 100 µl elution buffer (30 mM Tris/HCl, pH 7.9, 300 mM NaCl, 0.5 % SDS, 300 mM imidazole) were added to the column which was rotated for 5 min at RT and centrifuged at 1000 x g for 30 sec at RT. The elution step was repeated three times and the obtained fractions were pooled and concentrated to 100 µl using an Amicon® Ultra 0.5 ml filter unit (Merck KGaA (Darmstadt, Germany). The concentrated fraction was supplemented with 40 µl 4 x Laemmli buffer and separated via a 12.5 % SDS gel. The gel was reversibly stained using the zinc imidazole method and the band corresponding to Ps-OEP40 was excised from the gel. A second band was cut for controlling purposes. After

destaining, the excised bands were supplemented with water and sent to the group of Prof. Dr. R. Wagner, Biophysics, University of Osnabrück for reconstitution and lipid bilayer measurements. Parts of each band were placed in a well of a 12.5 % SDS gel and the contained proteins were separated. The presence of Ps-OEP40 was confirmed by immunoblotting using a specific antibody directed against Ps-OEP40.

Planar lipid bilayer measurements of Ps-OEP40

Further treatment of purified recombinant or *in vitro* translated Ps-OEP40 protein samples, reconstitution and electrophysiological measurements in a planar lipid bilayer to analyze the putative channel function of Ps-OEP40 were carried out at the group of Prof. Dr. R. Wagner (Biophysics, University of Osnabrück, Germany).

2.2.5 Metabolite analysis

Amino acids, organic acids, sugars

Complete plants were harvested without roots and immediately frozen in liquid nitrogen. The collected plant material was ground in liquid nitrogen and aliquots of 50 mg were prepared in the frozen state. The powder was extracted with 1.5 ml of a H_2O:methanol:chloroform mix (1:2,5:1). 50 mM Ribitol was added to the solvent mix as an internal standard. The samples were thoroughly mixed for 20 sec and then mixed by rotating for 6 min at 4 °C. After centrifugation at 20 000 x g for 2 min at RT, the supernatant was sent to the AG Weber, Plant Biochemistry, Heinrich-Heine University, Düsseldorf, Germany for analysis. Gas chromatography and subsequent mass spectroscopy were used to analyze the content of amino acids, organic acids and sugars according to the method described by Lee and Fiehn, 2008. The GC/MS TOF-analysis (GCT Premier by Waters) allowed the detection of amino acids (alanine, aspartate, cysteine, methionine, ornithine, asparagine, β-alanine, glycine, isoleucine, leucine, lysine, phenylalanine, proline, serine, threonine, tryptophane, valine, tyrosine), organic acids (malic acid, succinic acid, fumaric acid, glyceric acid, gluconic acid, γ-hydroxybutyric acid, quinic acid, citric acid, glycolic acid, malonic acid, glutamic acid, α-ketoglutaric acid, γ-aminobutyric acid, lactic acid, oxalic acid, shikimic acid, D-α-hydroxyglutaric acid) and sugars (glucose, fructose, sucrose, maltose, lactose, xylose, sorbitol, mannitol, raffinose, mannose, myoinositol).

2.2.6 Computational methods

Table 8: Software, databases and algorithms used in this study

Name	Reference	URL
ARAMEMNON 8.0	Schwacke et al., 2003	http://aramemnon.uni-koeln.de/
GeneDoc	Nicholas et al., 1997	http://www.nrbsc.org/gfx/genedoc/
VectorNTI	Invitrogen	http://www.lifetechnologies.com/de/de/home/life-science/cloning/vector-nti-software.html
MEGA6	Tamura et al., 2013	http://www.megasoftware.net/
TAIR (The Arabidopsis Information Resource)	Lamesch et al., 2011	http://www.arabidopsis.org/
ExPASy peptide cutter tool	Gasteiger et al., 2003	http://web.expasy.org/peptide_cutter/
BLAST (Basic local alignment search tool)	Altschul et al., 1997	http://www.ncbi.nlm.gov/BLAST

3 Results

3.1 PRAT2 in the inner chloroplast envelope

The two PRAT2 proteins, PRAT2.1 and PRAT2.2 show 82 % amino acid sequence similarity. *In vitro* import experiments, *in vivo* GFP targeting as well as immunoblotting experiments suggest a dual targeting for both isoforms to the inner membranes of chloroplast and mitochondria (Murcha et al., 2007, Pudelski et al., 2010). The sterile alpha motif (SAM) domain in the proteins' C-termini consists of about 70 amino acids and is an evolutionary highly conserved protein-binding domain present in various eukaryotic organisms (Schultz et al., 1997). SAM domains are known to mediate protein-protein or protein-nucleotide interactions (Kim and Bowie, 2003). Proteolysis experiments showed that the plastid PRAT proteins are orientated in the inner envelope with their N-termini and the SAM-domain containing C-termini facing the intermembrane space (Doctoral thesis S. Kraus, 2010). Dimers, tetramers and high molecular oligomers were demonstrated to form via the SAM domain by native gel electrophoresis, interaction studies in yeast and interaction chromatography (Doctoral thesis, Sabrina Kraus, 2010). The loss of one of the PRAT2 isoforms in *Arabidopsis* was analyzed using two independent T-DNA insertion lines for each isoform. None of the single mutant lines showed an obvious phenotype under standard growth conditions, which suggests that the presence of only one of the PRAT isoforms is sufficient to sustain normal plant development. However, the phenotypical analysis of two independent double mutant lines revealed a drastic chlorotic phenotype with lancet shaped leaves and stunted growth. Ultrastructural analysis showed the *prat2* double mutants to have an altered leave structure and fewer chloroplasts with reduced thylakoid membranes (Doctoral thesis S. Kraus, 2010). In summary, these results point to an important function of the PRAT2 proteins in plant growth and development. When grown under continuous light, a partial rescue of the phenotype could be observed independent of the light intensity. It was therefore assumed, that toxic metabolites accumulate if the plants pass through an 8-hour dark phase. Indeed, accumulation of reactive oxygen species (ROS), which is a response to various biotic and abiotic stresses, could be detected in *prat2-dm* mutants grown under longday (16 hrs light/8 hrs dark) but not under continuous light conditions. Interestingly, the reversed phenotypic effect was observed knockout plants for the *CS26*

gene encoding a plastid protein with S-sulfocysteine activity (Bermúdez et al., 2010) indicating a possible PRAT2 function in the homeostasis of sulphur-containing metabolites. The chlorotic phenotype of *prat2-dm* mutant plants points to alterations in the tetrapyrrole biosynthesis pathway. All measured pigments and tetrapyrrole intermediates were shown to be downregulated with the exception of magnesium protoporphyrine IX (Mg PPIX), which accumulates in *prat2* double mutant plants. Since Mg PPIX is converted to magnesium protoporphyrine IX monomethylesther (Mg PPIX MoMe) in an S-adenosylmethionine (SAM) dependent step, an additional connection to sulphur-containing metabolites could be possible. Transcriptome analysis revealed a downregulation of the enzyme NADPH:protochlorophyllide oxidoreductase (POR), which catalyzes the light-dependent reduction of protochlorophyllide, a phototoxic compound when accumulating, in the tetrapyrrole synthesis pathway (Doctoral thesis S. Kraus, 2010).

Aim of this part of the study was the assignment of a functional role to the plastid PRAT2 proteins. Based on the observations described above, a possible accumulation of a toxic compound in the dark was assumed. Therefore, metabolic analyses in *prat2*-dm mutant plants in the light and in the dark were conducted and the function and assembly of functional POR complexes necessary for protochlorophyllide conversion was analyzed. Further, a role of the plastid PRAT2 proteins in the transport of sulphur-containing metabolites was investigated.

3.1.1 Analysis of double mutants for *PRAT2.1* and *PRAT2.2* in *Arabidopsis thaliana*

Two independent T-DNA insertion lines for each, *PRAT2.*1 and *PRAT2.*2 did not show any phenotypic differences compared to wild-type plants when grown under standard longday conditions. This indicates that the presence of only one PRAT2 isoform is sufficient to sustain normal plant growth. To further analyze the physiological role of the PRAT2 proteins in *Arabidopsis*, double mutant lines lacking both PRAT2 isoforms where generated. At the beginning of this study, three independent double mutants generated by three independent crossings of two independent homozygous T-DNA insertion lines for each, *PRAT2.1* and *PRAT2.2*, were available and named *prat2-dm #1*, *#2* and *#3* (Figure 3, A, for an overview see doctoral thesis S. Kraus, 2010). The resulting lines were analyzed by RT-PCR to test whether they represent true knockout lines for *PRAT2.1* and *PRAT2.2*.

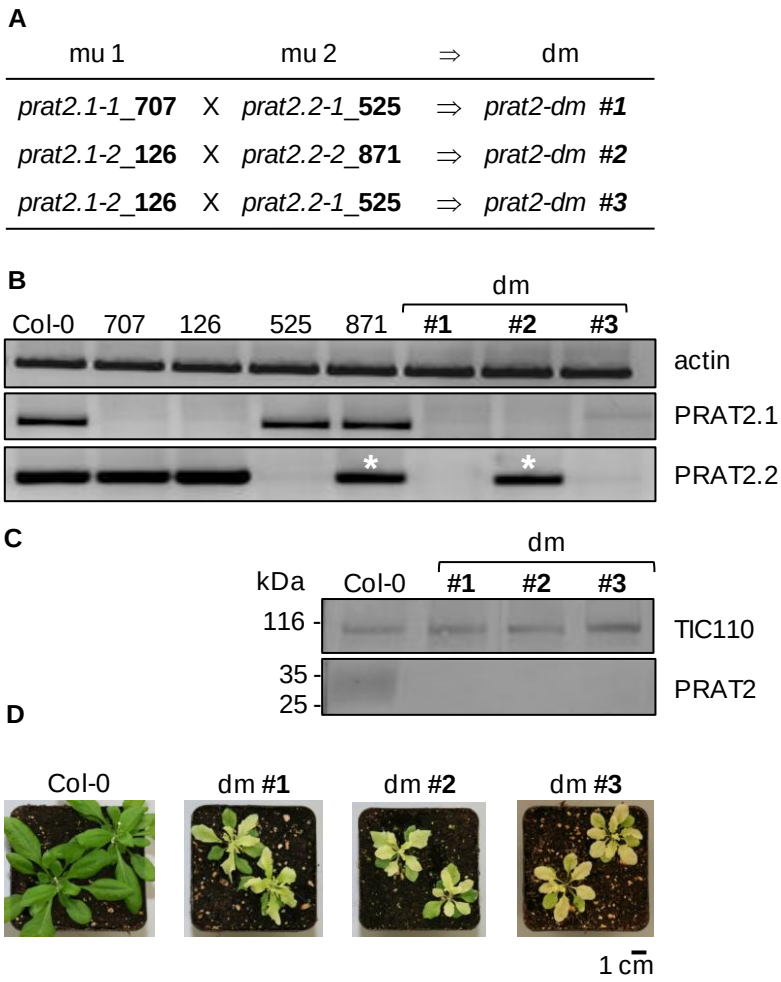

Figure 3: Mutation of the *PRAT2* genes in *Arabidopsis*

A) Generation of three independent *prat2* double mutant (dm) lines by crossing of different combinations of homozygous *prat2.1* (mu 1) and *prat2.2* (mu2) single mutant lines. For clarity, the last three digits of the SALK identifiers of the single mutants are indicated. In the following, the respective double mutant lines are designated as *prat2-dm #1, #2, #3*. B) PCR products of actin (435 bp), *PRAT2.1* (421 bp) and *PRAT2.2* (338 bp) after RT-PCR with the respective gene-specific primers on cDNA prepared from 14-day-old seedlings of Col-0 wild-type as well as the respective single and double mutant lines. Constitutively expressed actin was analyzed as a control. mRNA amplified on the single mutant *prat2.2-2* (871) and on the double mutant *dm #2* (*prat2.1-2* (126) X *prat2.2-2* (871)) is indicated by asterisks. C) Immunoblot of total protein extract (TPE) from Col-0 wild-type as well as *prat2-dm #1, #2* and *#3* homozygous mutant plants. 10 µg of TPE prepared from leaf material of 33-day-old plants was equally loaded and analyzed with a specific antibody directed against At-PRAT2. Antiserum against the inner envelope protein TIC110 was used as loading control. Numbers indicate the molecular mass of proteins in kDa. D) Representative individuals of 33-day-old Col-0 wild-type as well as *prat2-dm #1, #2* and *#3* homozygous mutant plants grown under longday conditions.

RT-PCR showed no *PRAT2.1* and *PRAT2.2* transcripts in the respective single and double mutant alleles except for a residual band in lines *prat2.2-2_871* and *prat2-dm #2*, which was generated by crossing of *prat2.1-2_126* and *prat2.2-2_871* (Figure 3, B). These lines contain the T-DNA insertion in the 5'-UTR of the *PRAT2.2* gene (Doctoral thesis S. Kraus, 2010) and therefore residual transcripts could be amplified by the gene specific primers binding the gene's C-terminal region. When total protein extracts from lines *prat2-dm #1*, *#2* and *#3* were analyzed by immunoblotting using a specific antibody directed against PRAT2 (Figure 3, C), no signals corresponding to PRAT2 could be detected in all three double mutant lines. Thus, the residual transcripts in line *prat2-dm #2* could not be translated into functional protein. The phenotypic appearance of all three double mutant lines was identical and characterized by a chlorotic phenotype, stunted growth and lancet shaped leaves (Figure 3, D). Therefore, all three *prat2* double mutant lines represent knockout lines for both PRAT2 isoforms. For all further analyses, lines *prat2-dm #1* and *prat2-dm #3* were chosen.

3.1.2 Phenotypic analysis of *prat2* double mutant plants

When grown under longday conditions (16 hrs light/8 hrs dark, LDC), *prat2* double mutant lines showed the chlorotic phenotype with stunted growth and lancet shaped leaves (Figure 3, D, Figure 4). The obvious reduction in chlorophyll content was visible already ten days after germination, whereas the delayed growth became visible when the plants reached the rosette stadium (Doctoral thesis S. Kraus, 2010). Ultrastructural analysis revealed fewer and smaller chloroplasts with reduced thylakoid membranes. When *prat2* double mutant plants were grown under continuous light conditions (CLC), the chlorotic phenotype could be partially complemented and the defects in plant growth could partly be reduced (Figure 4). Also, the stress symptoms of *prat2-dm* leaves such as accumulation of reactive oxygen species (e.g. H_2O_2, doctoral thesis S. Kraus, 2010) were reduced in continuous light. This indicates that the dark phase causes severe changes within the plant, possibly the accumulation of toxic substances, hindering normal plant development. This was supported by the occurrence of the chlorotic phenotype and growth defects in plants grown in ultra longday (ULDC, 2 hrs dark), longday (LDC, 8 hrs dark), and shortday (SDC, 16 hrs dark) conditions independently the length of the dark phase. When grown under continuous low light conditions (CLLC), no phenotypic differences between *prat2* double mutants and wild-type plants were detectable any more (Figure 4).

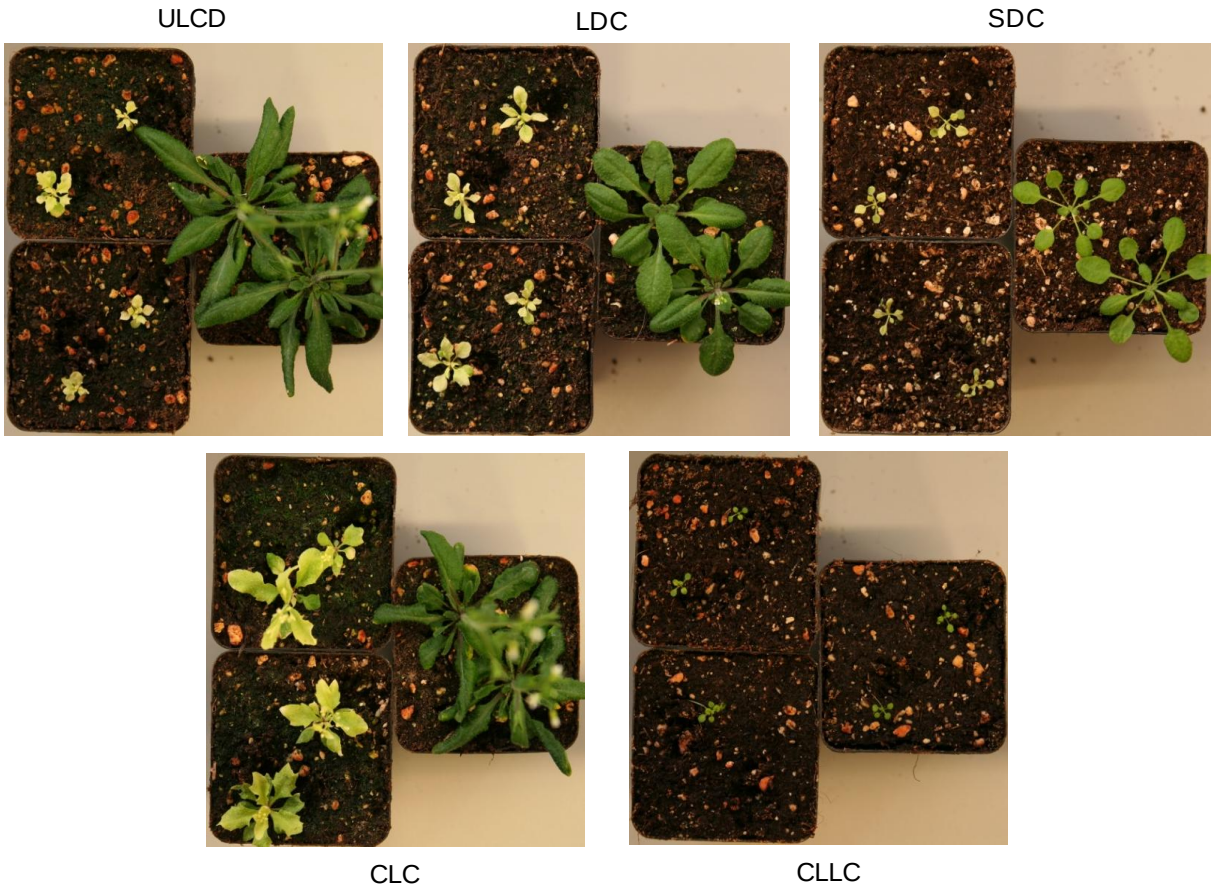

Figure 4: Phenotype of *prat2-dm* mutant plants under different light conditions
Representative individuals of 33-day-old plants of Col-0 wild-type as well as *prat2-dm#1* and *prat2-dm#3* homozygous plants grown under ultra longday (ULDC), longday (LDC), shortday (SDC), continuous light (CLC) and continuous low light (CLLC) conditions. All plants were germinated on ½ MS + 1 % sucrose plates and transferred to soil 14 days later.

3.1.3 POR expression in *prat2* double mutant plants

When differential gene expression was analyzed in wild-type plants compared to *prat2-dm* mutant plants grown under longday and continuous light conditions by DNA microarray analysis (for detailed results see doctoral thesis S. Kraus, 2010) it was found that all three isoforms of the gene coding for the enzyme NADPH:protochlorophyllide oxidoreductase (POR) were downregulated in *prat2-dm* mutant plants. In comparison to longday conditions, the reduction of *POR* expression under continuous light conditions was not as severe.

The downregulation of all three isoforms of POR revealed by DNA microarray analysis of *prat2-dm* mutant plants was analyzed on transcript and protein level using qRT-PCR and immunoblotting, respectively. To analyze whether the expression of *POR* is

impaired in plants during growth phases in the dark, *POR* expression was monitored during the greening process. For this purpose, the amount of *POR A*, *POR B* and *POR C* mRNA was analyzed in etiolated seedlings of Col-0 wild-type and crossed-out wild-type as well as *prat2-dm#1* and *prat2-dm#3* homozygous mutant plants by qRT-PCR (Figure 5). RNA was prepared from seedlings grown in the dark for 7 days after exposure to standard light conditions for 0, 1, 4 and 8 hrs. RNA was reversely transcribed into cDNA and qRT-PCR was performed with gene specific primers for *Arabidopsis PORA, PORB* and *PORC*. Results were normalized to 1000 actin molecules and the values for Col-0 and crossed-out wild-type as well as for both double mutants were combined. Values for wild-type samples at 0 hrs were set to 100 % (Figure 5).

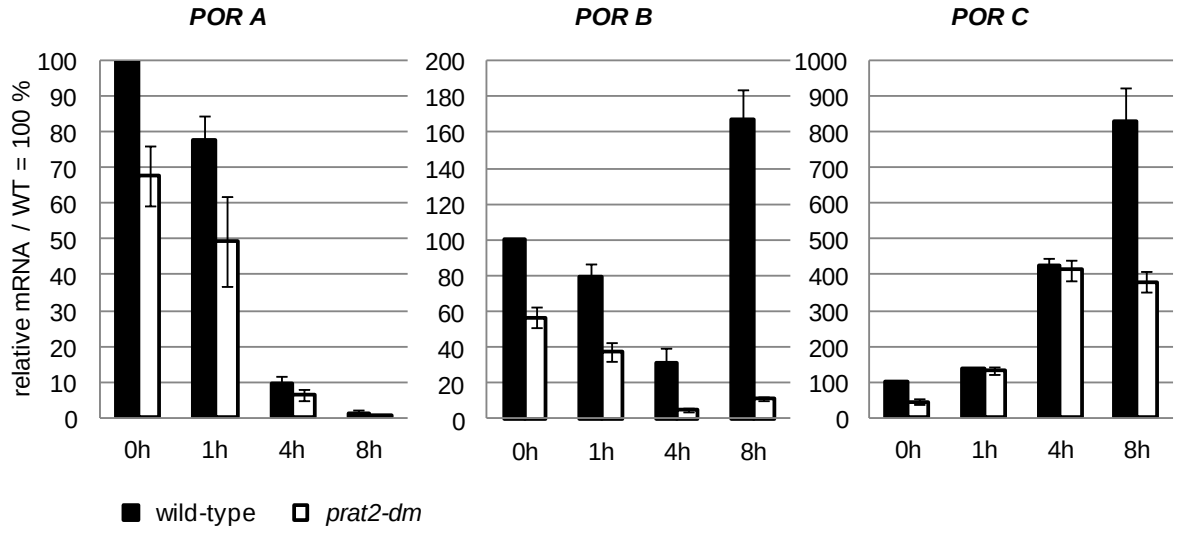

Figure 5: mRNA levels of *POR A*, *POR B* and *POR C* during greening

Quantification of *POR A*, *POR B* and *POR C* mRNA using qRT-PCR. mRNA was prepared from 7-day-old seedlings grown in the dark 0, 1, 4 and 8 hrs after the onset of light from Col-0 wild-type as well as crossed-out wild-type and from *prat2-dm#1* as well as *prat2-dm#3* homozygous mutant plants. Values for Col-0 and crossed out wild-type as well as for *prat2-dm#1* and *prat2-dm#3* were combined (n=2-6±SD) and normalized to 1000 actin transcript molecules. The wild-type at 0 hrs was set to 100 %.

The expression of all three *POR* isoforms in *prat2-dm* mutant in the first 4 hrs showed the same tendencies as in wild-type plants but with lower mRNA amounts. *POR A* expression was high in plants coming directly from the dark and decreased with prolonged exposure to light. *POR C* expression followed the opposite pattern being low in plants coming directly

from the dark and increasing with prolonged light exposure. In mutant plants, however, *POR C* expression did not further increase after 8 hrs. *POR B* expression first decreased after exposure to light and started to increase again after 8 hrs, however, the increase of *POR B* expression *prat2-dm* mutant plants was not as drastic as in wild-type plants. Therefore, all three *POR* isoforms are expressed as expected in the first 4 hrs but in lower amounts than in wild-type plants. After 8 hrs, however, *POR B* and *POR C* expression did only slightly or not at all increase, respectively.

To analyze POR protein levels in Col-0 wild-type and *prat2-dm* mutant plants, total protein extraction was performed on 200 mg leaf material from 33-day-old Col-0 wild-type as well as *prat2-dm#1* and *prat2-dm#3* mutant plants grown under longday and continuous light conditions (Figure 6). Appropriate amounts of protein were separated by SDS PAGE and subjected to immunoblotting with specific antibodies directed against POR, PRAT2 and (magnesium protoporphyrine IX methyltransferase, At4g25080). An antiserum directed against TIC 110 was used as a loading control. Because the POR isoforms cannot be separated via SDS PAGE, the detected band represents total amounts of POR A, B and C (Figure 6).

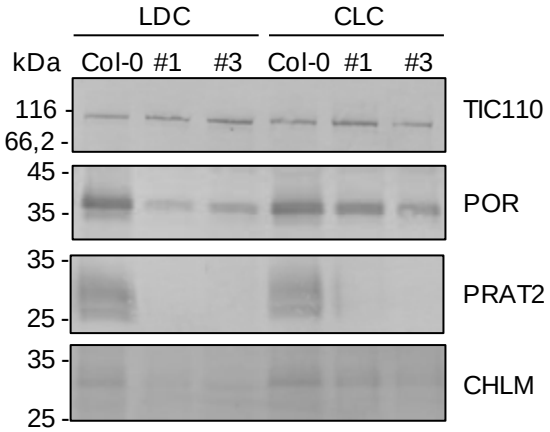

Figure 6: POR is reduced in *prat2-dm* mutant plants on the protein level

Immunoblot of total protein extract (TPE) from Col-0 wild-type (Col-0) as well as *prat2-dm#1* (#1) and *prat2-dm#3* (#3) homozygous mutant plants grown under longday (LDC) and continuous light (CLC) conditions. 10 µg (CHLM: 30 µg) of TPE prepared from leaf material of 33-day-old plants was equally loaded and analyzed with specific antibodies directed against POR, At-PRAT2 and At-CHLM. Antiserum against the inner envelope protein TIC110 was used as a loading control. Numbers indicate the molecular mass in kDa.

As depicted before in Figure 3, no residual band for PRAT2 could be detected in the double knockout mutants *prat2-dm#1* and *prat2-dm#3* (Figure 6). Equally strong bands corresponding to POR could be detected in protein extracts from Col-0 wild-type plants grown under both light conditions. In protein extracts from *prat2-dm#1* and *prat2-dm#3* plants grown under longday conditions, only faint bands corresponding to POR were detectable confirming the drastic reduction of POR observed in DNA microarray analysis results on protein level. In protein extracts from *prat2-dm#1* and *prat2-dm#3* plants grown under continuous light conditions, a reduction of POR could be observed on protein level which was less severe than under longday conditions (Figure 6). The same behavior was observed for CHLM underlining the general downregulation of the tetrapyrrole synthesis pathway in *prat2* knock-out mutants and the better overall shape of the mutants in response to continuous light.

3.1.4 Analysis of POR activity in *prat2-dm* plants

In order to analyze whether the residual amount of POR in *prat2-dm* plants is still assembled into functional, ternary POR complexes and therefore able to catalyze the light-dependent conversion of protochlorophyllide into chlorophyllide, the levels of protochlorophyllide and chlorophyllide were measured in etiolated Col-0 and *prat2-dm #1* seedlings which were either kept in the dark entirely before harvesting or treated with a light flash (1 flash, mecablitz 32 Z-2, Metz, Zirndorf, Germany) to trigger the light-dependent conversion right before harvesting. The plant material was frozen immediately in liquid nitrogen and protochlorophyllide, chlorophyllide as well as magnesium containing precursors were extracted using a phase-separating protocol with acetone, hexane and ethyl acetate and subsequently analyzed via HPLC (Dr. U. Oster, LMU, Munich). Since the seedlings were not supplemented with the chlorophyll precursor aminolevulinic acid before harvesting to enrich the amount of porphyrin-containing compounds, the amount of measurable intermediates was relatively low and did not allow reliable detection. The obtained preliminary results, however, indicate that the initial amount of convertible protochlorophyllide is already lower in *prat2-dm* seedlings and that the resulting rate of conversion of protochlorophyllide to chlorophyllide catalyzed by POR is the same in wild-type and *prat2-dm* seedlings. Therefore, functional, ternary POR complexes seem to be assembled correctly in *prat2-dm* mutant plants but in lower amounts than in wild-type (Dr. U. Oster, LMU, Munich, data not shown).

3.1.5 Analysis of SAM and tocopherol levels in *prat2-dm* mutant plants

In summary, data so far show an overall downregulation of tetrapyrrole biosynthesis on the transcript and protein level, which results in the overall reduction of chlorophyll precursors leading to a reduced content of chlorophyll a and b in *prat2-dm* mutant plants. The only exception was shown to be magnesium protoporphyrine IX (MgPP IX), which accumulates to about 1.5 times of the wild-type level. MgPP IX is formed by the ATP-dependent insertion of magnesium into protoporphyrine IX (PP IX) by the enzyme magnesium chelatase which marks the entry into the chlorophyll branch of tetrapyrrole biosynthesis. Subsequently, MgPP IX is methylated by the enzyme Mg protoporphyrin IX methyltransferase (MgMT) in an S-adenosylmethionine (SAM) dependent step resulting in the formation of magnesium protoporphyrine IX monomethyl ester (MgPP IX MoMe) (for an overview see Tanaka and Tanaka, 2007). The accumulation of MgPP IX could be due to an impaired export of MgPP IX from the chloroplast or, together with the decrease in other tetrapyrrole biosynthesis intermediates, could result from undermethylation due to a defect in the transfer of the methyl group from SAM. SAM, the predominant methyl group donor molecule, is solely produced in the cytosol. It therefore has to be imported into the chloroplast where it serves in various SAM-dependent reactions, e.g. the biosynthesis of tocopherols (Bouvier et al., 2006, Soll et al., 1985).

To analyze whether the overall availability of SAM for SAM-dependent methylation reactions is impaired in *prat2-dm* mutant plants, SAM levels were analyzed in Col-0 wild-type as well as *prat2-dm#1* and *prat2-dm#3* mutant plants grown under longday (38-day-old) and continuous light (32-day-old) conditions (Figure 7). The samples were sent to the group of Prof. R. Hell/ Dr. Markus Wirtz (Centre for Organismal Studies, University of Heidelberg) for further processing and HPLC measurements of SAM and S-methyl-5'-thioadenosin (MTA). MTA is produced when 1-aminocyclopropane-1-carboxylate (ACC) is synthesized from SAM, which is the committed step in ethylene biosynthesis (Bürstenbinder et al., 2007). Under longday conditions, neither for SAM nor for MTA levels, a significant difference between Col-0 and *prat2-dm* plants could be observed (Figure 7). Both, SAM and MTA levels were increased under continuous light conditions in all three lines but also no significant change between wild-type and mutant plants could be detected. If one of the *prat2-dm* lines

showed a more drastic difference compared to Col-0 wild-type (e.g. *prat2-dm#1* in MTA measurements, continuous light, Figure 7), the other *prat2-dm* line did not, which is why all changes in SAM and MTA levels were considered non-significant. Therefore, sufficient amounts of SAM seem to be present in *prat2-dm* mutant plants to serve all SAM-dependent reactions.

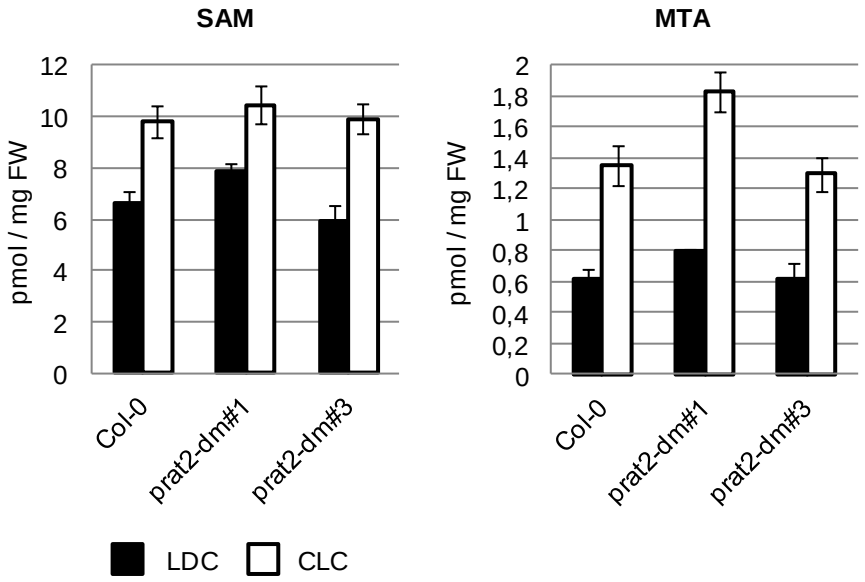

Figure 7: S-adenosylmethionine and methylthioadenosine levels in *prat2-dm* mutant plants
S-adenosylmethionine (SAM) and methythioadenosine (MTA) levels were analyzed in extracts from 200 mg leaf material of Col-0 wild-type as well as *prat2-dm#1* and *prat2-dm#3* homozygous mutant plants grown under longday (solid bars, 38-day-old) and continuous light (empty bars, 32-day-old) conditions. The absolute amounts (n=3-5±SD) are given in pmol / mg fresh weight (FW).

Tocopherol biosynthesis, a plastid intrinsic process also dependent on the transfer of methylgroups from SAM (for an overview see Hussain et al., 2013 and Soll et al., 1985), was chosen to analyze whether the methylation via SAM-dependent methyltransferases is impaired or whether the transport of SAM from the cytosol into the plastid is affected in *prat2-dm* mutant plants. Tocopherol levels were analyzed in 32-day-old Col-0 wild-type as well as *prat2-dm#1* and *prat2-dm#3* mutant plants grown under longday conditions. The samples were analyzed in the group of Prof. Dr. Uwe Sonnewald (Biochemistry, Dept. of Biology, University of Erlangen-Nürnberg, Germany) by HPLC measurements of α-, δ- and γ-tocopherol (Figure 8). For none of the three tocopherol derivatives measured, a significant difference in tocopherol content between Col-0 wild-type and *prat2-dm* mutant plants could

be observed. If one of the *prat2-dm* mutant lines showed a more drastic difference compared to Col-0 wild-type (e.g. *prat2-dm#1* in δ-tocopherol measurements, Figure 8), the other *prat2-dm* line did not, which is why all changes in tocopherol levels were considered non-significant. Synthesis of tocopherols and therefore SAM-dependent methylation does not seem to be affected in *prat2-dm* plants and sufficient amounts of SAM, at least for tocopherol methylation, seem to be available. Further, the transport of sufficient amounts of SAM into the plastid does not seem to be affected as well.

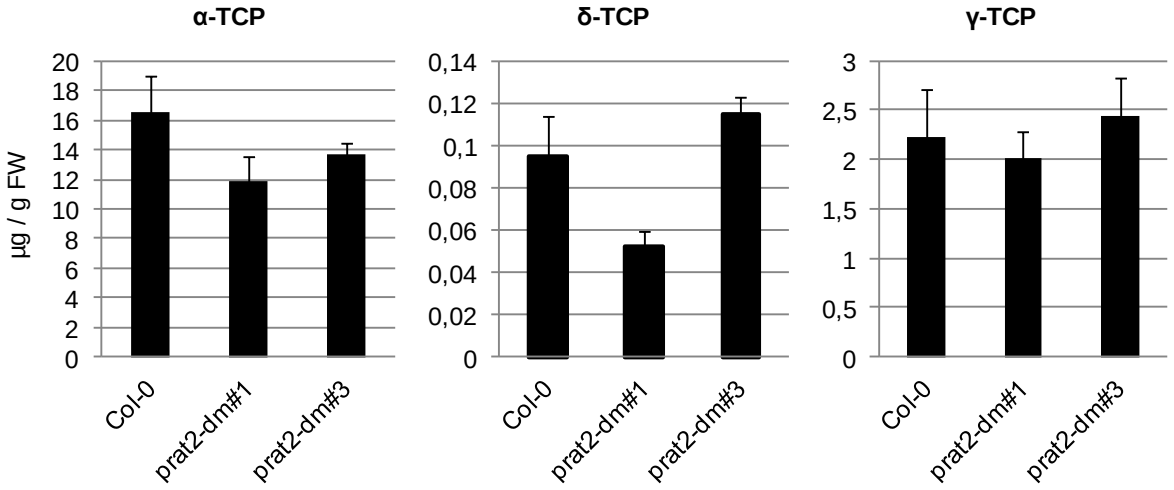

Figure 8: Levels of α-, δ- and γ-tocopherols in *prat2-dm* mutant plants

α-, δ- and γ-tocopherols (α-TCP, δ-TCP, γ-TCP) were analyzed in extracts from 100 mg leaf material of 32-day-old Col-0 wild-type as well as *prat2-dm#1* and *prat2-dm#3* mutant plants grown under longday conditions and harvested before the onset of light. The absolute amounts (n=3-5±SD) are given in µg / g fresh weight (FW).

3.1.6 Metabolite analysis in *prat2-dm* mutant plants

An analysis of a wide range of metabolites containing amino acids, carbohydrates and organic acids had already been conducted in collaboration with the group of Prof. Dr. Andreas Weber (Plant Biochemistry, University of Düsseldorf, Germany, for a detailed list of all measured metabolites, see 2.2.5) in Col-0 wild-type as well as *prat2-dm#1* and *prat2-dm#3* mutant plants grown under longday (30-day-old) and continuous light conditions (23-day-old, doctoral thesis S. Kraus, 2010). Phenotypic analysis under various light conditions (Figure 4) revealed that even only a short period of darkness leads to the described chlorotic phenotype with lancet shaped leaves and dwarfish, bushy growth in

prat2-dm mutant lines, whereas under continuous light conditions, the mutants were in much better shape. It was therefore concluded that any events causing the severe phenotype, possibly by the accumulation of toxic substances, occurs during the dark phase. The metabolite analysis was therefore extended with a set of samples from Col-0 wild-type as well as *prat2-dm#1* and *prat2-dm#3* mutant plants (29-day-old) grown under longday conditions but harvested in the dark before the onset of light. The results of both analyses were combined to obtain a more detailed picture of the metabolic situation in the *prat2-dm* mutant lines (Figure 9, 10 and 11).

The content of all measured metabolites was increased considerably in the new analysis with samples from longday conditions harvested before the onset of light in comparison to the previous analysis. This is due to the fact that the analyses of these samples were not conducted together with the samples harvested in the light (Doctoral thesis S. Kraus, 2010). The relative amounts obtained from both analyses are therefore not comparable but the ratios between wild-type and mutants can be compared (Figure 9, 10 and 11).

In summary, the analyses revealed an increase in the amino acids asparagine, aspartic acid, cysteine, isoleucine, leucine, lysine, methionine, phenylalanine, serine, and valine in *prat2-dm* mutant plants when compared to wild-type under longday conditions (Figure 9). Under continuous light conditions, the levels of asparagine, leucine, lysine, methionine and serine were increased less drastically, whereas cysteine, isoleucine and valine were still significantly increased. Cysteine showed to be the most drastically increased of all amino acids detected. In comparison to the harvest in the light under longday conditions, patterns of amino acid levels in *prat2-dm* mutant plants behaved similar as when harvested in the dark except for aspartatic acid and phenylalanine which were only increased in the dark.

Glycine was shown to be the only amino acid which was decreased in mutant plants compared to the wild-type under longday conditions. Interestingly, this difference was not observed under continuous light conditions where wild-type and mutant levels converged (Figure 9).

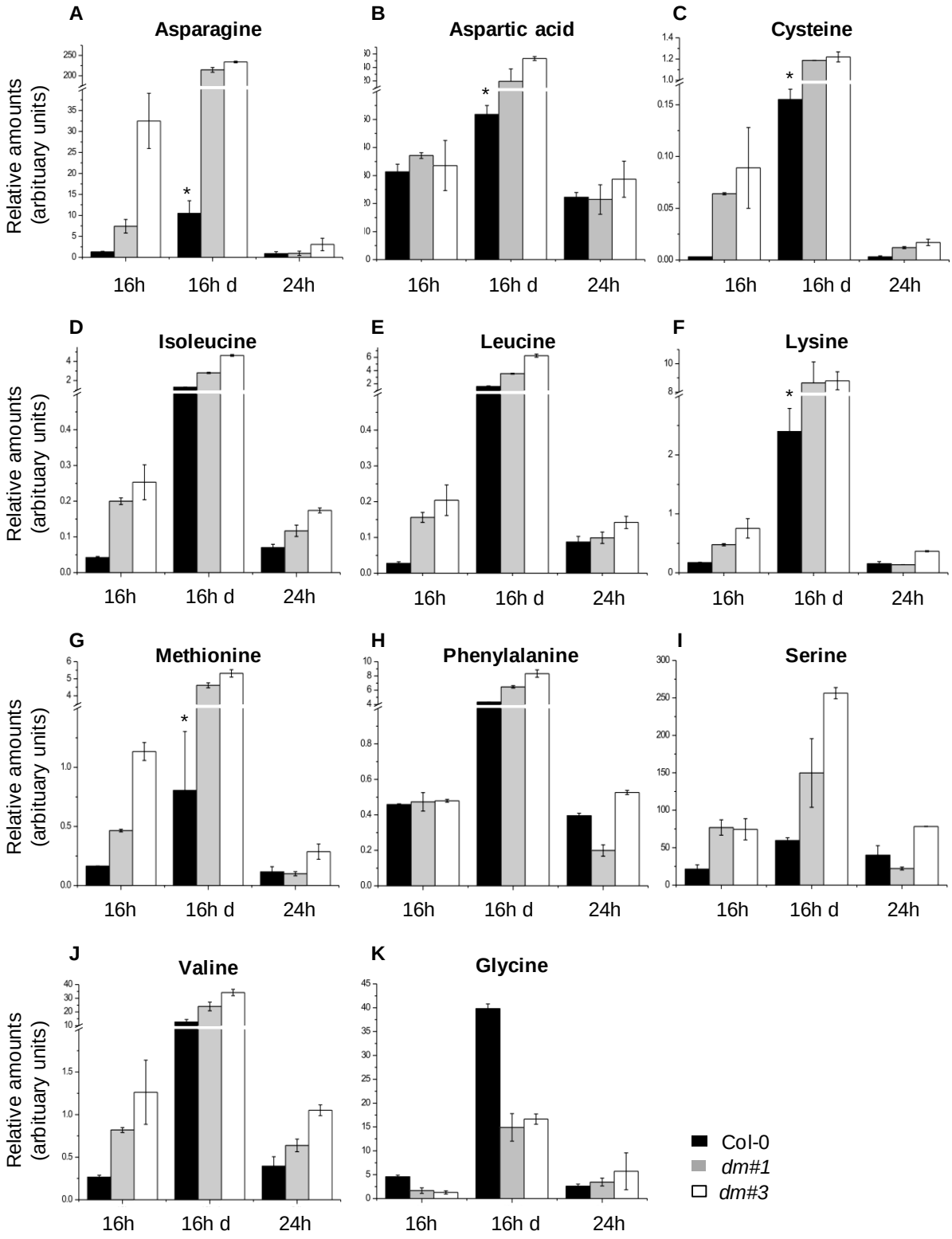

Figure 9: Changes in amino acid levels in *prat2-dm* mutant plants

Amino acid (AA) levels in Col-0 wild-type (black bars), *prat2-dm#1* (grey bars) and *prat2-dm#3* (white bars) homozygous mutant plants (n=2-3±SD). AA levels were measured in samples from longday conditions harvested in the light (16h), samples from longday conditions harvested in the dark (16h d) and in samples from continuous light conditions (24h). Please note the different scaling after the break of the y-axis and cases, in which values for Col-0 are not included in the break (asterisks).

The analysis of carbohydrates (Figure 10) revealed decreased levels for fructose, glucose, maltose, sucrose and xylose as well as the sugar alcohol myoinositol under longday conditions. Fructose, maltose and glucose levels were also decreased under continuous light conditions whereas sucrose, xylose and myoinositol were less increased in continuous light. In comparison to the harvest in the light under longday conditions, patterns of carbohydrate levels in *prat2-dm* mutant plants behaved similar as when harvested in the dark (Figure 10).

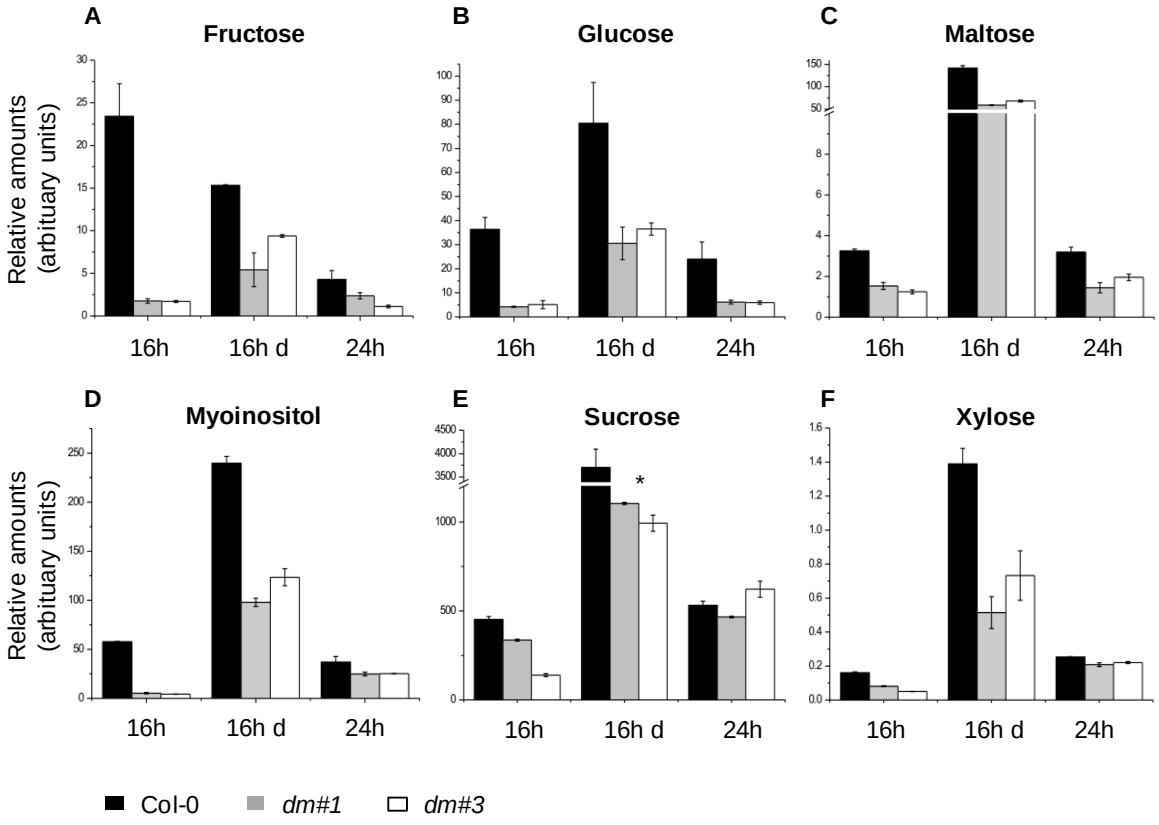

Figure 10: Changes in carbohydrate levels in *prat2-dm* mutant plants

Carbohydrate levels in Col-0 wild-type (black bars), *prat2-dm#1* (grey bars) and *prat2-dm#3* (white bars) homozygous mutant plants (n=2-3±SD). Carbohydrate levels were measured in samples from longday conditions harvested in the light (16h), samples from longday conditions harvested in the dark (16h d) and in samples from continuous light conditions (24h). Please note the different scaling after the break of the y-axis and cases, in which values for mutants are not included in the break (asterisks).

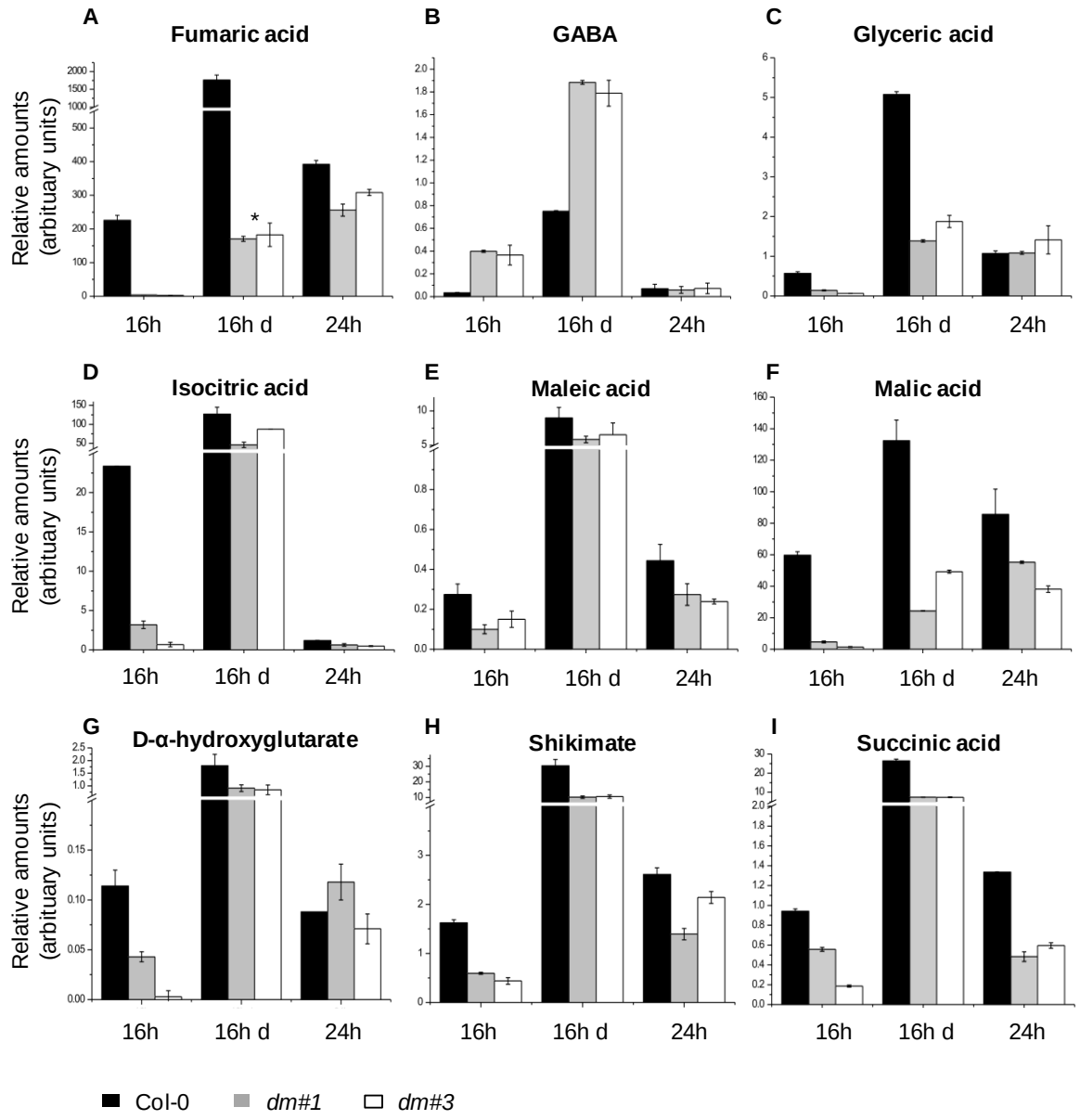

Figure 11: Changes in organic acid levels in *prat2-dm* mutant plants

Organic acid (OA) levels in Col-0 wild-type (black bars), *prat2-dm#1* (grey bars) and *prat2-dm#3* (white bars) homozygous mutant plants (n=2-3±SD). OA levels were measured in samples from longday conditions harvested in the light (16h), samples from longday conditions harvested in the dark (16h d) and in samples from continuous light conditions (24h). Please note the different scaling after the break of the y-axis and cases, in which values for mutants are not included in the break (asterisks).

The analysis of organic acids (Figure 11) revealed decreased levels of fumaric acid, glyceric acid, isocitric acid, maleic acid, malic acid, shikimate and D-α-hydroxyglutarate under longday conditions. Under continuous light conditions, levels of all these organic acids were elevated again, some (glyceric acid and D-α-hydroxyglutarate) even to or above wild-type

level. For γ-aminobutyric acid (GABA), a drastic increase was observed under longday conditions which reverted back to wild-type levels under continuous light conditions (Figure 11). For none of the measured organic acids, a change in samples harvested before the onset of light could be observed. A general decrease in organic acids could be registered *prat2-dm* mutant lines in comparison to Col-0 wild-type (Figure 11).

Overall, an increase in nitrogen-containing compounds (amino acids) in comparison to a decrease in mainly carbon containing compounds (carbohydrates, organic acids) could be observed in *prat2-dm* mutant lines (Figure 9, 10 and 11). Continuous light conditions reverted the changes for most of the measured metabolites back to wild-type levels. Harvest of samples before the onset of light did not reveal any changes to the harvest in light with the exception of the amino acids aspartic acid and phenylalanine. Here, increased levels were detected only in samples harvested in the dark (Figure 9, 10 and 11).

3.1.7 Analysis of sulphur-containing metabolites in *prat2-dm* mutant plants

The accumulation of MgPP IX pointing to a possible defect in SAM metabolism and the drastic increase of cysteine levels in *prat2-dm* lines along with, among other amino acids, an increase in methionine point to an overall perturbation of sulphur metabolism in *prat2-dm* lines. Also, the reversed phenotype to *prat2-dm* mutants observed in the *cs26* mutant (Bermúdez et al., 2010), in which a gene encoding a plastid protein with S-sulfocysteine activity is affected, supports this direction. Thus the question arose, whether the PRAT2 proteins in chloroplasts might be involved in the shuttling of sulphur-containing metabolites into and out of the chloroplast. To confirm the previous results from the metabolite analysis for cysteine and to gain further inside in the metabolic status of *prat2-dm* mutant plants concerning sulphur metabolism, cysteine, glutathione (GSH) and *O*-acetylserine (OAS) levels were analyzed in Col-0 wild-type as well as *prat2-dm#1* and *prat2-dm#3* mutant plants grown under longday (38-day-old) and continuous light (32-day-old) conditions (Figure 12). The samples were sent to the group of Prof. R. Hell/ Dr. Markus Wirtz (Centre for Organismal Studies, Universtiy of Heidelberg) for HPLC measurements.

The increase of cysteine levels in the *prat2-dm* mutant plants was confirmed in these measurements although not as drastic as seen before. Cysteine levels increased significantly by 2.3 fold in *prat2-dm#1* and by 1.9 fold in *prat2-dm#3* under longday conditions. Under continuous light conditions, cysteine levels were overall higher and also increased by 1.7 fold in *prat2-dm#1* and by 1.9 fold in *prat2-dm#3* (Figure 12).

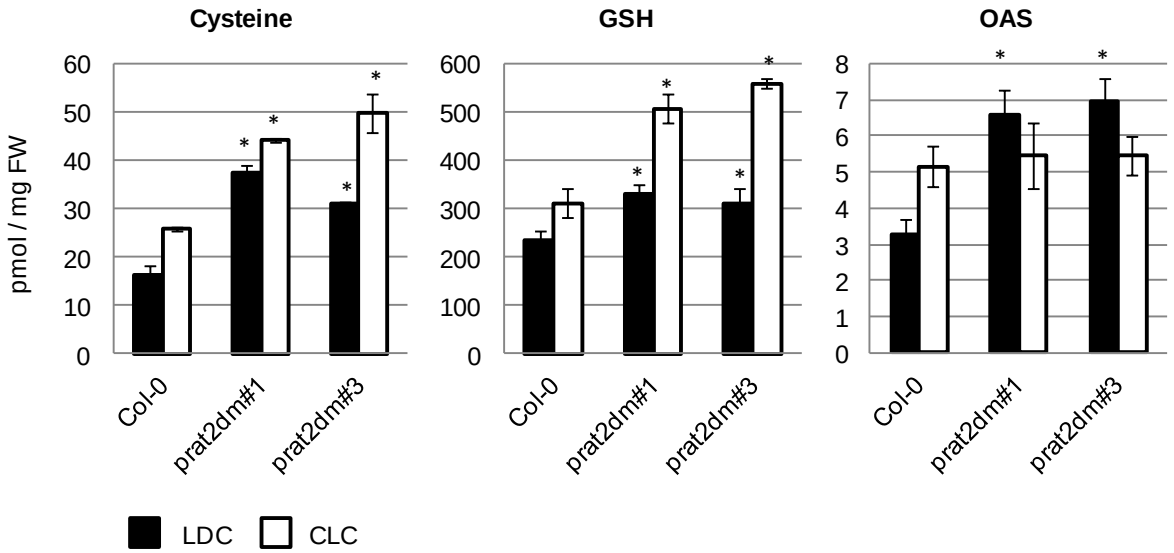

Figure 12: Cysteine, glutathione and *O*-acetylserine levels in *prat2-dm* mutant plants

Cysteine, glutathione (GSH) and *O*-acetylserine (OAS) levels were analyzed in extracts from 100 mg leaf material of Col-0 wild-type as well as *prat2-dm#1* and *prat2-dm#3* mutant plants grown under longday (black bars, 38-day-old) and continuous light (white bars, 32-day-old) conditions. The absolute amounts (n=3-5±SD) are given in pmol / mg fresh weight (FW). Asterisks indicate significant differences compared to Col-0 wild-type ($p<0,05$).

The same behavior was observed for GSH, a storage molecule for cysteine. GSH levels were significantly increased under longday conditions by 1.3 fold *prat2-dm#1* and by 1.4 fold in *prat2-dm#3.* Again, GSH levels were overall higher under continuous light conditions with a significant increase by 1.6 fold in *prat2-dm#1* and by 1.8 fold in *prat2-dm#3* (Figure 12). For OAS, the precursor of cysteine a significant increase could only be observed under longday conditions by 2 fold in *prat2-dm#1* and by 2.1 fold in *prat2-dm#3.* OAS levels under continuous light conditions were overall higher but no significant change between Col-0 wild-type and the *prat2-dm* mutant lines was detectable (Figure 12).

3.1.8 Transport activity studies in *Saccharomyces cerevisiae*

In order to test the transport capacity of the PRAT2 proteins for SAM, cysteine, and methionine, yeast cells expressing PRAT2.1 or PRAT2.2 in their plasma membrane were used for transport activity studies with radiolabelled SAM, cysteine, methionine and benzoic acid (BA) as a control. The empty pNEV vector was used as a control and 20 min after incubation, values of radioactivity inside yeast cells were calculated relative to the initial loading (Figure 13).

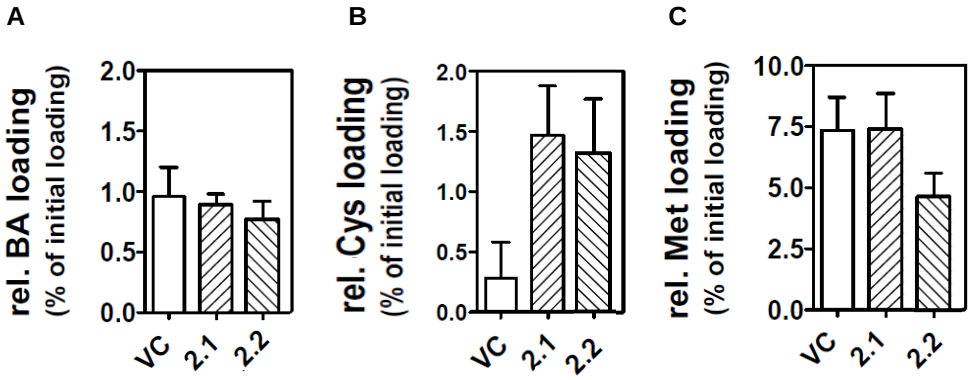

Figure 13: Transport activity of PRAT2 in yeast

Transport capacity for ^{35}S-cysteine (Cys) and ^{3}H-methionine (Met) of yeast cells (strain JK93da with reduced endogenous ABC transporter activity, Noh et al., 2001) expressing *PRAT2.1* and *PRAT2.2* was compared to the empty pNEV vector control (VC). ^{14}C-benzoic acid (BA) was used as a negative control. Values were calculated relative to the initial loading (mean activities±SD of 3 – 6 individual measurements).

As depicted in Figure 13, the control assay with BA did not show a difference in the uptake behavior of the yeast cells transformed with the empty pNEV vector compared to yeast cells expressing PRAT2.1 or PRAT2.2. The same is observed for yeast cells incubated with SAM (data not shown). For cysteine however, the loading in yeast cells expressing PRAT2.1 as well as PRTA2.2 was increased by about 5-fold compared to the empty vector control which points to cysteine import mediated by PRAT2. Yeast cells incubated with methionine show a decrease in loading by about 1.5-fold compared to the empty vector control only in cells expressing PRAT2.2, which might indicate a slight export activity for methionine (Figure 13).

3.2 IEP57 in the inner chloroplast envelope

The new inner envelope protein of 57 kDa (IEP57) was identified in an approach to isolate new OEPs from outer chloroplast envelopes pea (Docotral thesis I. Jeshen, 2012). *In silico* analysis revealed that IEP57 consists of 2 – 4 α-helical membrane regions and was annotated as a chloroplast protein due to the presence of a N-terminal cleavable transit peptide (cTP). The chloroplast localization of IEP57 was confirmed by GFP fusion proteins transiently transformed into protoplasts of *Arabidopsis* and immunoblot analysis of separated inner envelope (IE) vesicles with a specific antibody raised against the C-terminal part of the protein from pea. IEP57 was found to be integral to the inner chloroplast envelope by hydrophobicity analysis but its orientation towards stroma and intermembrane space still remained elusive (Doctoral thesis I. Jeshen, 2012). A motif rich in the amino acids aspartate and glycine was found in the N-terminal, soluble part of IEP57 which is a putative site for protein-protein interactions involving ankyrin repeats (Personal communication Prof. Dr. E. Neuhaus, Plant Physiology, University of Kaiserslautern, Germany and Wingenter et al., 2011). IEP57 is annotated as a putative solute transporter with plant-specific origin (Tyra et al., 2007, Doctoral dissertation I. Jeshen, 2012). It is similar to the RETICULATA-RELATED1 (RER-1) protein and belongs to the family of reticulata-related proteins (Personal communication with Prof. Dr. A. Weber, Plant Biochemistry, University of Düsseldorf, Germany and PD Dr. C. Bolle, Plant Molecular Biology/Botany, Ludwig-Maximilians University, Munich, Germany). All available T-DNA insertion lines for *At-IEP57* did not produce any homozygous descendants and detailed segregation and silique analysis of heterozygous offspring confirmed an embryo-lethal phenotype. In order to further characterize the physiological role of IEP57 in *Arabidopsis,* overexpression, inducible overexpression and inducible knockout lines were generated (Doctoral thesis I. Jeshen, 2012), which were available in the T2 generation at the beginning of this study.

Aims of this part of the study on IEP57 were the further biochemical characterization of the IEP57 protein in terms of a potential role in transport across the chloroplast membranes. Overexpression, inducible overexpression and inducible knockout lines were to be characterized genetically and phenotypically in order to elucidate the physiological role of IEP57 in *Arabidopsis.*

3.2.1 Biochemical characterization of IEP57

Heterologous overexpression of IEP57

To obtain heterologously overexpressed IEP57 protein to be used for the analysis of the N-terminal glycine and aspartate rich motif in terms of putative interaction partners, the full length coding sequences (At-IEP57-fl, Ps-IEP57-fl) as well as the N-terminal parts including the first transmembrane domain without the cTP (At-IEP57_42-278, Ps-IEP57_45-278) were subcloned into the following vectors: pET21d, which produces a C-terminal 6xhis fusion protein, pPROEX, which produces a N-terminal 6xhis fusion protein and, in case of At-IEP57_42-278, pCOLDII, which produces a N-terminal 6xhis fusion protein and allowing slow overexpression at 15 °C. For none of the overexpression approaches, a band corresponding to the respective overexpressed protein could be detected in coomassie stained SDS gels or by immunoblotting using specific antisera directed against Ps-IEP57 (data not shown).

Proteolysis experiments

Since the orientation of the IEP57 protein in inner envelope vesicles from pea and therefore the position of the glycine and aspartate rich motif in the protein's N-terminus could not be clearly determined via PEG-maleimide or proteolysis assays with the available antibody directed against the C-terminal part of PsIEP57, a second antibody directed against a synthetic peptide consisting of 30 amino acids from the soluble N-terminus of the protein from pea (see section 2.1, Pineda Antikörperservice, Berlin, Germany) was generated. When tested on separated outer and inner envelope preparations from pea, a double band appeared in the inner envelope fraction with the distinct upper band running at the expected size (Figure 14Figure 14, A, upper panel). The lower band was considered to be unspecific background since it did not vanish when IE vesicles were treated with the proteases thermolysin and trypsin (Figure 14, C and D). Although created against a peptide from the sequence of pea, the antibody also recognized IEP57 from *Arabidopsis* when tested on separated chloroplast envelope preparations (Figure 14, A, lower panel). However, when tested on separated total protein extract and separated total membrane protein extract from *Arabidopsis*, the protein was not recognized (data not shown). Because vesicles were prepared according to protocols (Keegstra and Youssif, 1986, Waegemann et al., 1992) giving a right-side out orientation (Heins et al., 2002, Balsera et al., 2009), only the parts of the

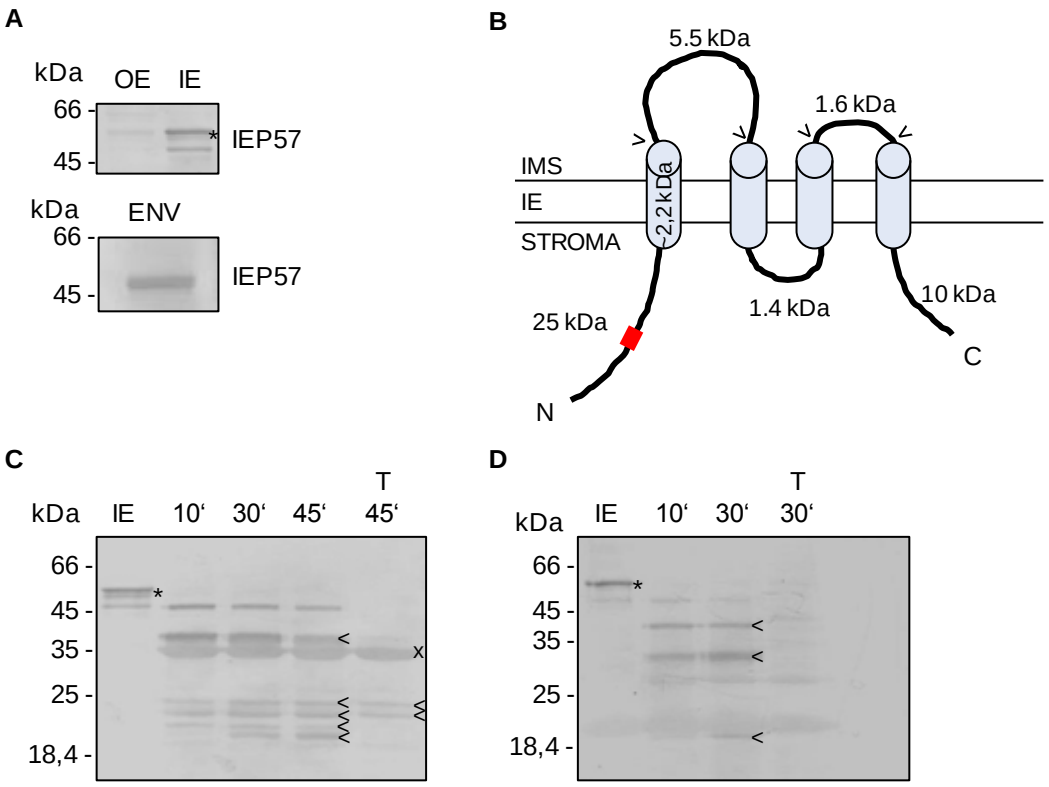

Figure 14: A new antibody specifically directed against the N-terminal of Ps-IEP57 used in proteolysis experiments

A) Immunoblots of outer (OE) and inner (IE) chloroplast envelope preparation of pea (left panel) and chloroplast envelope (ENV) preparation of *Arabidopsis* (right panel). 5 µg of OE/IE and 10 µg of ENV were separated via SDS PAGE (12.5 %) and analyzed with a specific antibody directed against a synthetic peptide from the N-terminal of Ps-IEP57. The asterisk in the left panel indicates the specific band corresponding to Ps-IEP57.B) Schematic model of Ps-IEP57 in the inner chloroplast envelope (IE) with the N-terminal (N) and C-terminal (C) oriented towards the chloroplast stroma and the loops connecting the transmembrane helices oriented towards the intermembrane space (IMS). The position of the synthetic peptide used for antibody production is marked with a red box, arrowheads indicate the closest proteolytic cleavage sites to the transmembrane helices accessible from the IMS side (modified from Doctoral thesis I. Jeshen, 2012). C) Proteolysis experiment with thermolysin. 5 µg of inner envelope (IE) vesicles were treated with 10 µg of thermolysin for 0 (IE), 10, 30, and 45 min. One sample containing 1 % Triton X-100 was treated for 45 min as a control, X indicates the band caused by the protease thermolysin. D) Proteolysis experiment with trypsin. 5 µg of inner envelope (IE) vesicles were treated with 5 µg of trypsin for 0 (IE), 10 and 30 min. One sample containing 1 % Triton X-100 was treated for 30 min as a control. Arrowheads indicate digestion fragments of Ps-IEP57.C + D) All samples were separated via SDS PAGE (12.5 %) and analyzed with a specific antibody directed against a synthetic peptide from the N-terminal of Ps-IEP57. Asterisks indicate the specific protein band corresponding to Ps-IEP57, arrowheads indicate digestion fragments of Ps-IEP57A, C + D) Numbers indicate the molecular mass in kDa.

protein facing the intermembrane space are accessible to protease digestion whereas parts facing the stromal side are protected.

In untreated inner envelope vesicles, a distinct protein band corresponding to IEP57 was detected which vanished after treatment with the proteases thermolysin and trypsin (Figure 14, C and D). This shows that parts of the protein facing the intermembrane space are successfully digested which decreases the proteins' size. In both cases, protein bands of lower molecular weight appeared that were recognized by the antibody directed against the N-terminus of IEP57. Even though the resulting band patterns could not be matched to the expected sizes of the proteolytic fragments (ExPASy PeptideCutter tool, Gasteiger et al., 2003), these results indicate that the N-terminal part of Ps-IEP57 protected from proteolytic digestion and therefore oriented towards the chloroplast stroma.

3.2.2 IEP57 *in planta*

IEP57 belongs to the RETICULATA-RELATED (RER) family of proteins

In *Arabidopsis*, the closest relative of At-IEP57 is annotated to be At-RER1 (RETICULATA-RELATED1), a protein possibly localized to the inner chloroplast envelope with yet unknown function (Doctoral dissertation I. Jeshen, 2012). At-RER1 belongs to the RETICULATA-RELATED (RER) family of proteins named after the first described family member RETICULATA (At-RE, Rédei and Hirono, 1964). Mutation of the gene encoding At-RE causes a reticulate class of leaf variegation, displaying pale-green interveinal tissue in contrast to a normal-green leaf vasculature (Lundquist et al., 2014). Two more mutants displaying the reticulated leaf phenotype, have been described for the RER family, *RETICULATA-RELATED 3* (*At-RER3*) and *4* (*At-RER4*) encoding for proteins which show high sequence similarity to RE (Pérez-Pérez et al., 2013). Three additional *A. thaliana* genes encoding for proteins with also high sequence similarities to At-RE were identified and named *At-RER2*, *At-RER5* and *At-RER6*. However, mutation of these genes does not cause the reticulated phenotype (Pérez-Pérez et al., 2013). When analyzed in terms of amino acid sequence similarity (Figure 15), the RER proteins form three pairs (RE-RER1, RER2-RER3, RER5-RER6) with RER4 as a single protein grouping with RER2-RER3 and IEP57 as a single protein grouping with RE-RER1 (Figure 15).

The RER family is plant-specific and all proteins of the family contain a plant-specific, conserved amino acid domain of unknown function, DUF3411 with a conserved RYQ motif at its end which is also present in IEP57 (Figure 16). At-RER5 and At-RER6 additionally contain a second domain of unknown function, DUF399 in their N-terminal parts which are prolonged compared to the other members of the family. At-IEP57 contains an aspartate- and glycine-rich motif and glycine-rich regions are also present in the other RER-family members except for At-RER5 and At-RER6 (Figure 16).

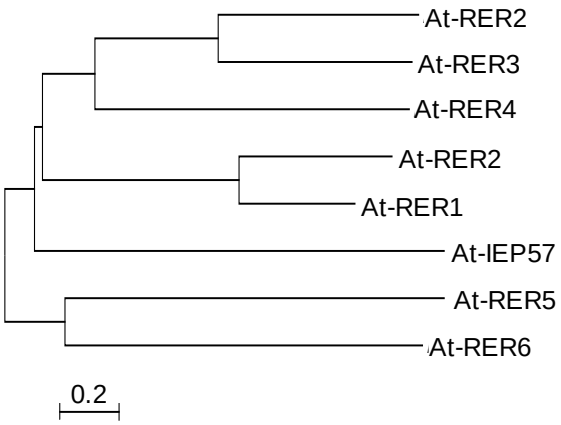

Figure 15: Phylogenetic tree of the proteins of the *Arabidopsis* RER family

The evolutionary history was inferred using the Neighbor-Joining method (Saitou and Nei, 1987). The optimal tree with the sum of branch length 8.761 is shown. The tree is drawn to scale, with branch lengths in the same units as those of the evolutionary distances used to infer the phylogenetic tree. The evolutionary distances were computed using the Poisson correction method (Zuckerkandl and Pauling, 1965) and are in the units of the number of amino acid substitutions per site. The analysis involved 8 amino acid sequences. All positions containing gaps and missing data were eliminated. There were a total of 337 positions in the final data set. Evolutionary analyses were conducted in MEGA6 (Tamura et al., 2013).

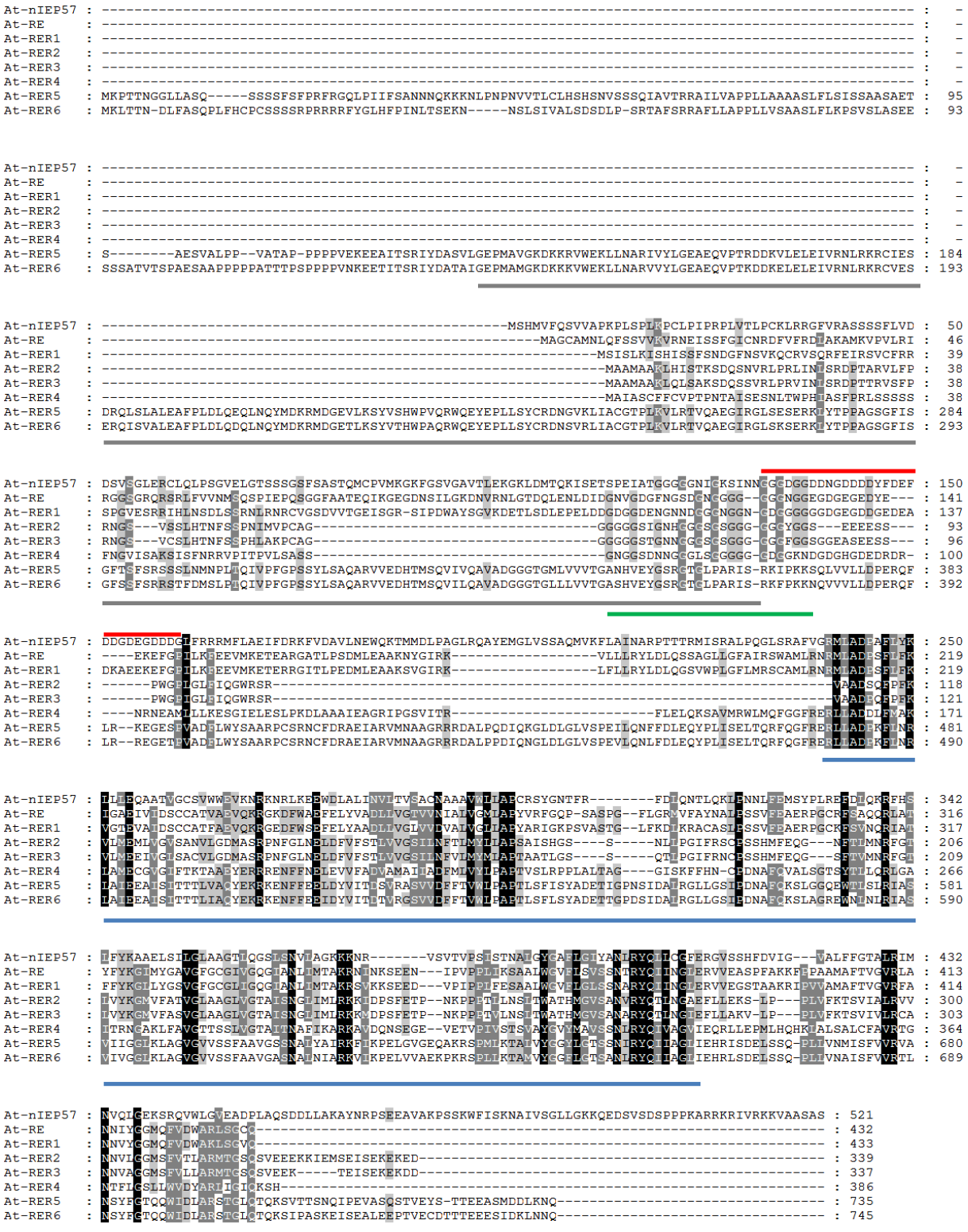

Figure 16: Alignment of the amino acid sequences of proteins of the *Arabidopsis* RER family
Identical and similar residues are shaded in black and grey, respectively. Numbers indicate amino acid positions. Blue line: DUF3411 domain, red line: glycine-aspartate rich motif in At-IEP57, green line: glycine-rich regions as in Pérez-Pérez et al., 2013, grey line: DUF399 domain in At-RER5 and At-RER6. Protein sequences were retrieved from NCBI, aligned with VectorNTI and shaded with GeneDoc (Nicholas et al., 1997).

3.2.3 Mutation of IEP57 in *Arabidopsis thaliana*

In order to study the physiological role of IEP57 *in planta* and to overcome the embryo lethality of homozygous T-DNA insertion lines for *IEP57* in *Arabidopsis*, overexpression as well as inducible overexpression and inducible RNAi lines (popON/popOFF system, Wielopolska et al., 2005) were generated and analyzed (Doctoral thesis I. Jeshen, 2012). Plants harboring an overexpression construct for At-IEP57 in the T2 generation exhibited spontaneous chlorosis randomly occurring during plant development. This phenotype was shown to be due to a transgene induced gene silencing initiated by 35S promoter controlling the overexpression of the *IEP57* cDNA (Doctoral thesis I. Jeshen, 2012). In the current study, plants were propagated to the T3 generation and homozygous lines were selected via PCR genotyping. The phenotype described above could be confirmed in the three obtained homozygous overexpression lines #6, #9 and #10 (data not shown).

However, no clear pattern could be associated with distinct developmental stages of plant organs. The phenotype was also not consistent in individuals within the same line. In order to analyze IEP57 *in planta* in a more reliable system, inducible overexpression and inducible RNAi lines, was chosen. In plants stably transformed with the popON/popOFF constructs, the overexpression or knock-down by RNA interference of a desired gene can be induced with dexamethasone and it is therefore possible to examine the phenotype at a specific point during plant development.

Inducible overexpression of *IEP57*

In order to confirm the observed phenotype of the 35S::*IEP57* overexpression lines, available lines harboring the inducible *At-IEP57*/popON construct in the T2 generation were propagated to the T3 generation and homozygous lines were selected via PCR genotyping. The two resulting lines (#2 and #5) were grown on agar medium-containing plates for 6 days and then transferred onto inducing medium-containing plates. Daily monitoring of the plants revealed that the chlorotic phenotype observed in 35S::*IEP57* lines could be confirmed for *At-IEP57*/popON lines #2 and #5 after the induction of overexpression with dexamethasone. Chlorosis started 8 to 10 days after transfer onto inducing medium from the middle of the rosette and spread over the petioles into the newly developing leaves (Figure 17).

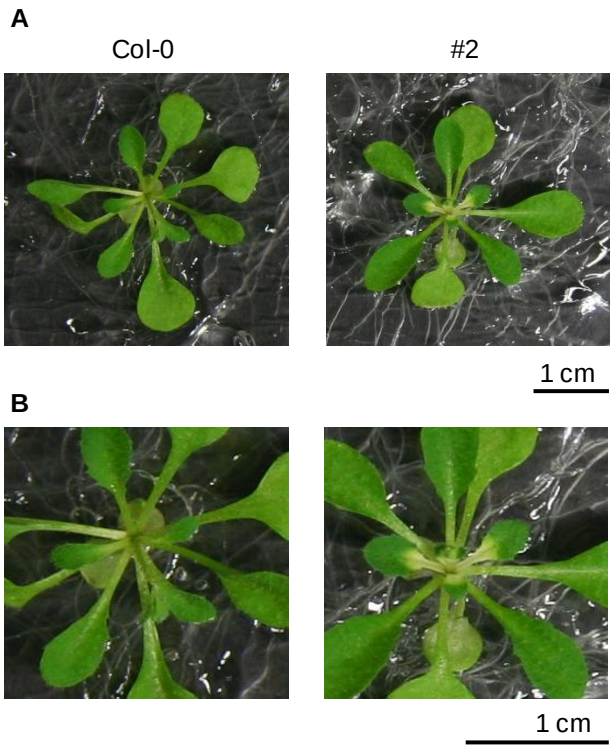

Figure 17: *At-IEP57*/popON inducible overexpressors display a chlorotic phenotype
A) Representative 17-day-old Col-0 wild-type and *At-IEP57*/popON line #2 (T3) homozygous plants 11 days after induction with 10 µM dexamethasone, B = magnification of A

Inducible knockdown of *IEP57*

When RNAi was induced in seedlings of transformants harboring the *At-IEP57*/popOFFII construct in the T2 generation, a phenotype similar to the one observed in the 35S and inducible overexpression lines could be detected (data not shown). Transformed lines were propagated to the T3 generation and lines homozygous for the *At-IEP57*/popOFFII construct were selected via PCR genotyping. The phenotypes of the resulting 4 lines (#1, 2, 5 and 7) were analyzed in the T4 generation. Seeds were either sown directly onto agar plates or on sterilized propyltex nets to facilitate the transfer to dexamethasone containing plates after 10 days. In general, plants grown on propyltex nets developed slower compared to plants directly grown on plates. In lines #1 (Figure 18) and #5 chlorosis started consistently 4 days after dexamethasone induction as previously described whereas no obvious phenotype occurred in lines 2 and 7.

Transcription analysis via qRT-PCR revealed a drastic reduction of *IEP57* transcript in all 4 lines 4 days after RNAi induction which slowly started to increase again 10 days after

induction, probably due to the complete consumption of dexamethasone. Functionality of the *At-IEP57*/popOFFII construct was also confirmed by GUS staining of plants after RNAi induction. It was therefore confirmed that the observed phenotype is due to the lack of *IEP57* transcript and lines #1 and #5 were chosen for all further applications (State examination thesis K. Winkler, 2013). Figure 18 shows representative Col-0 wild-type and *At-IEP57*/popOFFII line #1 plants and the displayed chlorosis upon RNAi induction with dexamethasone. The induction of a knock-down of the *IEP57* transcript in *Arabidopsis* using the dexamethasone inducible popOFFII system proved to be a reliable system to overcome the embryo lethality of T-DNA insertion lines for *IEP57*. Growth of transformants on propyltex nets (compare Figure 18) on plates was also shown to facilitate the transfer onto plates containing the knock-down inducing compound dexamethasone and allowed the production of large amounts of plant material for further analysis.

In order to induce the knock-down of *IEP57* in a more mature stage of plant development and to be able to analyze individual plants treated with different substances of interest, a hydroponic growth system was established. Individual seeds of *At-IEP57*/popOFF lines #1 and #5 were germinated on agar medium-containing seed holders allowing the roots to grow into a liquid-filled 1.5 ml Eppendorf tube attached underneath. (Figure 19, C). The used growth container allowed RNAi induction with dexamethasone of three-week-old plants and a subsequent monitoring of up to ten days. The expected phenotype occurred reliably with chlorosis starting from the middle of the rosette and spreading over the petioles into the newly developing leaves of the plants 4 days after RNAi induction (Figure 19, A). qRT-PCR analysis revealed a drastic reduction of *IEP57* transcripts in line #1, 7 days after induction (5 % of wild-type level), which increased slightly again 10 days after induction (12 % of wild-type level), probably due to the complete consumption of dexamethasone (Figure 19). Growth in hydroponic culture thus showed to be a reliable system for the induction of a knock-down of *IEP57* transcripts in mature plants and allowed further phenotypic analysis.

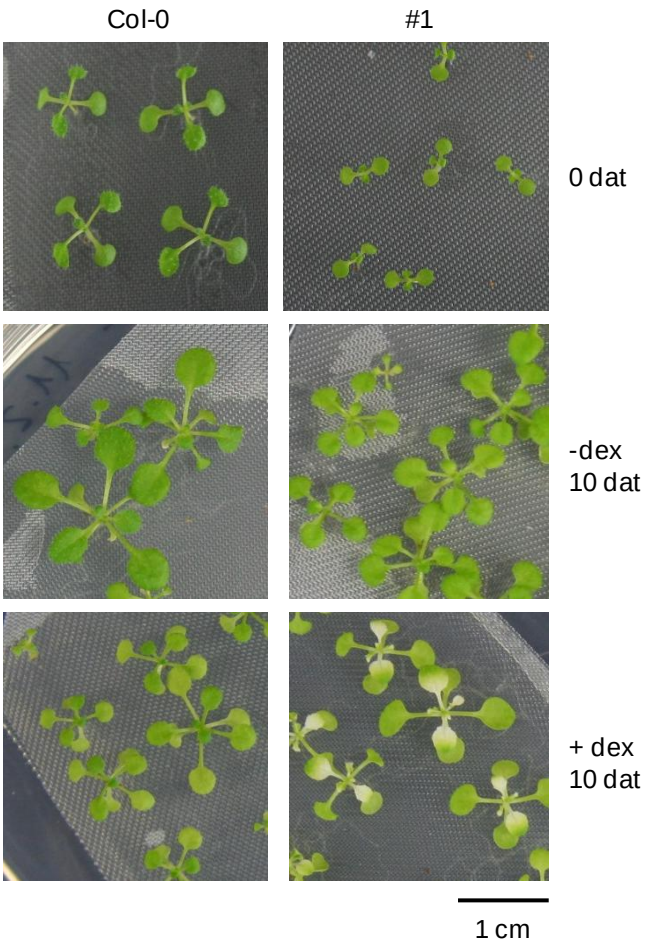

Figure 18: Inducible *At-IEP57* RNAi plants display a chlorotic phenotype

Representative Col-0 wild-type and *At-IEP57*/popOFF#1 (T3) homozygous seedlings grown on propyltex nets on non-inducing medium for 7 days (upper panel, 0 days after transfer (dat)) and 10 dat onto non-inducing (- dex, middle panel) and inducing medium containing 10 µM dexamethasone (+ dex, lower panel).

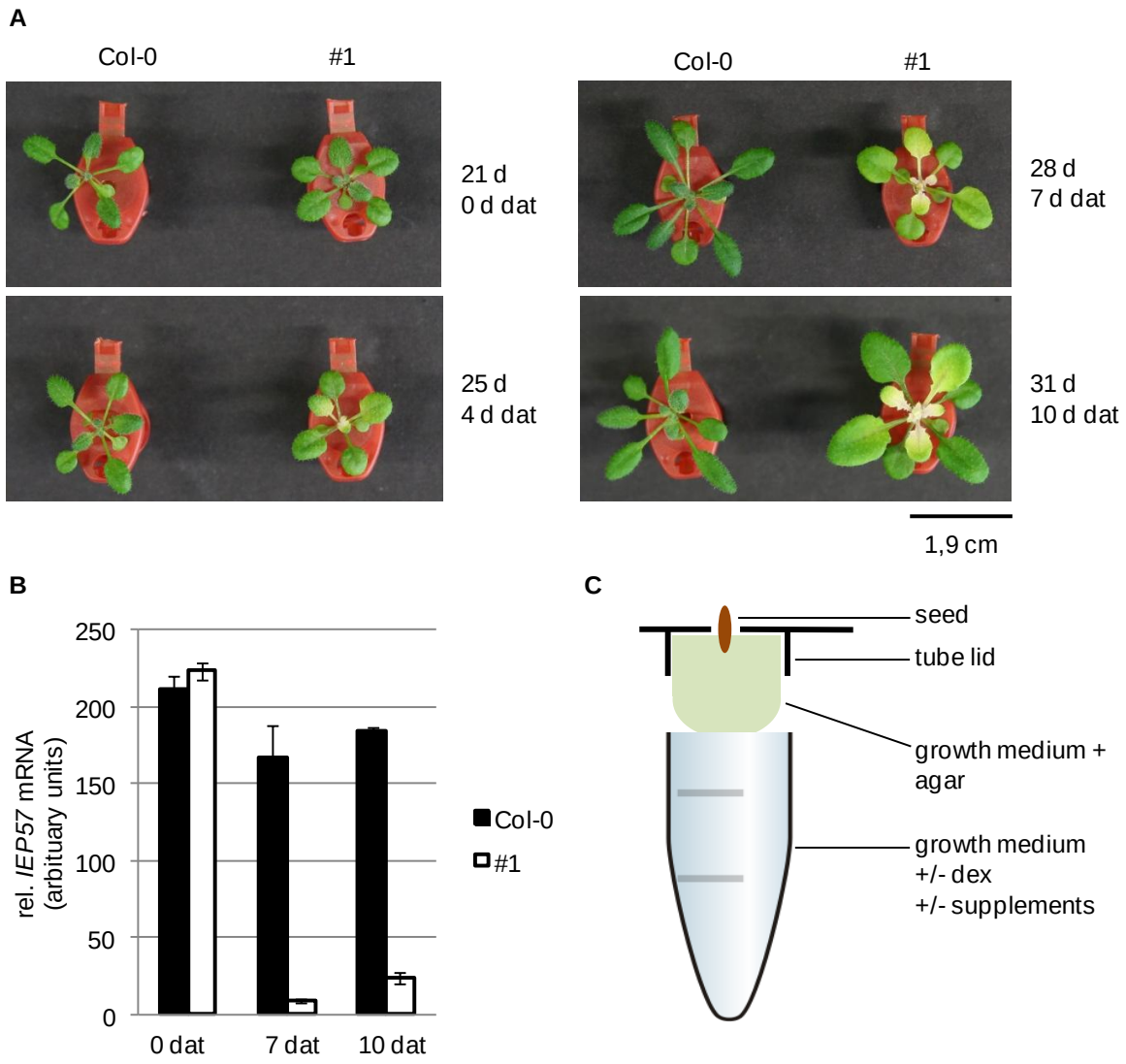

Figure 19: Induction of RNAi in *At-IEP57*/popOFF plants grown in hydroponic culture

A) Representative plants of Col-0 wild-type and *At-IEP57*/popOFF line #1 (T3) homozygous plants grown in hydroponic culture on non-inducing medium for 21 days (A,left upper panel, 0 days after transfer (dat)) and 4, 7 and 10 dat onto inducing medium.B) Quantification of *At-IEP57* mRNA using qRT-PCR. mRNA was prepared from three 21,28 and 31-day-old Col-0 wild-type (black bars) and *At-IEP57*/popOFF line #1 (white bars) plants plants grown in hydroponic culture 0, 7 and 10 dat onto inducing medium. The amount of mRNA (arbituary units, n=3±SD) was normalized to 1000 actin transcript molecules. C) Representation of the hydroponics system (modified after Conn et al., 2013).

3.2.4 Rescue of IEP57 mutant phenotypes

As described above, IEP57 belongs to the RER family of proteins. Metabolic profiles of *re* and *rer3* mutants revealed alterations in several biosynthetic pathways downstream of pyruvate and alterations in branched chain and aromatic amino acid metabolism (Pérez-Pérez

et al., 2013). A biosynthetic pathway, originating from pyruvate in the chloroplast is the production of the branched-chain amino acids valine, leucine and isoleucine (for an overview see Binder, 2010). A possible involvement of IEP57 in the metabolism of branched-chain amino acids, possibly in the transport of intermediates or end products was examined. Valine, leucine and isoleucine were added exogenously to analyze if the chlorotic phenotype caused by the reduction of *IEP57* transcripts can be rescued. Seeds of Col-0 wild-type and *At-IEP57*/popOFF line #1 were sown directly onto agar medium-containing plates with 10 µM dexamethasone to induce RNAi and 1 mM of the respective amino acid. Daily monitoring of the plants revealed no phenotypic alterations compared to Col-0 wild-type plants (Figure 20).

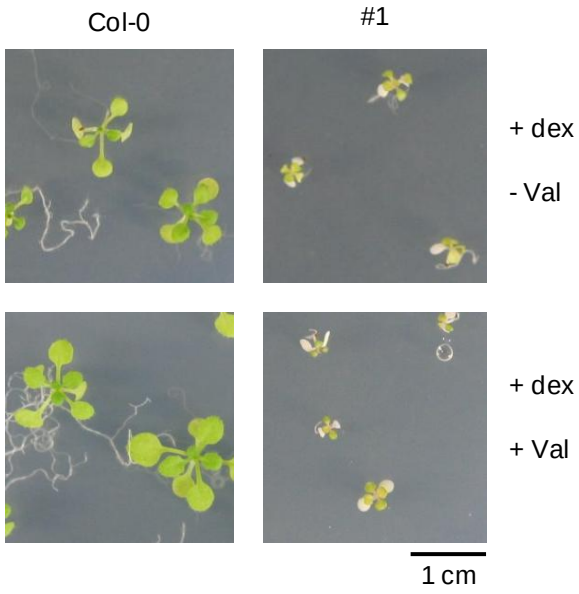

Figure 20: Feeding studies with the branched amino acid valine

Representative 21-day-old Col-0 wild-type and *At-IEP57*/popOFF line #1 seedlings grown directly on inducing medium (upper panel) and inducing medium supplemented with 1 mM valine (lower panel).

Other leaf reticulate mutants

Because IEP57 was found to be a member of the RER family of proteins in which the members *RE*, *RER3* and *RER4* cause the leaf reticulate phenotype when mutated, literature was searched for other mutants displaying a leaf reticulate phenotype.

Mutation in the gene *CUE1* encoding the phosphoenolpyruvate (PEP)/phosphate antiporter PPT1 in the inner chloroplast envelope leads to leaf reticulation (Li et al., 1995). PPT1 imports PEP synthesized in the cytosol into the chloroplast where it serves as a substrate for various biosynthetic pathways e.g. the shikimate pathway which produces numerous primary and secondary metabolites including the aromatic amino acids phenylalanine, tyrosine and tryptophan (Maeda and Dudareva, 2012). When all three aromatic amino acids were added simultaneously to the growth medium, the leaf reticulate phenotype was rescued in *cue1* mutant plants but not when they were applied individually (Streatfield et al., 1999). A possible involvement of IEP57 in the export of aromatic amino acids from the chloroplast was therefore analyzed. Seeds of the three homozygous *35S::IEP57* overexpression lines (#6, 9 and 10, T3 generation, Figure 21, A) as well as of the inducible RNAi lines *At-IEP57*/popOFF #1 (Figure 21, B) and #5 were sown directly on agar medium-containing plates, in case of the popOFF lines supplemented with 10 µM dexamethasone. Plates were supplemented with 1 mM phenylalanine, tryptophan or tyrosine or with 1 mM each of all three amino acids as described in Streatfield et al. (1999, Figure 21).

When the aromatic amino acids were applied individually, no phenotypic difference was observed, neither in *35S::IEP57* overexpression nor in *At-IEP57*/popOFF lines in comparison to control plates (data not shown). When all three aromatic amino acids were applied simultaneously, germination was very poor and Col-0 wild-type as well as *35S::IEP57* overexpression and *At-IEP57*/popOFF lines appeared small, weak and sickly. Still, Col-0 wild-type plants appeared somewhat bigger and greener whereas *35S::IEP57* overexpression and *At-IEP57*/popOFF seedlings displayed chlorosis. No phenotypic alterations could be observed in *35S::IEP57* overexpression and *At-IEP57/*popOFF plants (Figure 21).

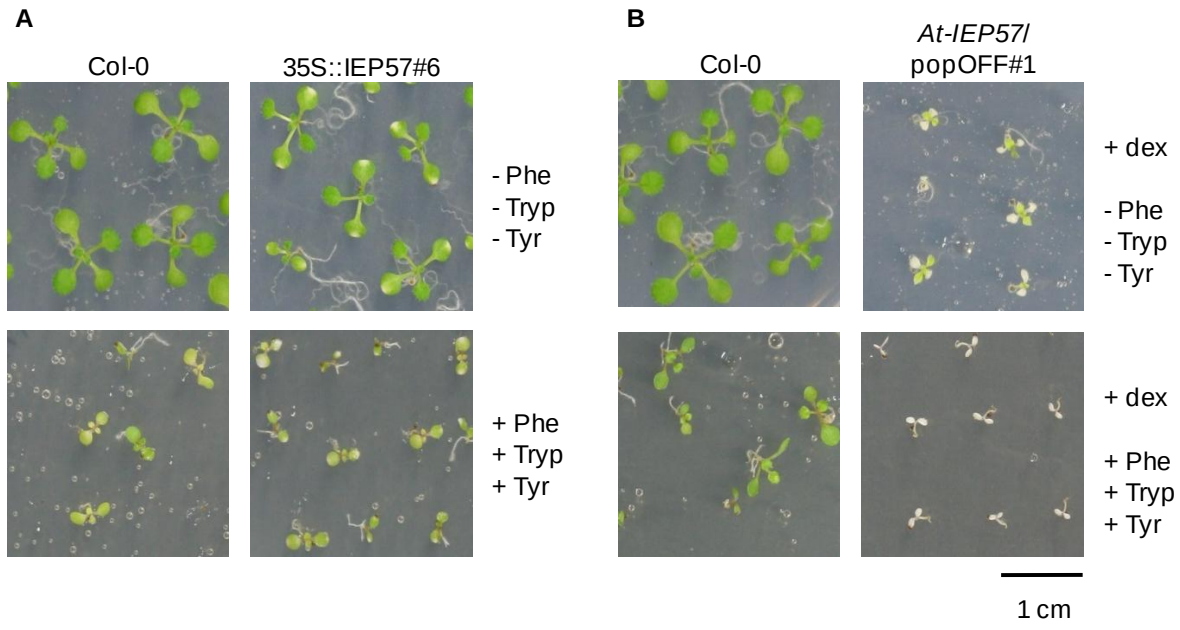

Figure 21: Feeding studies with the aromatic amino acids phenylalanine, tryptophan and tyrosine

A) Representative 11-day-old seedlings of Col-0 wild-type and 35S::IEP57 line #6 seedlings grown directly on agar medium-containing plates (upper panel) and on plates supplemented with 1 mM phenylalanine, tryptophan and tyrosine, each. B) Representative 11-day-old seedlings of Col-0 wild-type and *At-IEP57*/popOFF line #1 sown directly on inducing medium (upper panel) and on inducing medium supplemented with 1 mM phenylalanine, tryptophan and tyrosine, each.

Mutation of the genes *VEN3* and *VEN6* which encode the large (β) and the small (α) subunit of the plastid-localized carbamoylphosphate synthetase (CPS), respectively leads to leaf reticulation (Mollá-Morales et al., 2011). CPS catalyzes the conversion of glutamine and bicarbonate into carbamoyl phosphate (CP) and glutamate. CP together with ornithine is a precursor of citrulline used for the biosynthesis of arginine and pyrimidines (Slocum, 2005). A possible involvement of IEP57 in the transport of intermediates or end products of this pathway was therefore analyzed by exogenous application of ornithine, citrulline, arginine and proline, which can also be synthesized from ornithine (for an overview, see Szabados and Savouré, 2010). For this purpose, Col-0 wild-type and *At-IEP57*/popOFF line #1 plants were grown in hydroponic culture on non-inducing medium for 21 days and then transferred onto RNAi-inducing medium supplemented with 1 mM of the respective metabolite (Figure 22). Daily monitoring for 7 days did not show any phenotypic alterations for any of the four tested substances. Figure 22 shows representative plants supplemented with ornithine and citrulline 7 dat.

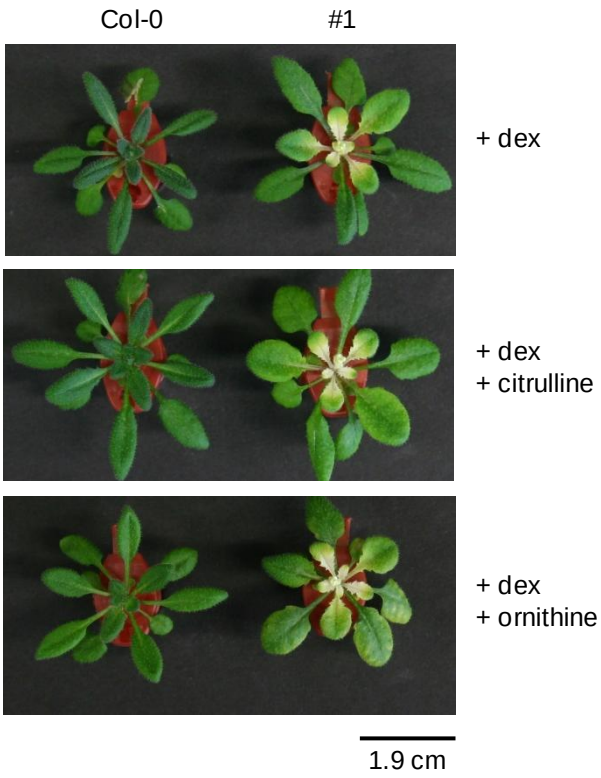

Figure 22: Feeding studies with citrulline and ornithine

Representative 28-day-old plants of Col-0 wild-type and *At-IEP57*/popOFF line #1 (T3) homozygous plants grown in hydroponic culture on non-inducing medium for 21 days. Pictures were taken 7 days days after transfer onto inducing medium supplemented with 1 mM citrulline or 1 mM ornithine.

In addition, plants can synthesize polyamines via two biosynthetic pathways from ornithine with the committed step located in the cytosol and from arginine with the committed step located to the plastid (Fuell et al., 2010, Carbonell and Blázquez, 2009). A possible involvement of IEP57 in the transport of intermediates or end products of these pathways was therefore analyzed by exogenous application of putrescine, spermidine and spermine. For this purpose, Col-0 wild-type and *At-IEP57*/popOFF line #1 plants were grown in hydroponic culture on non-inducing medium for 21 days and then transferred onto RNAi-inducing medium supplemented with 1 mM of the respective metabolite (Figure 23).

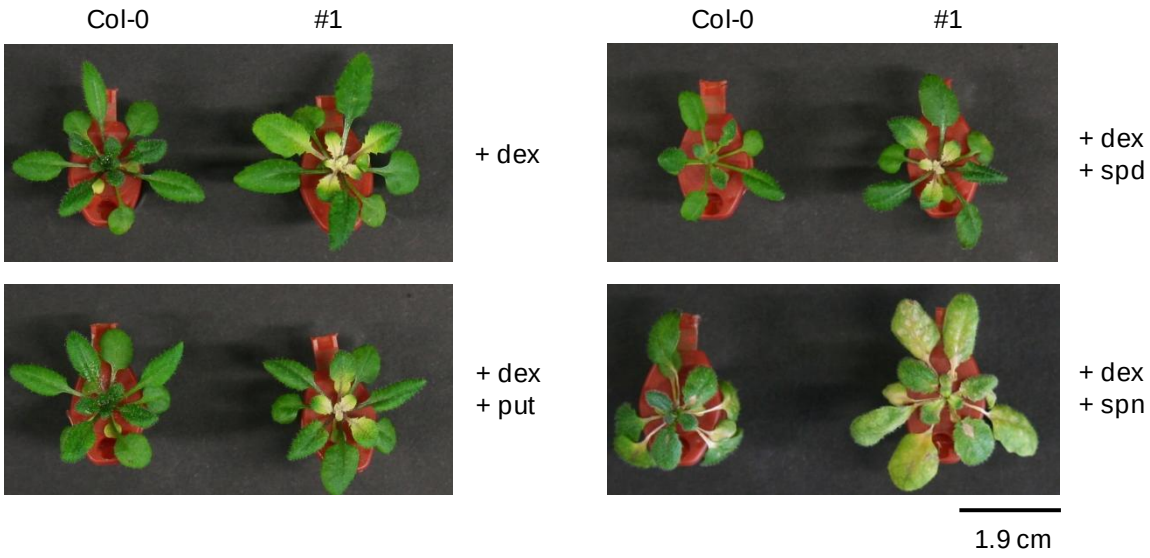

Figure 23: Feeding studies with the polyamines putrescine, spermidine and spermine
Representative 28-day-old plants of Col-0 wild-type and *At-IEP57*/popOFF line #1 (T3) homozyguous plants grown in hydroponic culture non-inducing medium for 21 days. Pictures were taken 7 days after transfer onto inducing medium supplemented with 1 mM putrescine (put, lefl lower panel), spermidine (spd, right upper panel) and spermine (spn, right lower panel).

Daily monitoring for 7 days did not show any phenotypic alterations for any of the three tested substances. Both, wild-type and mutant plants supplemented with spermine started to wilt after transfer and became limp and sickly (Figure 23). In a second approach, seeds of Col-0 wild-type and *At-IEP57*/popOFF line #1 were directly sown onto RNAi-inducing agar medium-containing plates supplemented with 1 mM putrescine, spermidine or spermine. Germination of wild-type as well as mutant plants was very poor on all three substances and mutant plants did also not show any phenotypic alterations (data not shown).

In another set of leaf reticulate mutants, *dov1*, *cia1*, a*td2* and *alx13*, the predominantly expressed isoform of glutamine phosphoribosyl pyrophosphate aminotransferase (ATase2) is affected. Together with ATase1 and 3 it catalyzes the deamination of glutamine into glutamate which is the first step in the partially plastid-localized biosynthesis of purines and purine-derived cytokinins (Lundquist et al., 2014, Rosar et al., 2012). A possible involvement of IEP57 in the transport of purines or downstream products was therefore analyzed by exogenous application of inosine 5'- monophosphate (IMP), adenosine 5'- monophosphate (AMP), guanosine 5'- monophosphate as well as the cytokinin derivative

6-benzylaminorpurine (BAP). For this purpose, Col-0 wild-type and *At-IEP57*/popOFF line #1 plants were grown in hydroponic culture on non-inducing medium for 21 days and then transferred onto RNAi-inducing medium supplemented with 0,1, 1 and 5 mM IMP, AMP and GMP (Figure 24).

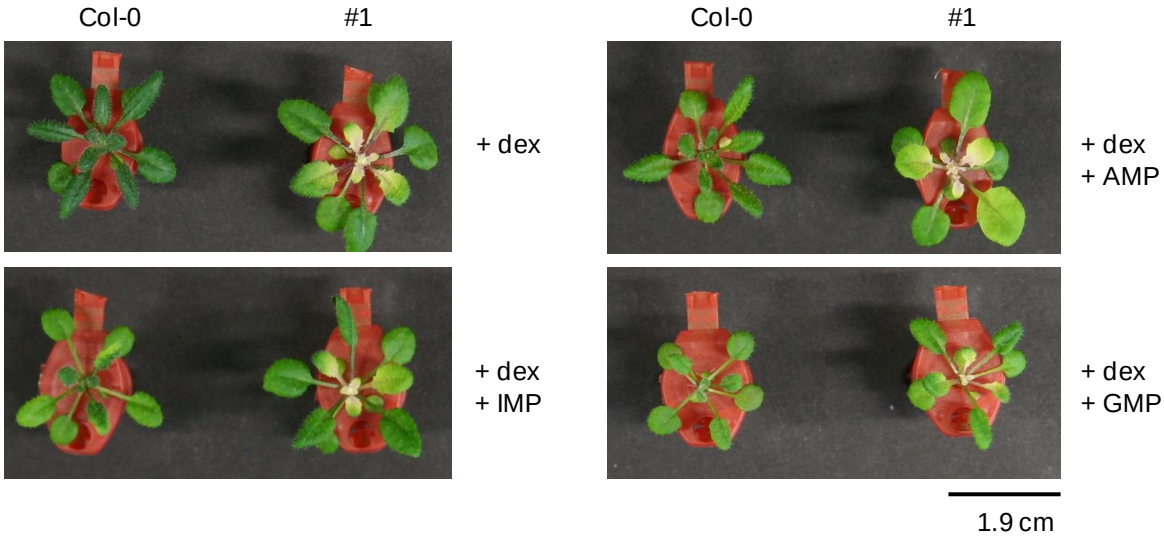

Figure 24: Feeding studies with the purines IMP, AMP and GMP

Representative 28-day-old plants of Col-0 wild-type and *At-IEP57*/popOFF line #1 (T3) homozygous plants grown in hydroponic culture non-inducing medium for 21 days. Pictures were taken 7 days after transfer onto inducing medium supplemented with 1 mM IMP (left lower panel), AMP (right upper panel) and GMP (right lower panel).

Daily monitoring for 7 days did not show any phenotypic alterations for any of the three tested substances (Figure 24). For BAP, seeds of Col-0 wild-type and *At-IEP57*/popOFF line #1 were directly sown onto RNAi inducing agar medium-containing plates supplemented with 0,1, 1, 10 and 100 nM BAP as described in Hung et al. (2004). Daily monitoring of the plants revealed no phenotypic alterations (data not shown).

3.2.5 IEP57 and the non-mevalonate pathway

Rescue of the *IEP57* mutant phenotype

The phenotype observed in 35S::*IEP57* transgenic lines is similar to the phenotype described by Hsieh et al. (2005) in 35S::*IspH* transgenic lines, in which the introduction of the *IspH* cDNA also led to transgene induced gene silencing of the respective *IspH* gene. This resulted in spontaneous chlorosis and the systemic spread of an albino phenotype in various

developmental stages and at several initiation sites. The encoded IspH protein functions as a non-mevalonate pathway enzyme involved in the biosynthesis of isoprenoids and localizes to the plastid stroma. Due to these phenotypic similarities, a possible role of IEP57 in the plastidic non-mevalonate pathway of isoprenoids was anticipated and an involvement of IEP57 in the transport of intermediate or end products of this pathway was tested. Two commercially available substances, 2-C-methyl-D-erythritol-2,4-cyclodiphosphate (MEcPP), an intermediate, and isopentenyl diphosphate (IPP), and end product of the non-mevalonate pathway were used for feeding studies in plants with an induced knock-down of *IEP57*. If the lack of functional IEP57 impairs the export of non-mevalonate pathway intermediates or end products from the chloroplast into the cytosol, external application of these substances would rescue the chlorotic phenotype. RNAi was induced in single *At-IEP57*/popOFF line #1 mutant plants grown in hydroponic culture for 14 days. Plants were then grown for 7 days until the phenotype had developed and were then transferred onto inducing medium containing 10 µM of MEcPP or IPP and monitored daily (Figure 25).

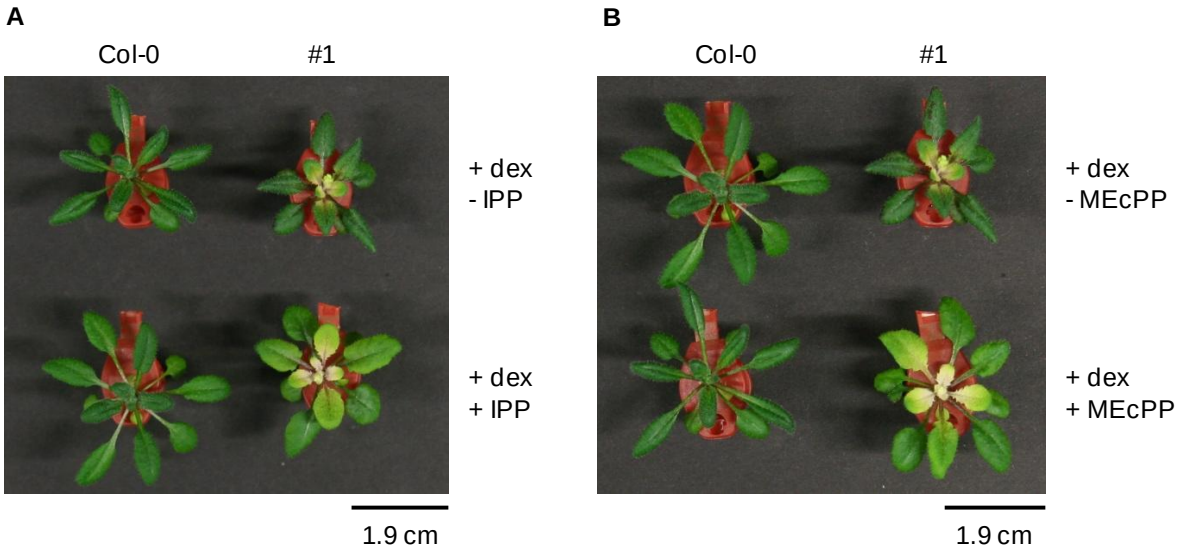

Figure 25: Feeding studies with IPP and MEcPP

Representative 28-day-old plants of Col-0 wild-type and *At-IEP57*/popOFF#1 (T3) homozygous plants grown in hydroponic culture. Plants were grown on ½ MS – sucrose for 14 days. Plants were then grown ½ MS – sucrose + 10 µM dexamethasone for seven days until the chlorotic phenotype developed. Pictures were taken after 28 days, 7 days after transfer onto ½ MS – sucrose + 10 µM dexamethasone and 10 µM isopentenyl pyrophosphate (IPP, A) or 10 µM 2-C-methyl-D-erythritol 2,4-cyclodiphosphate (MEcPP, B).

In a second approach, RNAi induction and supplementation of single *At-IEP57*/popOFF line #1 mutant plants with MEcPP and IPP occurred simultaneously after 21 days of growth (data not shown). In a third approach, a 10 µM MEcPP or IPP solution containing 0,01 % silwet-77 was applied externally onto the leaves of single *At-IEP57*/popOFF line #1 mutant plants by pipetting or by dipping and subsequent vacuum infiltration (data not shown). However, neither MEcPP nor IPP affected the development of the chlorotic *IEP57* RNAi phenotype in any of the approaches (Figure 25).

Induction of *HPL* expression by wounding

The non-mevalonate pathway intermediate MEcPP, a precursor of isoprenoids produced in the plastid was shown to act in retrograde signaling by inducing the expression of the stress responsive nuclear-encoded gene *HYDROPEROXID LYASE* (HPL), which encodes a plastid localized protein in the oxylipin pathway (Xiao et al., 2012.). The role of wounding in the induction of *HPL* induction is well established (Chehab et al., 2008, Chehab et al., 2006) and it was shown that plants treated with wounding stress accumulate endogenous MEcPP, which results in selective induction of *HPL* expression (Xiao et al., 2012). If IEP57 is involved in the export of MEcPP from the chloroplast, plants deficient in IEP57 should not be able to properly induce *HPL* expression in response to wounding stress. This was analyzed in 14- and 17-day-old Col-0 wild-type and *At-IEP57*/popOFF line #5 plants grown on agar medium-containing plates which were transferred either to inducing or to non-inducing agar-medium containing plates. 7 and 10 days after transfer, half of the RNAi induced and half of the non-induced plants were wounded with forceps in a way that every leaf of every plant was affected by tight compression. The other half of the plants was left unwounded and served as untreated controls. The reaction to wounding was allowed to proceed for 90 min before plants were harvested and frozen in liquid nitrogen. RNA was isolated, reversely transcribed into cDNA and *HPL* gene expression was analyzed using qRT-PCR (Figure 26).

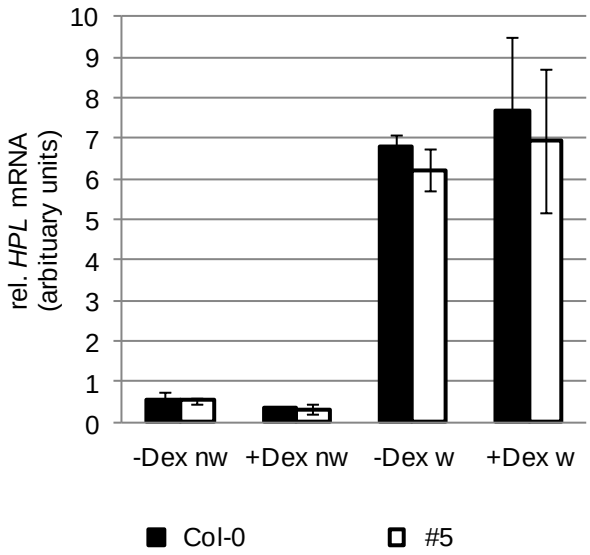

Figure 26: Induction of hydroperoxide lyase (HPL) after wounding

Relative expression levels of hydroperoxide lyase (HPL) in Col-0 wild-type (white bars) and *At-IEP57/*popOFF line #5 (black bars) (T3) homozygous plants. RNA was prepared from 17- day-old plants grown on non-inducing medium for 10 days and on non-inducing or inducing medium (-Dex/+Dex) for 7 days. Plants were either nonwounded (nw) or wounded (w) for 90 min before harvesting. The amount of mRNA (arbituary units, n=3, ±SD, 5 plants per replication) was normalized to 1000 actin transcript molecules.

Wild-type plants showed an increase of *HPL* expression after wounding stress under both, RNAi-inducing and non-inducing conditions. *HPL* expression also increased in *At-IEP57*/popOFF line #5 plants after wounding also under both, RNAi-inducing and non-inducing conditions (Figure 26).

3.3 OEP40 in the outer chloroplast envelope

In an approach to identify new proteins from the chloroplast envelopes, possibly involved in metabolite transport processes across the chloroplast membranes, the new outer envelope protein of 40 kDa (OEP40) was isolated from an outer envelope (OE) preparation from *Pisum sativum* (pea) due to its shifting running behavior when separated via SDS PAGE in the presence and absence of urea. This is a common feature of β-barrel pore forming proteins in the OE (Doctoral thesis Ingrid Jeshen, 2012, for an overview see Duy et al., 2007). After isolation of the cDNA for the respective proteins in pea and *Arabidopsis*, OEP40 was characterized *in silico* and the subcellular localization in the outer chloroplast envelope was confirmed. Further, an *Arabidopsis* T-DNA insertion line harboring the T-DNA insertion in the promoter region in front of the single exon of the *OEP40* gene was analyzed and shown to be a knockdown line for OEP40 with about 35 % of the wild-type expression level (compare Figure 31). Mutant plants further displayed an early flowering phenotype compared to wild-type plants when grown under low temperature conditions (Doctoral thesis I. Jeshen, 2012).

Aims of this part of the study on OEP40 were the further biochemical characterization of the protein in terms of its putative role in ion or metabolite transport. A second *Arabidopsis* T-DNA insertion line with the insertion disrupting the single exon of the gene was to be characterized genetically and phenotypically. Together with the mentioned knockdown line, this mutant was used to elucidate the metabolic events leading to the early flowering phenotype of *oep40* mutant plants.

3.3.1 Biochemical characterization of OEP40

Hydrophobicity analysis

To test whether OEP40 corresponds to an integral membrane protein or is just superficially attached to the membrane, OE vesicles prepared from *pea* were treated with high salt, high pH, urea and triton. After separation of membrane and soluble proteins by ultracentrifugation, pellet and supernatant fractions were separated via SDS-PAGE and analyzed by immunoblotting with specific antibodies raised against Ps-OEP40 and Ps-OEP37 as a control (Figure 27). Treatment with 1 mM NaCl removes proteins loosely attached to the membranes or to proteins integral to the membrane whereas 0.1 M Na_2CO_3, pH 11.3 removes proteins with tighter peripheral associations. Treatment with 6 M urea can

solubilize partly integral membrane proteins and stably integrated proteins can only be solubilized by treatment with 1 % of the membrane disrupting detergent Triton X-100 (Okamoto et al., 2001).

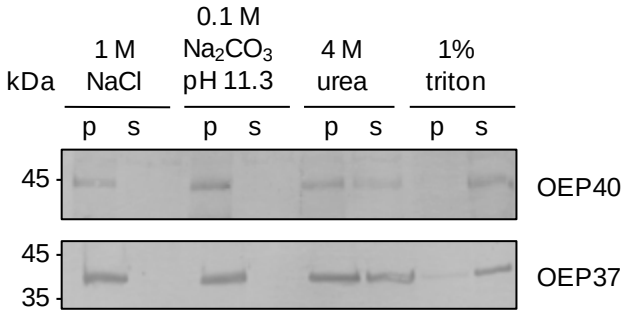

Figure 27: OEP40 is an integral protein of the outer chloroplast envelope membrane

Outer envelope preparation from *Pisum sativum* after treatment with 1 M NaCl, 0.1 M Na_2CO_3, pH 11.3, 4 M urea and 1 % Triton X-100. After ultracentrifugation, pelleted fractions (P) containing insoluble and supernatant fractions (S) containing soluble proteins were separated via SDS PAGE and analyzed by immunoblotting with a specific antibody directed against Ps-OEP40. An antibody against Ps-OEP37, a β-barrel protein integral to the outer chloroplast envelope (Schleiff et al., 2003) was used as a control. 20 µg of total protein were used for one treatment, the obtained samples of P and S fractions were separated equally for analysis with the mentioned antisera. Numbers indicate the molecular mass in kDa.

Treatment with high salt and high pH conditions was not sufficient to solubilize OEP40 from the outer chloroplast membrane because bands corresponding to Ps-OEP40 were only present in the pellet fraction (Figure 27) which indicates that OEP40 is not only superficially attached to the membrane surface. Urea treatment was able to only partly solubilize OEP40 because a strong band was still present in the pellet fraction but a second band appeared in the supernatant fraction containing soluble proteins. Finally, treatment with the detergent Triton X-100 fully solubilized OEP40 from chloroplast OE membranes and the corresponding band is only present in the soluble protein fraction. OEP40 behaves like the already described β-barrel forming outer envelope protein OEP37 (Figure 27, lower panel, Schleiff et al., 2003) and therefore most likely corresponds to an integral membrane protein of the outer chloroplast envelope as well.

Electrophysiological analysis of OEP40

To address the putative role in metabolite transport, the channel activity of OEP40 was analyzed using the planar lipid bilayer technique in collaboration with the group of Prof. Dr. Richard Wagner (Biophysics, University of Osnabrück). In a first approach, Ps-OEP40 was heterologously overexpressed in *E. coli* BL21 cells from the pET21d plasmid vector with a 6xhis tag fused to the proteins C-terminus. The protein was subsequently purified from cleaned inclusion bodies by Ni-affinity chromatography and the fractions containing the protein after imidazole elution were sent to Osnabrück for reconstitution into liposomes and electrophysiological measurements (Figure 28).

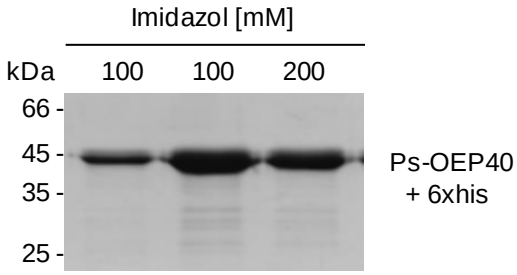

Figure 28: Purification of overexpressed Ps-OEP40 for electrophysiological measurements
Separation of samples from eluted fractions after Ni-affinity chromatography purification of overexpressed Ps-OEP40+6xhis, 12.5 % SDS gel, coomassie stained, load: 10 µl of 500 µl eluted fractions, numbers indicate the molecular mass in kDa.

In a second approach, the Ps-OEP40 protein was *in vitro* translated from the pET21d vector in reticulate lysate using the coupled transcription/translation system of the TNT Kit (Promega, Madison, WI, USA). After the reaction, samples were ultracentrifuged and the Ps-OEP40 protein was found to be in the supernatant when analyzed with a specific antibody after separation via SDS PAGE and immunoblotting (Figure 29, A). The protein containing supernatant was sent for reconstitution into liposomes and electrophysiological measurements. The supernatant of a reaction that did not contain plasmid DNA was used as a negative control. In a third approach, *OEP40* from pea was first *in vitro* transcribed from the pET21d plasmid vector using T7 polymerase and the resulting RNA was used to *in vitro* translate the protein using wheat germ lysate. The resulting translation product was purified via its 6xhis tag by Ni-affinity chromatography and the presence of the Ps-OEP40 protein in

the eluted fractions was confirmed by SDS PAGE and coomassie staining. The protein containing fractions were pooled, concentrated and separated by SDS PAGE. The resulting protein pattern was visualized by reversible imidazole/zinc staining. Two bands running at approximately 45 kDa, the expected size for Ps-OEP40 fused to the 6xhis tag, were excised from the gel, destained and sent for extraction of the contained protein, reconstitution into liposomes and electrophysiological measurements. Parts from each band were inserted into the wells of an SDS gel to separate the contained proteins. After immunoblotting with a specific antibody directed against Ps-OEP40, the presence of the protein was confirmed as expected in band two (#2). Band one (#1) was therefore used as a negative control (Figure 29, B).

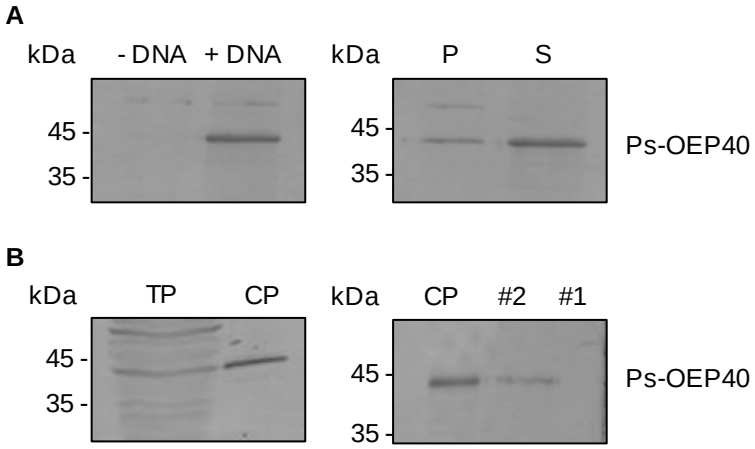

Figure 29: *in vitro* translation of Ps-OEP40 for electrophysiological measurements

A) Samples of in vitro translated Ps-OEP+6xhis using the TNT Kit (Promega). One reaction not containing DNA was used as a negative control. Left panel: 5 µl of the 50 µl reaction volume with and without DNA. Right panel: pellet (P) and supernatant (S) fraction after ultracentrifugation of the reaction assay containing DNA, 5 µl of the supernatant (~48 µl) and 5µl of the resuspended pellet fraction (in 48 µl 50 mM Tris/HCl pH8, 100 mM NaCl). B) Samples of in vitro translated Ps-OEP40+6xhis using wheat germ lysate. Left panel: 5 µl of translation product (TP) of a 100 µl reaction volume and 5 µl of the subsequently purified and concentrated Protein (CP) Right panel: 5 µl of purified and concentrated protein (CP) were loaded and excised gel slices (band #2 and band #1) of previously separated CP were inserted into the wells of an SDS gel to separate the contained proteins. All samples from A) and B) were separated on 12.5 % SDS gels and analyzed via immunoblotting with a specific antibody directed against Ps-OEP40. Numbers indicate the molecular mass in kDa.

Electrophysiological measurements

The obtained proteins from all three approaches could be successfully reconstituted into liposomes and were therefore functionally refolded into the membrane of lipid vesicles which were subsequently used for planar lipid bilayer measurements. This technique allows the analysis of the electrical properties of biological membranes and of channels inserted into these membranes. If the putative channel protein of interest is inserted into a planar lipid bilayer, it forms the main electrical connection between two electrolyte-filled half-chambers. Measurements are done in voltage clamp mode via two electrodes, one in each of the half-chambers. This way, an electric potential can be applied across the membrane and in case of an opening of the channel protein, the resulting ion current is recorded. Current changes due to conformational changes of the protein such as opening and closing as well as by interaction with added effector molecules can be monitored and quantified (Doctoral dissertation T. Götze, 2009). In the case of Ps-OEP40, after application of an electronic potential of ±120 mV in symmetric conditions at 250 mM in 10 mM MOPS/Tris pH7 in both cis/trans half-chambers, a current trace was observed which implies that Ps-OEP40 forms an ion channel with two conductance states of 400 and 540 pS (Figure 30). Ps-OEP40 forms a pore with a diameter of about 2 nm and in asymmetric electrolyte conditions Ps-OEP40 forms a cation selective channel (personal communication with Prof. Dr. Richard Wagner, Biophysics, University of Osnabrück, Germany). For all three approaches described, channel activity could be observed for Ps-OEP40. Since the proteins from all three approaches reacted identically to the analyzed parameters, they are not presented separately. Figure 30 representatively shows the single channel recordings for Ps-OEP40 from the first approach using recombinant Ps-OEP40 protein overexpressed in *E. coli*.

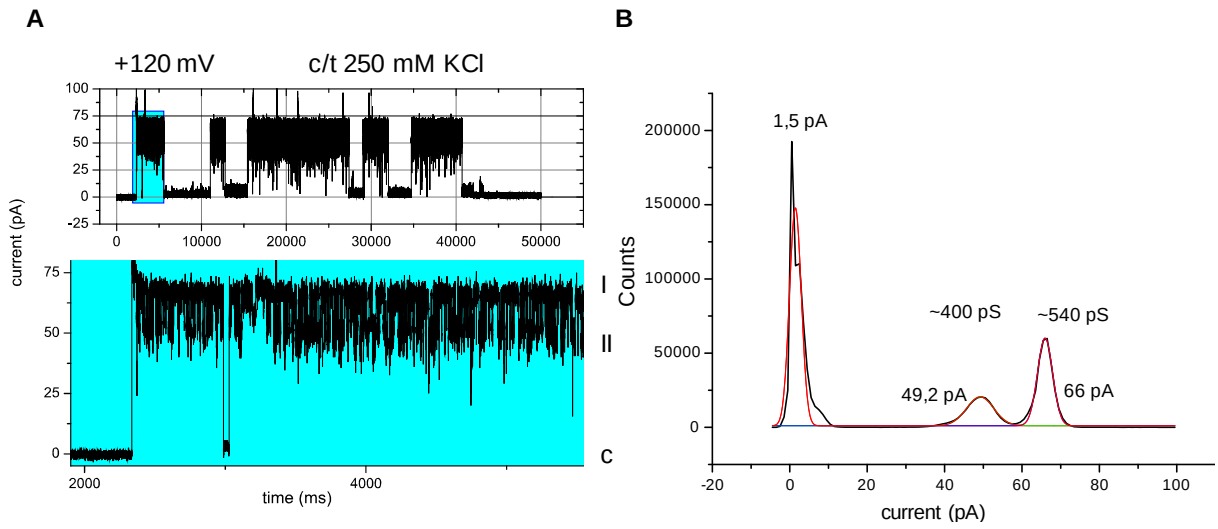

Figure 30: Single channel recording of Ps-OEP40 in planar lipid bilayer measurements

A) Single channel currents at V_m=120 mV in 250 mM KCl in both cis/trans half-chambers, current trace of the bilayer after a fusion event of recombinant Ps-OEP40 overexpressed in *E. coli* (lower pannel magnification of blue box in upper pannel) showing two conductance states (I, II) and the closed state (c). B) Histogram of the single channel currents at V_m=120 mV showing the two conductance states at 400 and 540 pS.

3.3.2 Mutation of OEP40 in *Arabidopsis thaliana*

At the beginning of this study, only one T-DNA insertion line for *OEP40* in *Arabidopsis*, *oep40-1* (SAIL_266_D10) was available which harbors the T-DNA insertion in the promoter region of the gene at -25 bp. It was shown via qRT-PCR that *oep40-1* corresponds to a knockdown line with about 35 % of wild-type transcript level (Doctoral thesis I. Jeshen, see Figure 31). When grown under various conditions, homozygous *oep40-1* mutant plants did not display any visible phenotypic differences when compared to wild-type plants except when grown at low temperature conditions. Under a longday light regime with a constant temperature of 10 °C, *oep40*-1 mutant plants showed earlier bolting, faster growth and earlier flowering than the wild-type (Doctoral dissertation I. Jeshen, Figure 32).

With the beginning of this study, a second T-DNA insertion line for *OEP40* in *Arabidopsis*, *oep40-3* (SAIL_759_A01) with the T-DNA insertion in the beginning of the single exon of the gene (Figure 31, A) became available. The plants were propagated to the F3 generation, PCR genotyped with gene and T-DNA specific primer pairs and segregated homozygous, heterozygous as well as wild-type lines were selected.

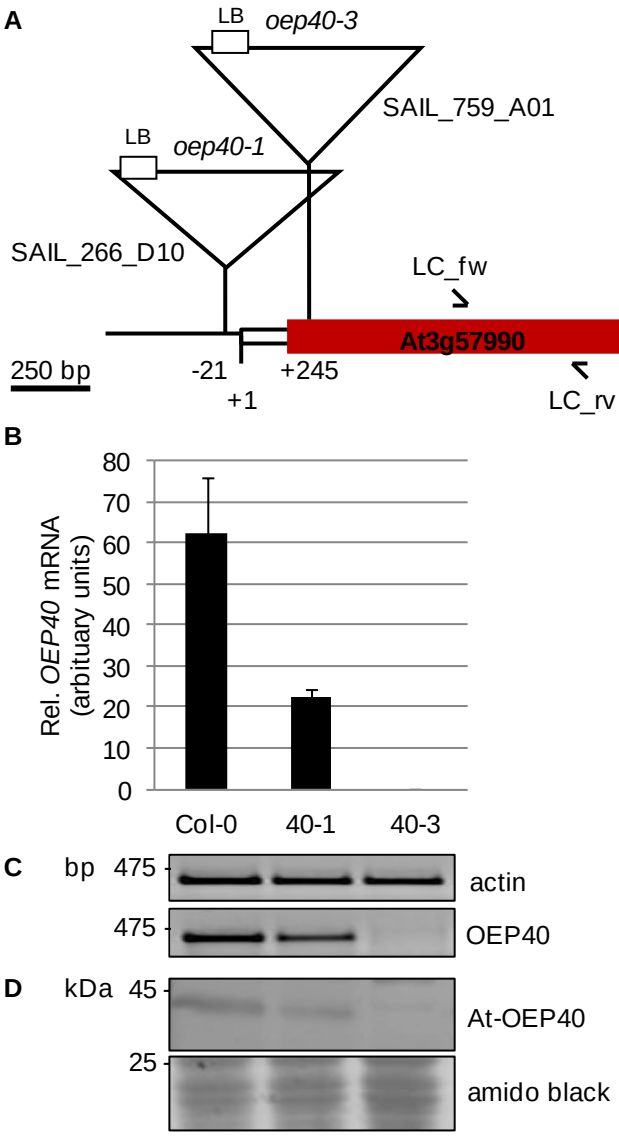

Figure 31: *oep40-1* corresponds to a knock-down and *oep40-3* to a knock-out line for *OEP40* in *Arabidopsis*

A) Schematic representation of *OEP40* from *Arabidopsis* (At3g57990). The red arrow indicates the single exon of the gene, the white bars the untranslated regions on the 5‘ and 3‘ ends. Insertion sites of T-DNAs in lines SAIL_266_D10 (*oep40-1*) and SAIL_759_A01 (*oep40-3*) are indicated by triangles. Open triangles indicate the binding sites for the gene specific primers used for RT-PCR (LC_fw, LC_rv).B) Quantification of *OEP40* mRNA using qRT PCR. mRNA was prepared from 14-day-old seedlings of Col-0 wild-type as well as *oep40-1* and *oep40-3* homozygous mutant plants. The amount of mRNA (arbitrary units, n=3±SD) was normalized to 1000 actin transcript molecules. C) PCR products of actin (435 bp) and *OEP40* (424 bp) after RT-PCR on cDNA prepared as in B) D) Immunoblot of total membrane protein extract (TMPE) from Col-0 wild-type as well as *oep40-1* and *oep40-3* homozygous plants. TMPE (110 µg/lane) was separated via SDS PAGE and analyzed with a specific antibody directed against At-OEP40. Staining of the lower part of the PVDF membrane with amidoblack was used as a loading control. Numbers in C) indicate the numbers of basepairs, numbers in D) indicate the molecular mass in kDa.

By amplification of a DNA fragment flanking the insertion site with T-DNA specific primers and subsequent sequencing, the specific T-DNA insertion site was mapped to +245 bp which corresponds to 47 bp after the translation start. To test whether the T-DNA disruption in the single exon led to true knockout mutants of *OEP40* in *Arabidopsis*, RNA from 14-day-old seedlings of the T4 generation was prepared and reversely transcribed into cDNA. The presence of *At-OEP40* transcripts was analyzed using semiquantitative RT-PCR which showed a clear product in wild-type, a reduced cDNA in *oep40-1* mutant and no residual product for *oep40-3* mutant plants (Figure 31, C). This result was confirmed by qRT-PCR (Figure 31, B).

An extract of total membrane protein (TMPE) was prepared from leaves of mature wild-type as well as *oep40-1* knockdown and *oep40-3* knockout plants and equal amounts of protein were separated via SDS PAGE and subjected to immunoblotting with the At-OEP40 antiserum. In the TMPE from wild-type, a distinct band corresponding to At-OEP40 at the expected size of around 45 kDa could be detected which was significantly weaker in the *oep40-1* knockdown and completely absent in the *oep40-3* knockout line (Figure 31, D). Therefore, *oep40-3* corresponds to a knockout line whereas *oep40-1* is a knockdown line for *At-OEP40*.

Phenotypic analysis of *OEP40* mutant plants

To confirm that the early flowering phenotype under low temperature conditions observed in the *oep40-1* mutant is due to the lack of OEP40 and to check whether the phenotype is also occurring in *oep40-3* knockout plants, a detailed phenotypic analysis of Col-0 wild-type, *oep40-1* and *oep40-3* plants was conducted. To accelerate the occurrence of the phenotype under the otherwise slow growth conditions at 10 °C, plants were preincubated at 21 °C for 7, 14 and 21 days. When plants were preincubated for 7 days at 21 °C, the early flowering phenotype at 10 °C could still be clearly observed whereas the difference in flowering time between wild-type and mutant plants decreased with elongation of the preincubation time at 21 °C (data not shown). Therefore, a 7-day incubation period at 21 °C prior to the transfer to 10 °C was chosen for all subsequent experiments. Representative individuals for the early flowering phenotype at 10 °C in *oep40* mutant plants compared to wild-type are shown in Figure 32.

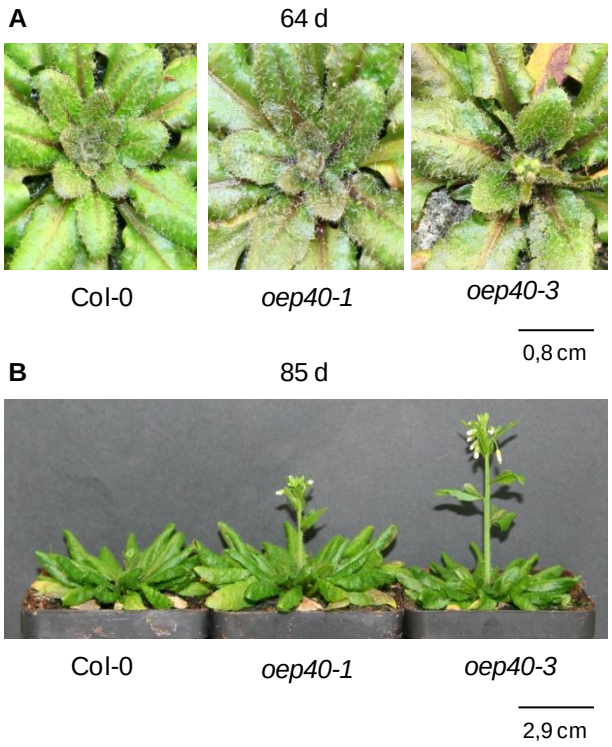

Figure 32: Phenotype of *oep40* mutant plants under low temperature conditions
Representative individuals of A) 64-day-old and B) 85 day-old-plants of Col-0 wild-type as well as *oep40-1* and *oep40-3* homozygous mutant plants. All plants were preincubated 7 d at 21 °C before transfer to 10 °C, age was counted as days after sowing.

For a detailed phenotypic analysis, days to bolting, days to flowering, number of rosette leaves and number of cauline leaves were recorded. A detailed list of all parameters recorded is given in Table 7. Daily monitoring of 27 plants from each, Col-0 wild-type, *oep40-1* and *oep40-3* mutants grown under low temperature conditions showed a significantly earlier bolting in mutant than in wild-type plants. While Col-0 needed a mean of 66 days until the inflorescence had elongated to 0.5 cm, *oep40-1* and *oep40-3* mutant plants only needed a mean of 59 and 60 days, respectively (Figure 33, A). A significant difference in approximately the same range could also be observed when days until flowering were recorded at 10 °C. While Col-0 wild-type needed about 96 days until the first flower appeared, *oep40-1* and *oep40-3* mutant plants showed the first flower after a mean of 87 to 88 days (Figure 33, B). Determination of the total leaf number at a primary inflorescence length of 15 cm showed that Col-0 wild-type produced a mean of 33 rosette and 8 cauline leaves whereas *oep40-1* and *oep40-3* mutant plants only produced an average of 27 to 28

rosette leaves and 7 to 8 cauline leaves at low temperature conditions (Figure 33, C). No significant differences in days to bolting, days to flowering and leaf numbers could, however, be detected in the set of control plants grown at 21 °C (Figure 33, D, E, F). The early flowering phenotype at low temperature conditions previously observed in *oep40-1* knockdown plants could therefore be confirmed in *oep40-3* knockout lines and the observed differences in plant development due to the reduction or lack of the OEP40 protein therefore seem to be connected to the ambient growth temperature.

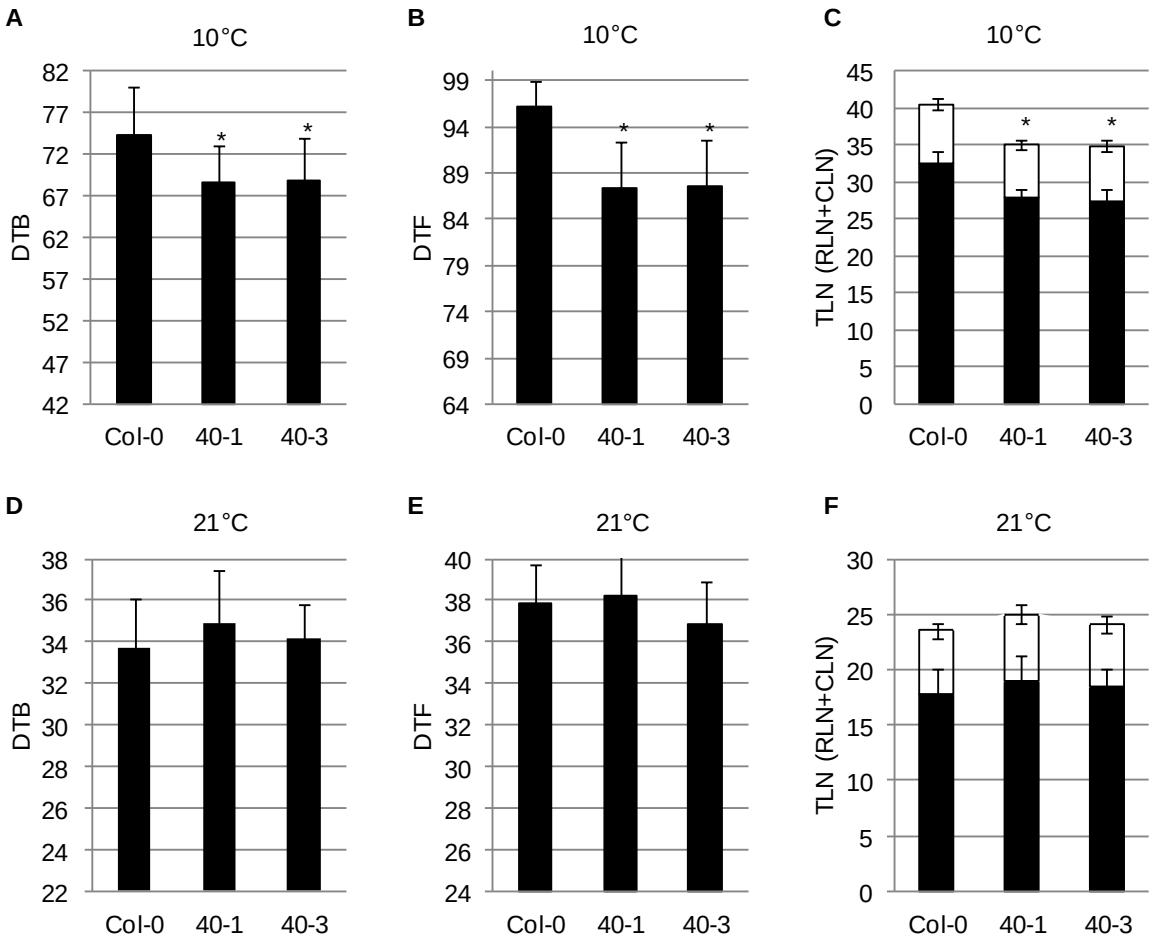

Figure 33: Detailed phenotypic analysis of *oep40* mutant plants

Recording of days to bolting [DTB, (A) and (D)], days to flowering [DTF, (B) and (E)] and total leaf number [TLN, (C) and (F)] in Col-0 wild-type as well as *oep40-1* and *oep40-3* homozygous mutant plants grown at 10 °C (preincubation: 7d at 21/16 °C) [(A) – (C)] and 21/16 °C [(D) – (E)] (n=27±SD). In (A) – (C) asterisks indicate significant differences in DTB, DTF and TLN in mutant plants compared to Col-0 ($p<0.05$). In (C) and (F), black bars represent rosette leave numbers (RLN) and white bars cauline leave number (CLN).

3.3.3 Analysis of floral induction in *oep40* mutant plants

Because OEP40 might be involved in metabolite transport, it is possible that the early flowering phenotype under low temperature conditions is due to a metabolic imbalance caused by the reduction of the lack of the OEP40 protein in the outer chloroplast envelope. This might lead to a change in the amount of inductive signals which are integrated into the complex network of the induction of flowering under the otherwise non-inductive conditions at 10 °C. However, once the phenotype can be observed in about 60-day-old *oep40* mutant plants at the time of bolting, the decision to flower has long been made and the transition from the vegetative to the reproductive state has already taken place. Consequently, any metabolic events that might be involved in producing signals needed to either induce flowering under optimal conditions or to repress flowering as long as conditions are not ideal yet, have to be analyzed earlier in plant development. It was therefore necessary to define a time point at which wild-type and *oep40* mutant plants differ in floral induction prior to the described visible phenotypic differences. In order to define a time frame suitable to harvest plant material for metabolite analyses, two approaches were used. First, expression analysis of various genes involved in the flowering induction process was conducted via qRT-PCR using a flowering gene primer platform available at the group of Prof. Dr. Mark Stitt at the Max Planck institute for molecular plant physiology, Golm, Germany. A time frame from 38 to 54 days was analyzed and plant material was harvested every 4 days at the end of the light period from Col-0 wild-type as well as *oep40-1* and *oep40-3* mutant plants with three biological replicates per line consisting of three individual plants for each time point. After RNA isolation and digestion of chromosomal DNA, cDNA was generated and qRT-PCR was carried out with 4 technical replicates each. A detailed list of the 90 genes analyzed is given in appendix X. An exact time point for floral transition which occurs earlier in *oep40* mutant plants than in Col-0 wild-type and reflects the differences of the phenotypic analysis could not be determined with this approach. Only for a minority of the 90 genes, changes in expression in the analyzed time frame could be detected (Figure 34, A).

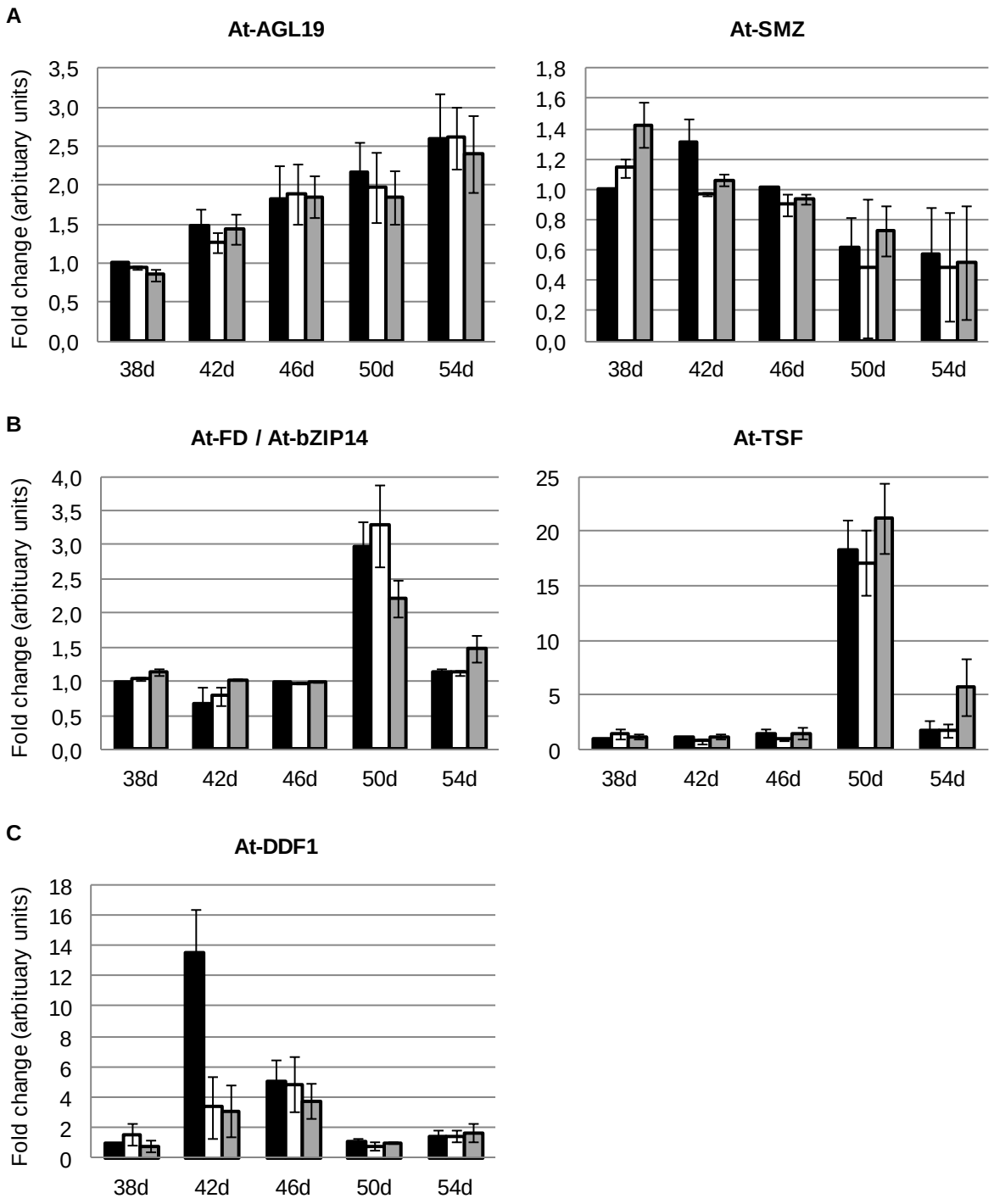

Figure 34: Expression of flowering genes in *oep40* mutant plants

Quantification of mRNA of the stated flowering genes using qRT-PCR. mRNA was prepared from Col-0 wild-type (black bars) as well as *oep40-1* (white bars) and *oep40-3* (grey bars) mutant plants grown under low temperature conditions 38, 42, 46, 50 and 54 days after sowing. The amount of mRNA was normalized to a reference gene index of four ubiquitously expressed genes (UBI, TUB, SAND, PDF2). Col-0 at 38 days was set to one and values are given as the respective fold changes (arbituary units). Error bars denote the SD of three biological replicates with four technical repetitions each.

Expression of factors promoting flowering was expected to increase over time whereas expression of factors repressing flowering should decrease. This was observed for *At-AGL19* (At4g22950, transcription factor promoting flowering) and *At-SMZ* (At3g54990, transcription factor repressing flowering, Figure 34, A) although a shift to earlier expression of the promoter *At-AGL19* in *oep40* mutant plants or a delay in expression of the repressor *At-SMZ* in Col-0 wild-type could not be observed. In all three lines, promoter and repressor increased and decreased gradually in the analyzed time frame, respectively. In most cases of changes in expression, however, an increase in transcript levels from day 46 to day 50 was observed which decreased again from day 50 to day 54 in all three lines analyzed. Figure 34 B shows two representative examples, *At-FD* (also *At-bZIP14*, At4g35900) and *At-TSF* (At4g20370). The same expression course was observed for *At-AGL8* (also *At-FUL*, At5g60910), *At-AGL7* (also *At-AP1*, At1g69120) and *At-FBGI* (At1g22770) (data not shown). All mentioned factors promote flowering but a shift to an earlier increase in transcript levels in the early flowering *oep40* mutant plants compared to Col-0 wild-type was not detected. The only case in which Col-0 wild-type displayed a different expression pattern than the *oep40* mutant plants is *At-DDF1* (At1g12610), a transcription factor expressed in response to various stresses including cold stress (Figure 34, C). *At-DDF* transcription only slightly increased in *oep40* mutant plants between 42 and 46 days whereas a drastic increase was detected in Col-0 wild-type after 42 days which decreased again after 46 days.

In a second approach, the transition to flowering was analyzed morphologically in the apices of Col-0 wild-type as well as *oep40-1* and *oep40-3* mutant plants. Emerging flower primordia were visualized by RNA *in situ* hybridization with a *LEAFY* (*LFY*) probe which is a marker gene for flower primordia but can also be weakly expressed in leaves (Dr. V. Wahl, personal communication). Plants were grown under low temperature conditions and meristem samples were collected 34 to 56 days after sowing (das) every two days by removing all but the smallest leaves or flowers and subsequent fixation. Dehydration, embedding into wax, sectioning and hybridization were carried out by Dr. V. Wahl (MPI of molecular plant physiology) as described in Wahl et al., 2013 (supplementary materials). After hybridization, the signal was detected colorimetrically and histological sections were imaged via microscopy and a digital camera (Figure 35).

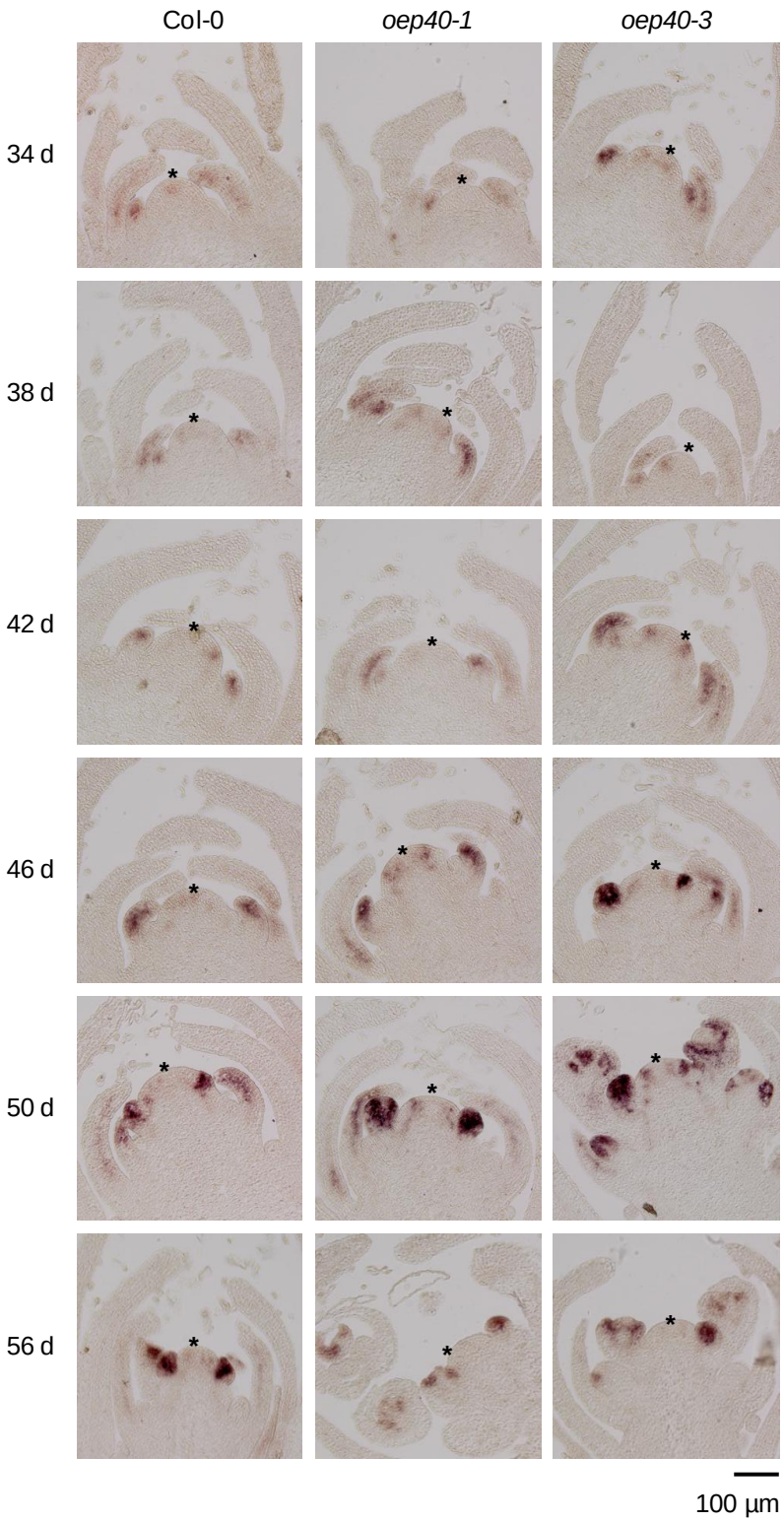

Figure 35: Floral transition occurs earlier in *OEP40* mutant lines compared to wild-type

Emergence of flower primordia was scored by RNA *in situ* hybridization with a *LEAFY* probe on longitudinal sections of Col-0 wild-type as well as *oep40-1* and *oep40-3* mutant lines. Sections were prepared from apices of plants grown under low temperature conditions and harvested every second day from 34 to 56 days after sowing. Asterisks indicate the meristem summit.

The distribution of the detected *LFY* signal to the left and the right of the meristem summit (Figure 35, asterisks) shows, that *oep40* mutant plants clearly express the floral primorida marker *LFY* earlier than wild-type plants with *noep40-3* knockout mutants being slightly ahead of *noep40* knockdown mutants. Compared to wild-type meristems, mutants show clearly developed flower primordia at earlier stages.

4 Discussion

4.1 PRAT2 in the inner chloroplast envelope

The aim of the work on the PRAT2 proteins of the inner chloroplast envelope was the further characterization of these proteins in *Arabidopsis* and their integration into plant metabolism in order to assign a functional role to these members of the PRAT family of proteins (for an overview see Murcha et al., 2007, Pudelski et al., 2010). For this purpose, two existing double loss-of-function mutants for *PRAT2.1* and *PRAT2.2* were analyzed regarding their metabolic status in comparison to wild-type plants under longday and continuous light conditions. These studies revealed that the severe chlorotic phenotype of *prat2-dm* mutant plants (see Figure 3) observed under longday conditions improved in continuous light with mutants almost resembling wild-type plants during the seedling stage. Phenotypic analysis under several light conditions (Figure 4) showed that the exposure to a phase of darkness during a 24 hour growth period leads to the manifestation of the described phenotype independent of the length of the dark phase.

PRAT2 and POR

Due to the phenotypic observations, the cause for the severe phenotypic reaction of *prat2-dm* mutant plants most likely occurs during these dark phases. Due to the obvious defect in chlorophyll biosynthesis, a possible accumulation of toxic intermediates of this pathway was assumed. Chlorophylls, the pathway's end products, are the most abundant tetrapyrroles in plants and occur in a protein-bound form. In this state, they are able to transfer absorbed light energy. Their biosynthetic precursors, however, mainly occur in a free, non-bound form and, when illuminated, act as photosensitizers producing highly toxic free radicals causing oxidative damage (Meskauskiene et al., 2001 and references therein). It is therefore necessary to keep the steady state level of chlorophyll biosynthetic intermediates during the daytime to a minimum. In the dark, chlorophyll biosynthesis only proceeds until the formation of protochlorophyllide, which is one of the major chlorophyll biosynthetic intermediates accumulating during the night. In angiosperms, the reduction of protochlorophyllide to chlorophyllide is catalyzed by NADPH:protochlorophyllide oxidoreductase (POR) in a light-dependent step (for an overview see Tanaka and Tanaka, 2007, Moulin and Smith, 2005). For this reaction, functional ternary complexes of the

substrate protochlorophyllide, the co-factor NADPH and the enzyme POR have to be formed (Masuda et al., 2003). In *prat2*-dm mutant lines, all three *Arabidopsis* isoforms of POR were found to be downregulated. This reduction was confirmed on mRNA and protein level (see Figure 6) and lead to the assumption that the reduced amount of POR is not able to sufficiently convert protochlorophyllide produced during the dark phase, thereby maybe causing it to accumulate to toxic concentrations. The analyses of the levels of chlorophylls and chlorophyll biosynthetic intermediates in *prat2-dm* mutant plants, however, did not reveal an accumulation of protochlorophyllide but an overall reduction of all analyzed substances compared to wild-type levels (Doctoral thesis S. Kraus, 2010). This overall reduction of chlorophyll biosynthesis in *prat2-dm* mutant plants was also confirmed on the transcript level of the respective enzymes of the pathway by DNA microarray analysis. In this current study, *POR* transcript levels were analyzed in etiolated seedlings during the greening process (see Figure 5) and the reduction of all three isoforms was again observed. However, the *POR* expression patterns in response to light otherwise were as in wild-type and in accordance with published results. POR A performs a specialized function during the initial stages of greening and *POR A* expression rapidly declines within hrs of illumination (Armstrong et al., 1995). Expression of *POR C*, in contrast, is induced by light (Oosawa et al., 2000, Su et al., 2001). *POR B* was reported to decrease in the first hrs of greening and to reaccumlate during illumination (Armstrong et al., 1995). Not only the light regulated expression of the three *POR* isoforms but also the activity of POR did not seem to be affected in *prat2-dm* mutant plants. Illumination of etiolated seedlings with a short flash of light revealed decreased levels of protochlorophyllide and chlorophyllide but the conversion rate was comparable to the one in wild-type seedlings (data not shown). In summary, the data suggest that the ternary POR complexes together with the substrate protochlorophyllide and the cofactor NADPH are assembled correctly in *prat2-dm* mutant plants and that POR is not impaired in its protochlorophyllide-reducing activity. The significantly reduced amounts of functional POR are sufficient to convert the also reduced amounts of protochlorophyllide and a role of the PRAT2 proteins in the import or assembly of functional POR is therefore unlikely.

PRAT2 and SAM

Instead of protochlorophyllide, the analyses of the levels of chlorophyll biosynthetic intermediates in *prat2-dm* mutant plants revealed increased levels of magnesium protoporphyrine IX (MgPP IX). MgPP IX is formed by the ATP-dependent insertion of magnesium into protoporphyrine IX (PP IX) by the enzyme magnesium chelatase which marks the entry into the chlorophyll branch of tetrapyrrole biosynthesis (Walker and Willows, 1997). Subsequently, MgPP IX is methylated by the enzyme Mg protoporphyrine IX methyltransferase (MgMT) in an S-adenosylmethionine (SAM) dependent step resulting in the formation of magnesium protoporphyrine IX monomethyl ester (MgPP IX MoMe). In *Arabidopsis*, the enzyme is located at both, envelope and thylakoid membranes (Block et al., 2002) and forms a ternary complex with its substrate MgPP IX and the methylgroup donor SAM (Shepherd and Hunter, 2004). Possibilites for the accumulation of MgPP IX could be that the functionality of the MgMT enzyme is impaired due to the lack of the PRAT2 proteins in the inner chloroplast envelope or that MgPP IX can only be sufficiently exported from the chloroplast. Like the other enzymes of chlorophyll biosynthesis, MgMT (At4g25080, *At-CHLM*) was shown to be downregulated on transcript level and also protein levels were decreased under longday conditions.

SAM is an essential metabolite for all organisms because it serves as the predominant donor of methyl groups in reactions catalyzed by methyltransferases. In plants, SAM is produced solely in the cytosol by several soluble isoenzymes, which lack organellar targeting sequences making mitochondria and chloroplasts strictly dependent on SAM import from the cytosol (for an overview, see Bouvier et al., 2006). SAM is used by several plastid methyl transferases whose substrates range from prenyllipids such as chlorophylls, plastochinones and tocopheroles to plastid DNA and Rubisco (Bouvier et al., 2006 and references therein). In the course of the methylation, each molecule of SAM releases one molecule of S-adenosylhomocysteine (SAHC) which acts as an inhibitor of SAM-dependent methyltransferases for example in the methylation of MgPP IX to MgPP IX MoMe or the methylation of γ-tocopherol to α-tocopherol (Shepherd et al., 2003, Koch et al., 2003). Therefore, the efficiency of methyl transferases depends on the efficient removal of SAHC via SAHC hydrolase, a cytosolic enzyme catalyzing the hydrolysis of SAHC into adenosine and homocysteine. Chloroplasts thus have to import cytosolic SAM and export SAHC. In

Arabidopsis, this exchange was shown to be mediated by the plastid SAM TRANSPORTER1 (SAMT1, Bouvier et al., 2006). Homozygous T-DNA knock-out mutants display a pale-green leaf phenotype and severe growth retardation, which is similar to the phenotype observed in the *prat2-dm* plants. Further, expression analysis revealed *PRAT2.1* among the 68 genes contained in a highly correlated cluster with *SAMT1* (Bouvier et al., 2006). However, levels of SAM and S-methyl-5'-thioadenosin (MTA), a product from the conversion of SAM to 1-aminocyclopropane-1-carboxylate (ACC), were not significantly changed in *prat2-dm* mutant plants compared to wild-type (see Figure 7). Also the levels of tocopherols, which are synthesized in the chloroplast in a SAM-dependent step (for an overview see Hussain et al., 2013, Soll et al., 1985) were not significantly changed in *prat2-dm* mutant plants compared to wild-type, which confirms the overall observation, that the lack of the PRAT2 proteins does not lead to insufficient SAM levels and that an undermethylation status does not seem to be the cause for the severe phenotype.

In plastids, SAM acts as an allosteric activator of threonine synthase (Curien et al., 1998) and thereby its presence controls the flux of *O*-phosphohomoserine into the biosynthesis pathways of threonine and methionine. If, due to the lack of the PRAT2 proteins, SAM was not available in sufficient amounts in the chloroplast, the SAM-mediated activation of threonine synthase could not take place which would result in a higher flux of *O*-phosphohomoserine into the methionine branch of the synthesis pathway. This then would lead to an increase of methionine and a decrease of threonine levels in *prat2-dm* mutant plants. Indeed, an increase of methionine levels was detected but levels of threonine, however, were not decreased but increased in *prat2-dm* mutant plants (see Figure 9, data for threonine not shown). Again, this indicates, that sufficient amounts of SAM are present in the chloroplast when the PRAT2 proteins are lacking.

PRAT2 and thiol-group amino acid metabolism

Previous metabolite analyses in *prat2-dm* mutant plants revealed that metabolite levels that were changed under longday conditions converged back to wild-type levels under continuous light (Doctoral thesis S. Kraus, 2010). Overall, a shift of the ratio of carbon- and nitrogen-containing compounds towards nitrogen was observed. The extension of the metabolite analysis with a set of samples harvested before the onset of light in longday conditions did not reveal any significant changes in the metabolite pattern of *prat2-dm*

mutant plants except for aspartic acid and phenylalanine. For those two amino acids, increased levels could only be detected in samples harvested in the dark. Overall, an increase in amino acid levels in *prat2-dm* mutant plants was observed with the most drastic increase for cysteine.

Interestingly, a reversed phenotypic effect was observed for knockout plants for the *CS26* gene encoding a plastid protein with S-sulfocysteine (S-Cys) activity (Bermúdez et al., 2010). Here, mutant plants displayed a more severe phenotype under continuous light conditions and improved when the phase of darkness was prolonged. Under longday conditions, the *cs26* mutant showed elevated levels of reactive oxygen species, which were absent when grown under shortday conditions therefore increasing with the length of the light period. In *prat2-dm* mutant plants, in contrast, the ROS levels decreased with the length of the light period (Doctoral dissertation S. Kraus, 2010). It could therefore be speculated, that CS26 and the PRAT2 proteins of the chloroplast are involved in the same metabolic pathway of thiol group amino acids.

Because of the opposite phenotype in the *cs26* mutant with a defect in plastidic S-sulfocysteine synthesis, the accumulation of MgPP IX, which is methylated in a SAM-dependent step and the increased levels of cysteine and methionine in *prat2-dm* mutant plants, a possible role of the PRAT2 proteins in thiol compound transport was further investigated. The increased cysteine levels in *prat2-dm* plants were confirmed in a renewed analysis of metabolites involved in thiol compound metabolism (Figure 12). Due to the use of internal standards, absolute values of metabolite contents were obtained this time. Cysteine levels under both, longday and continuous light, were increased by about 2-fold with levels under continuous light being generally higher. The cysteine precursor *O*-acetylserine (OAS) was increased by about 2-fold under longday conditions but levels were not changed in continuous light. The cysteine storage compound glutathione (GSH) was slightly increased under longday conditions and more drastically in continuous light.

In plants, the synthesis of cysteine can be subdivided into three steps: first, reduced sulphur is assimilated in the form of sulfide by sulfate reduction in the plastid stroma. Second, the carbon- and nitrogen-containing backbone for cysteine is synthesized and thirdly, the reduced sulphur is incorporated into the organic backbone (reviewed in Wirtz and Droux, 2005). The synthesis of the organic backbone is catalyzed by the serine acetyltransferase

(SAT), which transfers an acetyl-moiety from acetyl-Coenzyme A (acetyl-CoA) to serine leading to OAS formation. Subsequently, OAS is converted into cysteine in the presence of sulfide by the enzyme *O*-acetylserine(thiol)lyase (OAS-TL). SAT and OAS-TL form a multienzyme complex called cysteine synthase complex, which, in contrast to sulfide production and the synthesis of most amino acids in higher plants, is not only active in plastids but also in the cytosol and in mitochondria. It has been shown that mitochondria seem to have a large impact on cellular OAS biosynthesis whereas the biosynthesis of cysteine mainly takes place in the cytosol (Krueger et al., 2009). It is therefore assumed, that OAS and cysteine are efficiently transported between the cytosol, chloroplasts and mitochondria (Heeg et al., 2008, Krueger et al., 2009).

The biosynthesis of the sulphur containing amino acid methionine is also tripartite with the organic backbone coming from a phosphorylated homoserine, the methylgroup from folates and the sulphur atom from cysteine. The transfer of the sulphur atom from cysteine to homocysteine through the transsulphuration pathway occurs only in plastids, thus making chloroplasts the unique site for *de novo* methionine synthesis (Wirtz and Droux, 2005). Most of the methionine synthesized in the plant cell is subsequently converted into SAM, a process located in the cytosol (for an overview, see Bouvier et al., 2006). If the transport of sulphur containing amino acids across the chloroplast membrane was impaired due to the lack of the PRAT2 proteins, cysteine could not be shuttled correctly between compartments leading to an overall accumulation because it was not further metabolized, e.g. into methionine. If *de novo* synthesized methionine was not exported from the chloroplast, it could accumulate possibly leading to a backlog in the transfer of sulphur from cysteine. This scenario could also explain the increase in GSH levels because excess cysteine could be shuttled into the reserve pool GSH instead.

In the *cs26* mutant, which displays the opposite phenotype as the *prat2*-dm mutants, the protein catalyzing the synthesis of S-Cys from *O*-acetylserine (OAS) is affected (Bermúdez et al., 2010). S-Cys, which is synthesized from OAS like cysteine, can be degraded to cysteine but is thought to have another important role in the chloroplast. Lack of *CS26* gene activity leads to elevated levels of glutathione, a reserve pool for cysteine, but cysteine levels are not changed. If S-Cys cannot be synthesized from OAS, it seems to be converted to cysteine instead and then stored in the glutathione pool. If cysteine levels in chloroplasts of the

prat2-dm mutants were elevated because of insufficient cysteine export across the inner chloroplast envelope, it might not only be stored in the glutathione pool which leads to the observed increase in glutathione levels (see Figure 12). Also, a higher flux of OAS into S-Cys synthesis instead of into cysteine and subsequent methionine synthesis might be possible, which would result in higher S-Cys levels in *prat2-dm* mutants explaining the opposite phenotype to the *cs26* mutant, in which S-Cys levels are decreased. However, S-Cys levels could not been determined in the *prat2-dm* mutants so far.

An involvement of the PRAT2 proteins sulphur metabolism was further supported by transport studies in yeast cells expressing PRAT2.1 and PRAT2.2 in their plasma membranes. Loading with radiolabelled cysteine and methionine showed import activity of cysteine for both, PRAT2.1 and PRAT2.2 and a slight export activity of methionine in the case of PRAT2.2 (see Figure 13)

In summary, an involvement of the PRAT proteins in POR assembly and the sufficient conversion of protochlorophyllide is unlikely. The tetrapyrrole pathway intermediate Mg PP IX could accumulate to toxic concentrations or its export from the chloroplast could be impaired due to the lack of PRAT2. Taken together, the results point to a role of the PRAT2 proteins in the transport of thiol containing amino acids or intermediates of sulphur metabolism.

4.2 IEP57 in the inner chloroplast envelope

Initially, IEP57 was isolated from outer envelopes of pea chloroplasts in an approach to identify new OEPs. However, biochemical analysis revealed that IEP57 corresponds to an integral membrane protein of the inner chloroplast envelope with predictions for α-helical transmembrane domains and a cleavable chloroplast transit peptide For IEP57, 4 transmembrane α-helices are predicted which is supported by previous assays with PEG-malmeide (Doctoral thesis I. Jeshen, 2012). The orientation of IEP57 in the inner envelope membrane, however, still is not completely clear. A previously proposed orientation of the N- and C-terminal facing the intermembrane space could not be confirmed in the current study with a newly ordered antibody directed against a synthetic peptide from the N-terminal of Ps-IEP57. Even though proteolysis with the proteases thermolysin and trypsin lead to a set of bands corresponding to digestion fragments, none of these fragments could be matched to the predicted fragment sizes. The antibody directed against the N-terminal still detected protein bands after proteolysis, which indicates that the N-terminal is protected from digestion and, therefore, most likely, is oriented towards the inside of the inner envelope membrane vesicles corresponding to the chloroplast stroma. The long N-terminal part of IEP57 might be involved in recognition of the substrates to be transported. If the N-terminal is indeed oriented toward the chloroplast stroma, this would indicate that IEP57 might be involved in the export of substances produced inside the chloroplast.

The long, soluble N-terminal part of IEP57 contains an aspartate- and glycine-rich repeat. Wingenter et al. (2011) showed that the aspartate-rich motif of At-TMT1, a glucose transporter in the vacuolar membrane, interacts with the VIK kinase (RAF17) via its ankyrin repeat. Personal communication with Prof. Dr. E. Neuhaus (Plant Physiology, University of Kaiserslautern) revealed that the aspartate- and glycine-rich motif of IEP57 is also suitable for possible protein-protein interactions via an ankyrin repeat. Of the 5 other members of the VIK kinase family, 4 were shown not to localize to the chloroplast (Personal communication with Prof. Dr. E. Neuhaus, Plant Physiology, University of Kaiserslautern). The remaining kinase RAF25 as well as three other ankyrin-containing proteins (Becerra et al., 2004) with chloroplast predictions could not be localized to the plastid by GFP targeting in tobacco protoplasts (State examination thesis K. Winkler, 2013). Further interaction

studies or the precipitation of interaction partners from chloroplast extracts with recombinant IEP57, however, were not possible to be conducted because neither the full length proteins from *Arabidopsis* or pea nor truncated versions containing the soluble N-terminal parts of IEP57 could be heterologously overexpressed in *E. coli*. The full length coding sequences for IEP57 from both plant species were further subcloned into suitable vectors to be used in the Split-Ubiquitin-system in yeast, which is a two component system to analyze protein-protein-interactions (Johnsson and Varshavsky, 1994). However, preliminary control experiments failed, proving this system unsuitable for interaction studies with IEP57 (data not shown). Also further experiments concerning IEP57's structure, e.g. CD spectroscopy, or channel activity analysis as described for OEP40 could not be performed due to the lack of suitable protein samples.

IEP57 mutant phenotypes

In *Arabidopsis*, homozygous T-DNA insertion lines for *IEP57* were shown to be embryo lethal, pointing to an essential role of IEP57 in plant development (Doctoral thesis I. Jeshen, 2012). *Arabidopsis* plants overexpressing *IEP57* under control of the constitutively active 35S promoter in a wild-type background displayed spontaneous chlorosis which randomly occurred during plant development. This phenotype was shown to be due to a transgene-induced gene silencing initiated by the introduction of the 35S::*IEP57* overexpression construct (Doctoral thesis I. Jeshen, 2012). However, the occurrence of the chlorotic phenotype in the three obtained homozygous 35S lines #6, #9 and #10 could not be pinpointed to specific plant organs or developmental stages. Further chlorosis patterns did not only differ between the three lines but also between individuals of one line, making this system unsuitable for further phenotype-rescue studies. In order to be able to control the phenotypic changes in *IEP57* mutant plants and to overcome the embryo lethality in *IEP57* knockouts, the popON/popOFF system (Wielopolska et al., 2005) was used to generate inducible *IEP57* overexpression as well as inducible *IEP57* RNAi lines. Here, overexpression of *IEP57* and knock-down by RNA interference can be induced by the exogenous application of dexamethasone. When *IEP57* overexpression was induced, the chlorotic phenotype observed in 35S::*IEP57* overexpression lines was confirmed. The main focus, however, was set on the inducible RNAi lines in which the induction with dexamethasone leads to a knockdown of *IEP57* transcripts by RNA interference. Upon RNAi induction,

At-IEP57/popOFFII lines again displayed chlorosis. In both cases, induced overexpression and knockdown of *IEP57*, chlorosis occurred consistently in all plants after transfer onto inducing medium. Chlorosis started at the center of the rosette and spreading over the petioles into the leaves. This pattern is probably due to the uptake of the inducing compound dexamethasone by the roots and its distribution by the vascular tissue. Chlorosis in RNAi lines appeared faster than in inducible overexpression lines. Induction of the chlorotic phenotype worked well at the seedling stage on inducing medium-containing agar plates but was limited to the first two to three weeks of plant development. Induction of the phenotype in mature plants, however, proved to be more difficult. Application of exogenous dexamethasone by watering of mature plants grown on soil was not followed because a constant application of equal amounts of dexamethasone on all plants could not be ensured and the chlorotic phenotype therefore occurred randomly or not at all (data not shown). This was overcome by the establishment of a hydroponic growth system (see Figure 19), which allowed the phenotypic analysis of single plants above the seedling stage up to 28 days and ensured a constant and equal supply with dexamethasone-containing growth medium. The phenotype appeared reliably four days after induction and *IEP57* transcripts where shown to be reduced to 5 % of wild-type levels 7 days after induction. The subsequent reincrease after 10 days is probably due to the complete consumption of all dexamethasone. The experimental setup also allowed facilitated supplementation of the growth medium with different substances of interest because the required amount of medium and supplements could be kept relatively small and the individual plants were easily transferable onto new media. In summary, hydroponic culture proved to be a reliable system to induce RNAi *At-IEP57*/popOFFII lines and was therefore used for further phenotype-rescue studies to identify a potential substrate transported by IEP57.

The search for IEP57 transport substrates

IEP57 was annotated as a putative solute transporter (Tyra et al., 2007) and was found to be part of the plant-specific RETICULATA-RELATED (RER) family of proteins all members of which contain a plant-specific, conserved amino acid domain of unknown function (DUF3411) with a conserved RYQ motif (Pérez-Pérez et al., 2013, see Figure 16). Most of the RER family proteins (RE, RER1, RER3 and RER4) were identified as integral components of the chloroplast envelope except for RER5 and 6, which were identified in the thylakoid lumen

(Pérez-Pérez et a., 2013 and references therein). For none of the members of the RER protein family, a precise function has been discovered so far, but co-expression analysis revealed strong association with a number of genes of amino acid and nucleotide metabolism (Lundquist et al., 2014, Pérez-Pérez et al., 2013). Also, metabolic profiling of *re* and *rer3* pointed to affected pathways downstream of pyruvate and to an altered metabolism of branched chain and aromatic amino acids, a pattern that is repeated in many reticulate mutants. In addition, several other products downstream of the plastid pool of phosphoenolpyruvate (PEP) were decreased, pointing to a misregulated shikimate pathway or insufficient supply of PEP to the plastid (Lundquist et al., 2014, Pérez-Pérez et al., 2013). These observations together with the results on other leaf reticulate mutants (for an overview see Lundquist et al., 2014), which are often affected in plastid-localized metabolic pathways, were used to identify a potential substrate possibly transported across the chloroplast envelope by IEP57.

If IEP57 was involved in the export of intermediates or end products of plastid-localized metabolic pathways, the exogenous application of these metabolites to plants lacking IEP57 should rescue the chlorotic phenotype and restore a wild-type like appearance. This approach was used to test various substances retrieved from publications on the RER family of proteins or other leaf reticulate mutants.

The aromatic acids Phe, Tyr and Tryp were investigated, because double mutant analysis of the two reticulate leaf mutants *cue1* and *re*, revealed that the *cue1* mutation is epistatic to the *re* mutation indicating an involvement in the same developmental pathway (González-Bayón et al., 2006). In addition, the gene encoding for the second isoform of the phosphoenol-pyruvate (PEP)/phosphate translocator, PPT2, was found among the 20 most downregulated genes in DNA microarray analyses from induced *At-IEP57*-RNAi plants (State examination thesis K. Winkler, 2013). It might therefore be speculated, that IEP57 is involved in aromatic acid transport.

For the *cue1* mutant which displays leaf reticulation and in which the gene encoding the plastid phosphoenol-pyruvate (PEP)/phosphate translocator 1 (PPT1) is affected, a successful rescue of the reticulate phenotype by the simultaneous, exogenous application of the three aromatic amino acids phenylalanine (Phe), tryptophan (Tryp) and tyrosine (Tyr) has been reported (Streatfield et al., 1999). In this study, surface sterilized seedlings were grown on

MS agar plates containing 1 mM of all three amino acids. The phenotype-rescue studies for IEP57 RNAi lines with Phe, Tryp and Tyr as well as with the branched-chain amino acids valine (Val), leucine (Leu) and isoleucine (Ile) were therefore carried out using MS agar plates supplemented with the respective amino acids. Neither for the individual nor for the simultaneously applied aromatic amino acids, a phenotype rescue was observed in *At-IEP57*-RNAi plants.

Although the branched chain amino acids (BCAAs) Val, Leu and Ile are synthesized in plastids originating from pyruvate, exogenous application of the BCAAs Val, Leu and Ile, however, did not lead to a rescue of the *IEP57* mutant phenotype.

For all other tested substances retrieved from publications on other leaf reticulate mutants the same results were observed. None of the exogenously applied substances was able to rescue the chlorotic phenotype in *At-IEP57*/popOFFII plants grown in the presence of dexamethasone.

However, the exogenous application of certain intermediates or end products can only compensate for metabolic imbalances caused by the lack of IEP57 if the respective compound is thereby hindered from leaving the chloroplast and being transported to its final destination in the plant cell, where it is further metabolized. This also requires that the exogenously added compounds are even taken up by the plant and are correctly distributed to their destination in the cell. Further, the approach requires that the tested compounds are stable in sufficient amounts over a number of days after being added to the growth medium. For all these reasons, if the application of a certain compound does not lead to a rescue of the phenotype, it cannot automatically be excluded from the pool of potential transport substrates of IEP57. An additional fact to bear in mind for all phenotype rescue studies is that they were carried out in the presence of dexamethasone to induce a knockdown of *IEP57* transcripts by RNAi using the popOFF system. In tobacco, no inhibitory effect of dexamethasone on plant development has been reported using the pop6/LhGR system (Samalova et al., 2005). In *Arabidopsis*, plants grown in the presence of dexamethasone were slightly smaller than plants grown without the inducing compound but otherwise did not seem to be impaired in growth and development. However, a successful rescue of a phenotype caused by dexamethasone-induced gene expression by the addition

of exogenous substances has not been reported to date and it is not clear, whether the effects caused by dexamethasone can be compensated for.

IEP57 and the plastid nonMVA pathway

Due to phenotypic similarities to the 35S::*IspH* mutant, a possible involvement of IEP57 in the plastid non-mevalonate (nonMVA) pathway was investigated. In higher plants, two unrelated distinct biosynthetic routes to the five-carbon precursors of isoprenoids, isopentenyl diphosphate (IPP) and demethylallyl diphosphate (DMAPP), exist (Figure 36, Lange et al., 2000). The cytosolic acetate/mevalonate (MVA) pathway was long thought to be the only route to synthesize IPP and DMAPP. It starts from acetyl-CoA and proceeds to the intermediate mevalonate (Laule et al., 2003). The plastidic non-MVA pathway involves a condensation of pyruvate and glyceraldehydes-3-phosphate via 1-deoxy-D-xylulose-5-phosphate (DOXP) and is therefore also called DOXP or MEP pathway due to its first committed intermediate 2C-methyl-D-erythritol-4-phosphate (Figure 36). Sesquiterpenes, sterols and polyterpenes are derived from the cytosolic MVA pathway whereas isoprene, phytol and carotenoids as well as the plant hormones gibberellins and absciscic acid are synthesized via the plastidic non-MVA pathway. (Hsieh and Goodman, 2005 and references therein). However, the compartmental separation of the two pathways is not absolute and metabolic crosstalk between the pathways is highly possible. Defects in either of the isoprenoids pathways can be compensated for by crosstalk between the cytosol and the plastid only to a certain extent which is underlined by the strong mutant phenotypes described (Flügge and Gao, 2005 and references therein).

The fact that the plastid nonMVA pathway starts from pyruvate, the metabolite downstream of which metabolic profiles of the *re* and *rer3* mutants seem to be altered (Pérez-Pérez et al., 2013) fits to a possible involvement of the RER family member IEP57. A mutation in the *Arabidopsis ISPH* gene encoding the enzyme catalyzing the pathway's final step from 1-hydroxy-2-methyl-2(E)-butebyl-4-diphosphate (HMBPP) to IPP lead to led to an albino phenotype with altered chloroplast structure (Hsieh and Goodman, 2005) but, in contrast to *IEP57* mutants, homozygous mutant plants were viable. The subsequent attempt to create *Arabidopsis* 35S::*IspH* overexpression lines led to transformants showing various albino phenotypes strongly resembling those observed in all *IEP57* mutant lines.

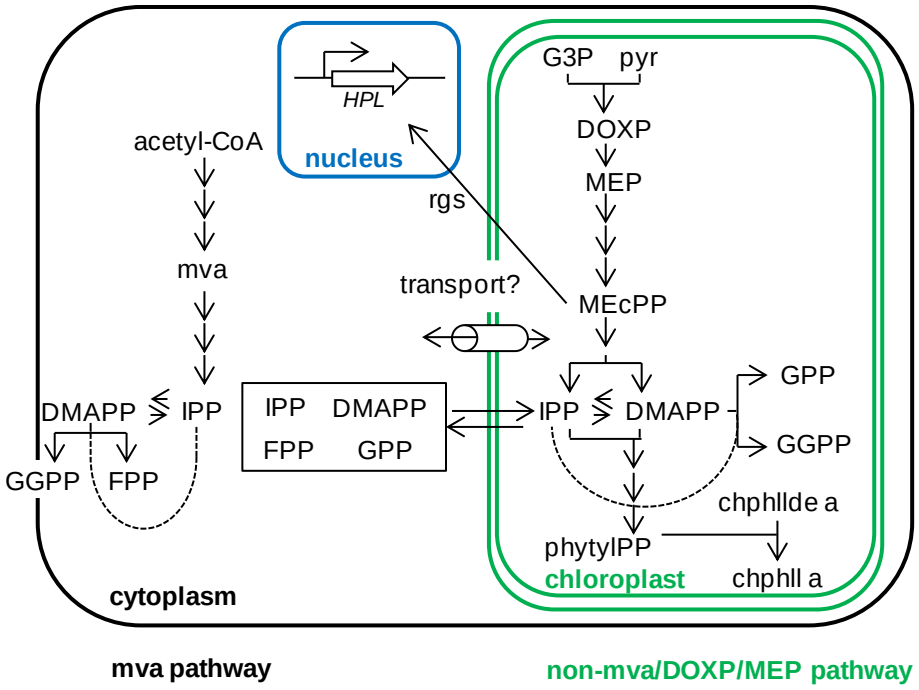

Figure 36: Suggested compartmentation of isoprenoid precursor biosynthesis in higher plants
The cytosolic mevalonate (mva) pathway proceeds from acetyl-CoA via the intermediate mva to isopentenyldiphosphate (IPP) which can be reversely converted into dimethylallyl diphosphate (DMAPP). The plastidic non-mevalonate or 1-deoxy-D-xylulose-5-phosphate (DOXP) pathway proceeds from glyceraldehyde-3-phosphate (G3P) and pyruvate (pyr) via the intermediates DOXP, methylerythritol (MEP) and 2-C-methyl-D-erythritol-2,4-cyclodiphosphate (MEcPP) to IPP and DMAPP. In the cytoplasm, addition of IPP units to DMAPP leads to the production of geranylgeranyldiphosphate (GGPP) and farnesyldiphosphate (FPP). In the plastid, addition of IPP units to DMAPP leads to the production of geranylgeranyldiphosphate (GGPP) and geranyldiphosphate (GPP). In the plastid, phytyldiphosphate (phytylPP) is produced from GGPP which serves as the phytol moiety for chlorophyll a (chphll a) produced from chlorophyllide a (chphllde a). The intermediates IPP, DMAPP, FPP and GPP are thought to be shuttled between chloroplast and cytosol. MEcPP has been shown to act in retrograde signaling (rgs) and is shuttled from the chloroplast to the nucleus by a yet unknown mechanism where it leads to the expression of *HYDROPEROXID LYASE (HPL)* in response to stress (Xiao et al., 2012). (Adapted from Laule et al., 2003 and Vranová et al., 2013).

It was shown, that the occurrence of these chlorotic plant parts is also due to transgene-induced gene silencing with *IspH* overexpressed in the green tissue and silenced in the albino tissue of the same plant. Additionally, RNAi lines for nonMVA pathway genes also displayed green and albino leaf sectors (Xiao et al., 2012) and *Arabidopsis* seedlings treated with fosmidomycin, an inhibitor of the plastid nonMVA pathway, leaves started bleaching within

48 hrs. Xiao et al. (2012) further showed, that the nonMVA intermediate 2-C-methyl-D-erythritol-2,4-cyclodiphosphate (MEcPP) acts as a specific retrograde signaling metabolite regulating the expression of nuclear stress-response genes. It is therefore evident, that transport of nonMVA pathway intermediates and endproducts as well as of those of the MVA pathway has to be mediated across the chloroplast membrane.

Feeding studies with the two commercially available substrates MEcPP and IPP, however, did not lead to a rescue of the chlorotic phenotype in -induced *At-IEP57* RNAi plants grown in hydroponic culture. Application was conducted in adaption to Xiao et al. (2012) where the external application of MEcPP was shown to induce the induction of the nuclear stress gene *HYDROPEROXID LYASE (HPL)*. In addition to adding the substances to the growth medium, MEcPP and IPP solutions were supplemented with 0.01 % silwet and added externally onto the leaves or by dipping the plants into the solution and applying a vacuum.

The nonMVA pathway intermediate MEcPP was shown to act as a retrograde signal produced in the chloroplast and inducing the expression of the stress responsive gene *HPL* upon wounding (Figure 36, Xiao et al., 2012). In order to fulfill its role as a retrograde signaling molecule, MEcPP needs to be exported from the plastid but the mechanism of transport still remains elusive. If IEP57 was involved in the export of MEcPP from the plastid, it could be assumed that plants lacking IEP57 are not able to induce *HPL* expression in response to wounding stress. Wounding of Col-0 wild-type plants grown on the inducing compound dexamethasone showed that dexamethasone treatment alone does not lead to an impaired *HPL* expression in response to wounding stress. RNAi-induced *At-IEP57*/popOFFII plants, however, also responded to wounding stress with *HPL* expression. This indicates, that either the knockdown of *IEP57* transcripts by induced RNAi is not sufficient to reduce the IEP57 protein to levels where transport of MEcPP is so diminished that a proper induction of *HPL* is not possible any more. Or, the non-MVA pathway up to the intermediate MEcPP is as well as the export of this retrograde signaling molecule are not impaired in plants lacking IEP57.

In summary, a role of IEP57 in the transport of aromatic amino acids still seems to be likely. However, further analyses have to be conducted in order to assign a functional role to IEP57. With the established growth system in hydroponic culture, a reliable system for further metabolite and DNA microarray analyses is available.

4.3 OEP40 in the outer chloroplast envelope

The outer envelope protein of 40 kDa, OEP40, was isolated from outer envelope of pea chloroplasts in an approach to identify new OEPs. When analyzed towards its association with the membrane (see Figure 27), Ps-OEP40 displayed the same behavior as the well described β-barrel protein OEP37 (Schleiff et al., 2003) which is integral to the outer chloroplast envelope. The analysis of the protein sequence of At-OEP40 in comparison to the well described β-barrel proteins At-OEP37 and At-VDAC with the PROF Secondary Structure Prediction System software (Ouali and King, 2000) confirmed the prediction that At-OEP40 might form a β-barrel (Bachelor thesis J. Beratis, 2013). Attempts to confirm the structural prediction by CD-spectroscopy failed so far due to purification problems but should be continued to establish OEP40 as a classical outer envelope β-barrel protein.

Electrophysical studies of Ps-OEP40 in the planar lipid bilayer system (Group of Prof. Dr. Richard Wagner, Biophysics, Universtiy of Osnabrück, Germany) showed that Ps-OEP forms a cation-selective channel with two conductance states (see Figure 30). Equal channel activities were observed for Ps-OEP40 protein samples obtained from three different purification approaches, which implies that the same channel was analyzed in all the channel recordings and that this channel indeed is Ps-OEP40 and not a contamination from the used expression system, e.g. the outer bacterial membrane.

OEP40 and the induction of flowering

The link between the potential role of OEP40 as a metabolite transport protein and the phenotype in *oep40* knock-down mutants, which were observed to flower earlier under low temperature conditions (10 °C) than wild-type plants (Doctoral dissertation I. Jeshen, 2012), is assumed to be a metabolic imbalance caused by the lack of the OEP40 transport function leading to an excess of promoting or a shortage of repressing signals for floral transition. The transition from vegetative growth to the reproductive state is the result of responses to a variety of endogenous and exogenous signals that have to be integrated and eventually result in flowering. The perceived signals from different interacting pathways are directed by a complex network of activators and repressors, which converge in the activation of a set of integrator genes in the shoot apex where flowers are eventually formed (for an overview see Srikanth and Schmid, 2011). So far, several physiological, plant-derived signals have been shown to affect flowering (reviewed in Matsoukas et al, 2012 and Bernier et al., 1993).

Hormonal control of flowering is mediated by gibberellins which promote flowering by activating the promoter of *LEAFY* (*LFY*), a floral meristem identity gene (Blázquez et al., 1998). In addition, gibberellins degrade DELLA proteins thereby lifting repression of PHYTOCHROME INTERACTIN FACTOR 4 (PIF4) activity, leading to the expression of *FLOWERING LOCUS T* (FT) (Kumar et al., 2012). FT acts as a long-distance signal, which is transported from the leaves to the shoot meristem where it initiates flowering (Wigge et al., 2005).

In addition to the *oep40* knock-down line on which phenotypic analysis had already been started (*oep40-1*, doctoral dissertation I. Jeshen, 2012), a knock-down line with no residual *oep40* transcript and OEP40 protein, *oep40-3* was characterized in this study (Figure 31). Detailed phenotypic analysis confirmed the early flowering phenotype under low temperature conditions (10 °C). The knock-down as well as the knock-out line for *OEP40* displayed the same shift to an earlier flowering time point which implies that even a partial loss on OEP40 is sufficient to shift the metabolic status of the plant so that flowering is induced.

The transition from vegetative growth to the reproductive state and flowering is made long before flowers and possible flowering phenotypes actually become visible. The phase change is characterized by multiple morphogenetic changes and the initial developmental switch itself responsible for this phase change cannot be detected directly (Pouteau and Albertini, 2009). Therefore, any event leading to the observed phenotype must take place at a developmental stage where wild-type and *oep40* mutant plants cannot be phenotypically distinguished yet. To detect a possible metabolic imbalance in *oep40* mutant plants causing early flowering at 10 °C, a time frame from 38 days to 54 days after sowing was chosen for further analysis. The goal was to define detailed time points prior to the visible phenotype in wild-type and *oep40* mutant plants, which reproduce the visible difference in bolting and flowering time on the transcript level using qRT-PCR with a primer platform of 90 flowering genes (Dr. A. Schlereth, Group of Prof. M. Stitt, MPI for molecular plant physiology, Golm, Germany). However, for the majority of the genes, no significant changes in expression level between wild-type and *oep40* mutant plants could be detected in the analyzed time frame between 38 to 54 days. This might be due to the fact that most of the analyzed genes encode for transcription factors, which are only expressed for a short time to activate their

downstream target. Also, only small changes in their expression might be sufficient. It might therefore be possible that those subtle changes cannot be captured with the 4 day interval between time points in analyzed time frame keeping in mind that the difference in flowering between Col-0 wild-type and *oep40* mutant plants is relatively small. As expected, expression of floral inducers and repressors was increasing and decreasing over time, respectively but this expression was not shifted to a respectively earlier or later time point in *oep40* mutant plants.

The only gene which was differentially expressed in Col-0 wild-type compared to the *oep40* mutant plants was *DWARF AND DELAYED FLOWERING 1* (*At-DDF1*), encoding for an AP2 transcription factor which, was shown to enhance tolerance to abiotic stressed including cold when overexpressed (Kang et al., 2011). *At-DDF1* expression drastically increased in Col-0 wild-type between day 38 and day 42, whereas expression in *oep40* mutants remained almost unchanged. In wild-type *Arabidopsis*, *DDF1* was shown to be upregulated by cold, salt stress, drought and heat (Kang et al., 2011). Upregulation of *DDF1* under low temperature conditions only in Col-0 wild-type leads to the assumption that the lack of OEP40 alters the status of the mutant plant in a way that impairs the induction of *DDF1* expression as a stress response.

In the literature, the phenotype of mutant plants overexpressing *At-DDF1* was restored when plants were treated with exogenous gibberellins, indicating an involvement of a gibberellin pathway in the stress tolerance mediated by *At-DDF1*. DELLA proteins, a family of nuclear, growth-repressing proteins were shown to accumulate in response to the low temperature-induced C-repeat/drought-responsive element binding factor (CBF1, Achard et al., 2008, Figure 37). Constitutive expression of *CBF1* leads to the accumulation of less bioactive gibberellins which in turn stimulate the degradation of DELLA proteins. The global *della* mutant, which is homozygous for mutant alleles at all 5 *Arabidopsis* DELLA loci (Koini et al., 2009), has been reported to flower early at low temperature (Kumar et al., 2012). DELLA proteins control the activity of the bHLH transcription factor PIF4 through repressing activity and prevent PIF4 from binding DNA. PIF4 has been shown to regulate the expression of *FT* in a temperature-dependant manner at the level of chromatin accessibility (Kumar et al., 2012, Figure 37). The PIF4-repressing DELLA proteins are degraded by the phytohormone gibberellin which triggers their degradation. Therefore, gibberellin plays a key permissive

role in the induction of the floral inducer FT. As DELLA proteins have been shown to regulate the way by which gibberellins influences PIF4 and the finding that PIF4 can directly activate FT suggests a possible mechanism by which changes in gibberellins levels may influence flowering (Figure 37). If the lack of OEP40 led to an increased level of gibberellins, DELLA protein accumulation would be prevented even though *CBF1* is expressed in response to cold. DELLA degradation allows PIF4 to activate *FT* expression leading to flowering even though overall environmental conditions at 10 °C are non-inducing.

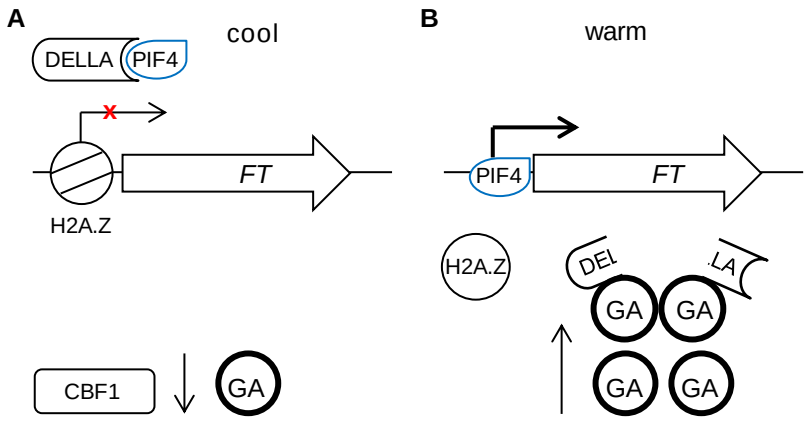

Figure 37: Temperature-dependent *FT* regulation

Schematic representation of phytochrome interacting factor 4 (PIF4) activitating *FLOWRING LOCUS T* (FT) in a temperature-dependent manner. Temperature-induced H2A.Z nucleosome dynamics regulate PIF4 binding to target loci for transcriptional activation. In addition, DELLA proteins repressively control the activity of PIF4 and prevent it from binding DNA. The phytohormone gibberellin (GA) triggers DELLA protein degradation and therefore free PIF4 to directly activate *FT* expression. The low temperature-induced C-repeat/drought-responsive element binding factor (CBF1) leads to the accumulation of less bioactive gibberellins (Adapted and extended from Kumar et al., 2012).

In a second approach to follow flowering induction in *oep40* mutants, the emergence of flower primordia was analyzed on shoot apical meristem (SAM) sections by RNA *in* situ hybridization with a LEAFY probe, which is a marker gene for floral primordia (Wahl et al., 2013). The chosen time frame from 34 to about 50 or 54 days seems to cover the transition from vegetative growth to the reproductive state and flowering. *Oep40* mutant

plants show an earlier expression of the floral primordia marker *LFY* and, in comparison to wild-type meristems, flower primordia develop at earlier stages. The time frame from 34 to 54 days cantherefore be used for further analyses in order to detect metabolic imbalances due to the lack of OEP40.

OEP40 and metabolic signals

Little is known about the contribution of carbohydrates to flowering regulation but analysis of mutants of sugar and starch metabolism have shown to affect various developmental aspects including flowering (summarized in Matsoukas et al., 2012 and Bernier et al., 1993). The level of trehalose-6-phosphate (T6P), a metabolite with hormone-like metabolic activities is closely linked to the level of sucrose, functioning as a signal of the sucrose status (Lunn et al., 2006). The T6P pathway was shown to affect the induction of flowering in both, leaves and the SAM (Wahl et al., 2013) thereby linking the carbohydrate status of the plant to flowering control. In the search of a potential substrate transported by OEP40 which might be connected to the control of flowering, trehalose-6-phosphate (T6P) was further investigated. Signaling by trehalose-6-phosphate (T6P) has been shown to be involved in the regulation flowering in *Arabidopsis* (Wahl et al., 2013). In leaves, the activity of TREHALOSE-6-PHOSPHATE SYNTHASE (TPS1) is required for the induction of the expression of *FT*. Thereby, the physiological signal of high carbohydrate levels indicated by T6P, is integrated with environmental signals into floral induction. This ensures, that *FT* is expressed only when conditions are optimal, that is when day lengths has reached a certain minimum and when carbohydrate resources are sufficient to support the energy-demanding process of flowering and seed production. In the SAM, the T6P pathway affects the expression of flowering-time and flowering-patterning genes. T6P is synthesized from UDP-glucose and glucose-6-phosphate by TPS1 in the cytoplasm (Figure 38). It is subsequently converted to trehalose which in turn is hydrolyzed to 2 molecules of glucose. It hast been suggested that T6P is transported into chloroplasts by a yet unknown mechanism where it induces starch synthesis via thioredoxin-mediated activation of AGPase. In plastids, T6P might also be converted into trehalose, which has been shown to regulate starch breakdown (Figure 38, for an overview, see Ponnu et al., 2011). If OEP40 was responsible for the transport of T6P into the chloroplast, the lack on OEP40 would lead to an increased level of T6P in the cytosol possibly acting in the T6P signaling pathway leading to flowering. Under low temperature

conditions, the increase of T6P in the cytoplasm might produce an excess of inducing signal leading to flowering under otherwise non-inducing conditions. Only very recently, channel recordings of reconstituted Ps-OEP40 in a planar lipid bilayer showed that the OEP40 channel specifically reacts to T6P but not to trehalose by dramatically increasing the channel conductance. T6P affected the channel only from one side, which is thought to be the cytosolic side (Personal communication Prof. Dr. R. Wagner, Biophysics, University of Osnabrück).

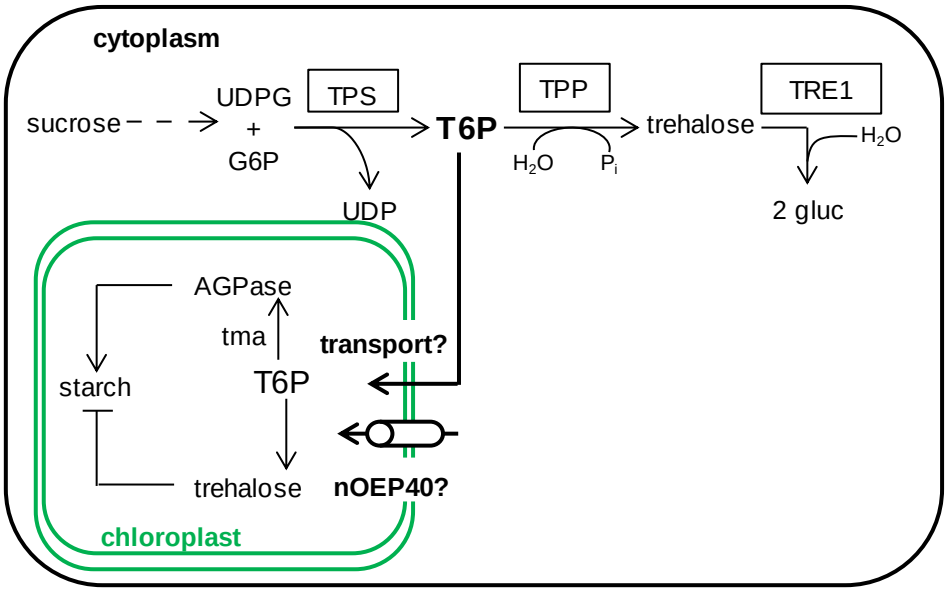

Figure 38: Trehalose-6-phosphate in the plant cell

Trehalose-6-phosphate (T6P) is synthesized from UDP-glucose (UDPG) and glucose-6-phosphate (G6P) by trehalose-6-phosphate synthase (TPS). T6P is subsequently converted to trehalose by T6P phosphatase (TPP). Trehalose is then hydrolyzed to two molecules glucose (gluc) by trehalase 1 (TRE1). The precursors of T6P are derived from sucrose metabolism. T6P is transported into plastids by a yet unknown mechanism possibly by OEP40. In plastids, T6P induces starch synthesis via thioredoxin-mediated activation (tma) of AGPase. T6P might also be converted to trehalose which has been shown to regulate starch breakdown in plastids (adapted from Ponnu et al., 2011).

Therefore, a broad range metabolite analysis (Group of Prof. Dr. A. Weber, Plant Biochemistry, University of Düsseldorf, Germany) is in preparation and also levels of T6P and other phosphorylated carbohydrates will be analyzed (Dr. J. Lunn, MPI of molecular plant biology, Golm, Germany). This should provide a widespread overview of the metabolic situation in *oep40* mutant plants and might reveal a metabolic imbalance caused by the lack

of OEP40 which can then be linked to the early flowering under low temperature conditions. In addition, the presence of DELLA proteins in *oep40* mutants could be analyzed on transcript level by qRT-PCR and the levels of gibberellins could be determined in order to analyze a possible involvement of OEP40 in gibberellin metabolism.

References

Achard, P., F. Gong, S. Cheminant, M. Alioua, P. Hedden and P. Genschik (2008). "The cold-inducible CBF1 factor-dependent signaling pathway modulates the accumulation of the growth-repressing DELLA proteins via its effect on gibberellin metabolism." Plant Cell **20**(8): 2117-2129.

Altschul, S. F., T. L. Madden, A. A. Schaffer, J. Zhang, Z. Zhang, W. Miller and D. J. Lipman (1997). "Gapped BLAST and PSI-BLAST: a new generation of protein database search programs." Nucleic Acids Res **25**(17): 3389-3402.

Armstrong, G. A., S. Runge, G. Frick, U. Sperling and K. Apel (1995). "Identification of NADPH:protochlorophyllide oxidoreductases A and B: a branched pathway for light-dependent chlorophyll biosynthesis in Arabidopsis thaliana." Plant Physiol **108**(4): 1505-1517.

Balsera, M., T. A. Goetze, E. Kovacs-Bogdan, P. Schurmann, R. Wagner, B. B. Buchanan, J. Soll and B. Bolter (2009). "Characterization of Tic110, a channel-forming protein at the inner envelope membrane of chloroplasts, unveils a response to Ca(2+) and a stromal regulatory disulfide bridge." J Biol Chem **284**(5): 2603-2616.

Becerra, C., T. Jahrmann, P. Puigdomenech and C. M. Vicient (2004). "Ankyrin repeat-containing proteins in Arabidopsis: characterization of a novel and abundant group of genes coding ankyrin-transmembrane proteins." Gene **340**(1): 111-121.

Bechthold, N., J. Ellis and G. Pelletier (1993). "In planta Agrobacterium mediated gene transfer by infiltration of adult Arabidopsis thaliana plants." C.R. Acad.Sci.Paris/Life Sciences **316**: 1194-1199.

Bermudez, M. A., M. A. Paez-Ochoa, C. Gotor and L. C. Romero (2010). "Arabidopsis S-sulfocysteine synthase activity is essential for chloroplast function and long-day light-dependent redox control." Plant Cell **22**(2): 403-416.

Bernier, G., A. Havelange, C. Houssa, A. Petitjean and P. Lejeune (1993). "Physiological Signals That Induce Flowering." Plant Cell **5**(10): 1147-1155.

Binder, S. (2010). "Branched-Chain Amino Acid Metabolism in Arabidopsis thaliana." Arabidopsis Book **8**: e0137.

Blazquez, M. A., R. Green, O. Nilsson, M. R. Sussman and D. Weigel (1998). "Gibberellins promote flowering of arabidopsis by activating the LEAFY promoter." Plant Cell **10**(5): 791-800.

Block, M. A., R. Douce, J. Joyard and N. Rolland (2007). "Chloroplast envelope membranes: a dynamic interface between plastids and the cytosol." Photosynth Res **92**(2): 225-244.

Block, M. A., A. K. Tewari, C. Albrieux, E. Maréchal and J. Joyard (2002). "The plant S-adenosyl-L-methionine:Mg-protoporphyrin IX methyltransferase is located in both envelope and thylakoid chloroplast membranes." FEBS Lett **269**: 240-248.

Bölter, B. and J. Soll (2001). "Ion channels in the outer membranes of chloroplasts and mitochondria: open doors or regulated gates?" EMBO J **20**(5): 935-940.

Bölter, B., J. Soll, K. Hill, R. Hemmler and R. Wagner (1999). "A rectifying ATP-regulated solute channel in the chloroplastic outer envelope from pea." EMBO J **18**(20): 5505-5516.

Bouvier, F., N. Linka, J. C. Isner, J. Mutterer, A. P. Weber and B. Camara (2006). "Arabidopsis SAMT1 defines a plastid transporter regulating plastid biogenesis and plant development." Plant Cell **18**(11): 3088-3105.

Bradford, M. M. (1976). "A rapid and sensitive method for the quantitation of microgram quantities of protein utilizing the principle of protein-dye binding." Anal Biochem **72**: 248-254.

Bürstenbinder, K., G. Rzewuski, M. Wirtz, R. Hell and M. Sauter (2007). "The role of methionine recycling for ethylene synthesis in Arabidopsis." Plant J **49**(2): 238-249.

Carbonell, J. and A. Blázquez (2009). "Regulatory mechanisms of polyamine biosynthesis in plants." Genes & Genomics **31**(2): 107-118.

Chehab, E. W., R. Kaspi, T. Savchenko, H. Rowe, F. Negre-Zagharov, D. Kliebenstein and K. Dehesh (2008). " Distinct Roles of Jasmonates and Aldehydes in Plant-Defense Responses." PLoS One **3**(4): e1904.

Chehab, E. W., G. Raman, J. W. Walley, J. V. Perea, G. Banu, S. Theg and K. Dehesh (2006): "Rice HYDROPEROXIDE LYASES with unique expression patterns generate distinct aldehyde signatures in Arabidopsis." Plant Physiol **141**: 121-134.

Clausen, C., I. Ilkavets, R. Thomson, K. Philippar, A. Vojta, T. Mohlmann, E. Neuhaus, H. Fulgosi and J. Soll (2004). "Intracellular localization of VDAC proteins in plants." Planta **220**(1): 30-37.

Conn, S. J., B. Hocking, M. Dayod, B. Xu, A. Athman, S. Henderson, L. Aukett, V. Conn, M. K. Shearer, S. Fuentes, S. D. Tyerman and M. Gilliham (2013). "Protocol: optimising hydroponic growth systems for nutritional and physiological analysis of Arabidopsis thaliana and other plants." Plant Methods **9**(1): 4.

Curien, G., D. Job, R. Douce and R. Dumas (1998). "Allosteric activation of Arabidopsis threonine synthase by S-adenosylmethionine." Biochemistry **37**(38): 13212-13221.

Duy, D., J. Soll and K. Philippar (2007). "Solute channels of the outer membrane: from bacteria to chloroplasts." Biol Chem **388**(9): 879-889.

Embley, T. M. and W. Martin (2006). "Eukaryotic evolution, changes and challenges." Nature **440**(7084): 623-630.

Flügge, U. I. and W. Gao (2005). "Transport of isoprenoid intermediates across chloroplast envelope membranes." Plant Biol (Stuttg) **7**(1): 91-97.

Fuell, C., K. A. Elliott, C. C. Hanfrey, M. Franceschetti and A. J. Michael (2010). "Polyamine biosynthetic diversity in plants and algae." Plant Physiol Biochem **48**(7): 513-520.

Gasteiger, E., A. Gattiker, C. Hoogland, I. Ivanyi, R. D. Appel and A. Bairoch (2003). "ExPASy: The proteomics server for in-depth protein knowledge and analysis." Nucleic Acids Res **31**(13): 3784-3788.

Goetze, T. A., K. Philippar, I. Ilkavets, J. Soll and R. Wagner (2006). "OEP37 is a new member of the chloroplast outer membrane ion channels." J Biol Chem **281**(26): 17989-17998.

Gonzalez-Bayon, R., E. A. Kinsman, V. Quesada, A. Vera, P. Robles, M. R. Ponce, K. A. Pyke and J. L. Micol (2006). "Mutations in the RETICULATA gene dramatically alter internal architecture but have little effect on overall organ shape in Arabidopsis leaves." J Exp Bot **57**(12): 3019-3031.

Gould, S. B., R. F. Waller and G. I. McFadden (2008). "Plastid evolution." Annu Rev Plant Biol **59**: 491-517.

Gross, J. and D. Bhattacharya (2009). "Mitochondrial and plastid evolution in eukaryotes: an outsiders' perspective." Nat Rev Genet **10**(7): 495-505.

Hanahan, D. (1983). "Studies on transformation of Escherichia coli with plasmids." J Mol Biol **166**(4): 557-580.

Heeg, C., C. Kruse, R. Jost, M. Gutensohn, T. Ruppert, M. Wirtz and R. Hell (2008). "Analysis of the Arabidopsis O-acetylserine(thiol)lyase gene family demonstrates compartment-specific differences in the regulation of cysteine synthesis." Plant Cell **20**(1): 168-185.

Heins, L., A. Mehrle, R. Hemmler, R. Wagner, M. Kuchler, F. Hormann, D. Sveshnikov and J. Soll (2002). "The preprotein conducting channel at the inner envelope membrane of plastids." EMBO J **21**(11): 2616-2625.

Hemmler, R., T. Becker, E. Schleiff, B. Bolter, T. Stahl, J. Soll, T. A. Gotze, S. Braams and R. Wagner (2006). "Molecular properties of Oep21, an ATP-regulated anion-selective solute channel from the outer chloroplast membrane." J Biol Chem **281**(17): 12020-12029.

Hsieh, M. H. and H. M. Goodman (2005). "The Arabidopsis IspH homolog is involved in the plastid nonmevalonate pathway of isoprenoid biosynthesis." Plant Physiol **138**(2): 641-653.

Hung, W-F., L-J. Chen, R. Boldt, C-W. Sun and H-M. Li (2004): Characterization of Arabidopsis glutamine phosphoribosyl pyrophosphate amidotransferase-deficient mutants." Plant Physiol **135**: 1314-1323.

Hussain, N., F. Irshad, Z. Jabeen, I. H. Shamsi, Z. Li and L. Jiang (2013). "Biosynthesis, structural, and functional attributes of tocopherols in planta; past, present, and future perspectives." J Agric Food Chem **61**(26): 6137-6149.

Jarvis, P. and J. Soll (2001). "Toc, Tic, and chloroplast protein import." Biochim Biophys Acta **1541**(1-2): 64-79.

Johnsson, N. and A. Varshavsky (1994). "Split ubiquitin as a sensor of protein interactions in vivo." Proc Natl Acad Sci U S A **91**(22): 10340-10344.

Kang, H. G., J. Kim, B. Kim, H. Jeong, S. H. Choi, E. K. Kim, H. Y. Lee and P. O. Lim (2011). "Overexpression of FTL1/DDF1, an AP2 transcription factor, enhances tolerance to cold, drought, and heat stresses in Arabidopsis thaliana." Plant Sci **180**(4): 634-641.

Keegstra, K. and A. E. Youssif (1986). "Isolation and characterization of chloroplast envelope membranes." Methods Enzymology **118**: 316-325.

Kim, C. A. and J. U. Bowie (2003). "SAM domains: uniform structure, diversity of function." Trends Biochem Sci **28**(12): 625-628.

Knappe, S., U. I. Flugge and K. Fischer (2003a). "Analysis of the plastidic phosphate translocator gene family in Arabidopsis and identification of new phosphate translocator-homologous transporters, classified by their putative substrate-binding site." Plant Physiol **131**(3): 1178-1190.

Knappe, S., T. Lottgert, A. Schneider, L. Voll, U. I. Flugge and K. Fischer (2003b). "Characterization of two functional phosphoenolpyruvate/phosphate translocator (PPT) genes in Arabidopsis--AtPPT1 may be involved in the provision of signals for correct mesophyll development." Plant J **36**(3): 411-420.

Koch, M., R. Lemke, K. P. Heise and H. P. Mock (2003). "Characterization of gamma-tocopherol methyltransferases from Capsicum annuum L and Arabidopsis thaliana." Eur J Biochem **270**(1): 84-92.

Koini, M. A., L. Alvey, T. Allen, C. A. Tilley, N. P. Harberd, G. C. Whitelam and K. A. Franklin (2009). "High temperature-mediated adaptations in plant architecture require the bHLH transcription factor PIF4." Curr Biol **19**(5): 408-413.

Koncz, C. and J. Schell (1986). "The Promoter of the T1-DNA gene 5 controls the tissue-specific expression of chimeric genes carried by a novel type of Agrobacterium binary vector." Molecular & General Genetics **204**(3): 383-396.

Krueger, S., A. Niehl, M. C. Lopez Martin, D. Steinhauser, A. Donath, T. Hildebrandt, L. C. Romero, R. Hoefgen, C. Gotor and H. Hesse (2009). "Analysis of cytosolic and plastidic serine acetyltransferase mutants and subcellular metabolite distributions suggests interplay of the cellular compartments for cysteine biosynthesis in Arabidopsis." Plant Cell Environ **32**(4): 349-367.

Kumar, S. V., D. Lucyshyn, K. E. Jaeger, E. Alos, E. Alvey, N. P. Harberd and P. A. Wigge (2012). "Transcription factor PIF4 controls the thermosensory activation of flowering." Nature **484**(7393): 242-245.

Kyhse-Andersen, J. "Electroblotting of mutliple gels: a simple apparatus without buffer tank for rapid transfer of proteins from polyacrylamide to nitrocellulose." J Biochem Biophys Methods **10**(3-4):203-209.

Laemmli, U. K. (1970). "Cleavage of structural proteins during assembly of head of Bacteriophage T4." Nature **227:** 680-685.

Lamesch, P., T. Z. Berardini, D. Li, D. Swarbreck, C. Wilks, R. Sasidharan, R. Muller, K. Dreher, D. L. Alexander, M. Garcia-Hernandez, A. S. Karthikeyan, C. H. Lee, W. D. Nelson, L. Ploetz, S. Singh, A. Wensel and E. Huala (2012). "The Arabidopsis Information Resource (TAIR): improved gene annotation and new tools." Nucleic Acids Res **40**(Database issue): D1202-1210.

Lange, B. M., T. Rujan, W. Martin and R. Croteau (2000). "Isoprenoid biosynthesis: the evolution of two ancient and distinct pathways across genomes." Proc Natl Acad Sci U S A **97**(24): 13172-13177.

Laule, O., A. Furholz, H. S. Chang, T. Zhu, X. Wang, P. B. Heifetz, W. Gruissem and M. Lange (2003). "Crosstalk between cytosolic and plastidial pathways of isoprenoid biosynthesis in Arabidopsis thaliana." Proc Natl Acad Sci U S A **100**(11): 6866-6871.

Li, H., K. Culligan, R. A. Dixon and J. Chory (1995). "CUE1: A Mesophyll Cell-Specific Positive Regulator of Light-Controlled Gene Expression in Arabidopsis." Plant Cell **7**(10): 1599-1610.

Lundquist, P. K., C. Rosar, A. Brautigam and A. P. Weber (2014). "Plastid signals and the bundle sheath: mesophyll development in reticulate mutants." Mol Plant **7**(1): 14-29.

Lunn, J. E., R. Feil, J. H. Hendriks, Y. Gibon, R. Morcuende, D. Osuna, W. R. Scheible, P. Carillo, M. R. Hajirezaei and M. Stitt (2006). "Sugar-induced increases in trehalose 6-phosphate are correlated with redox activation of ADPglucose pyrophosphorylase and higher rates of starch synthesis in Arabidopsis thaliana." Biochem J **397**(1): 139-148.

Maeda, H. and N. Dudareva (2012). "The shikimate pathway and aromatic amino acid biosynthesis in plants." Annu Rev Plant Biol **63**: 73-105.

Masuda, T., N. Fusada, N. Oosawa, K. Takamatsu, Y. Y. Yamamoto, M. Ohto, K. Nakamura, K. Goto, D. Shibata, Y. Shirano, H. Hayashi, T. Kato, S. Tabata, H. Shimada, H. Ohta and K. Takamiya (2003). "Functional analysis of isoforms of NADPH: protochlorophyllide oxidoreductase (POR), PORB and PORC, in Arabidopsis thaliana." Plant Cell Physiol **44**(10): 963-974.

Matsoukas, I. G., A. J. Massiah and B. Thomas (2012). "Florigenic and antflorigenic signaling in plants." Plant Cell Physiol **53**(11): 1827-1842.

Meskauskiene, R., M. Nater, D. Goslings, F. Kessler, R. op den Camp and K. Apel (2001). "FLU: a negative regulator of chlorophyll biosynthesis in Arabidopsis thaliana." Proc Natl Acad Sci U S A **98**(22): 12826-12831.

Molla-Morales, A., R. Sarmiento-Manus, P. Robles, V. Quesada, J. M. Perez-Perez, R. Gonzalez-Bayon, M. A. Hannah, L. Willmitzer, M. R. Ponce and J. L. Micol (2011). "Analysis of ven3 and ven6 reticulate mutants reveals the importance of arginine biosynthesis in Arabidopsis leaf development." Plant J **65**(3): 335-345.

Moulin, M. and A. G. Smith (2005). "Regulation of tetrapyrrole biosynthesis in higher plants." Biochem Soc Trans **33**(Pt 4): 737-742.

Moustafa, A., A. Reyes-Prieto and D. Bhattacharya (2008). "Chlamydiae has contributed at least 55 genes to Plantae with predominantly plastid functions." PLoS One **3**(5): e2205.

Murashige, T. and F. Skoog (1962). "A revised medium for rapid growth and bio assays with tobacco tissue culture." Physiologia Plantarum **15**: 473-497.

Murcha, M. W., D. Elhafez, R. Lister, J. Tonti-Filippini, M. Baumgartner, K. Philippar, C. Carrie, D. Mokranjac, J. Soll and J. Whelan (2007). "Characterization of the preprotein and amino acid transporter gene family in Arabidopsis." Plant Physiol **143**(1): 199-212.

Nicholas, K. B. and H. B. Nicholas (1997). "GeneDoc: a tool for editing and annotating multiple sequence alignments." Distributed by the authors

Noh, B., A. S. Murphy and E. P. Spalding (2001). "Multidrug resistance-like genes of Arabidopsis required for auxin transport and auxin-mediated development." Plant Cell **13**(11): 2441-2454.

Nohr, J. and K. Kristiansen (2003). "Site-directed mutagenesis." Methods Mol Biol **232**: 127-131.

Okamoto, T., R. B. Schwab, P. E. Scherer and M. P. Lisanti (2001). "Analysis of the association of proteins with membranes." Curr Protoc Cell Biol **Chapter 5**: Unit 5 4.

Oosawa, N., T. Masuda, K. Awai, N. Fusada, H. Shimada, H. Ohta and K. Takamiya (2000). "Identification and light-induced expression of a novel gene of NADPH-protochlorophyllide oxidoreductase isoform in Arabidopsis thaliana." FEBS Lett **474**(2-3): 133-136.

Ouali, M. and R. D. King (2000). "Cascaded multiple classifiers for secondary structure prediction." Protein Sci **9**(6): 1162-1176.

Perez-Perez, J. M., D. Esteve-Bruna, R. Gonzalez-Bayon, S. Kangasjarvi, C. Caldana, M. A. Hannah, L. Willmitzer, M. R. Ponce and J. L. Micol (2013). "Functional Redundancy and Divergence within the Arabidopsis RETICULATA-RELATED Gene Family." Plant Physiol **162**(2): 589-603.

Pohlmeyer, K., J. Soll, R. Grimm, K. Hill and R. Wagner (1998). "A high-conductance solute channel in the chloroplastic outer envelope from Pea." Plant Cell **10**(7): 1207-1216.

Pohlmeyer, K., J. Soll, T. Steinkamp, S. Hinnah and R. Wagner (1997). "Isolation and characterization of an amino acid-selective channel protein present in the chloroplastic outer envelope membrane." Proc Natl Acad Sci U S A **94**(17): 9504-9509.

Ponnu, J., V. Wahl and M. Schmid (2011). "Trehalose-6-phosphate: connecting plant metabolism and development." Front Plant Sci **2**: 70.

Pouteau, S. and C. Albertini (2009). "The significance of bolting and floral transitions as indicators of reproductive phase change in Arabidopsis." J Exp Bot **60**(12): 3367-3377.

Pudelski, B., S. Kraus, J. Soll and K. Philippar (2010). "The plant PRAT proteins - preprotein and amino acid transport in mitochondria and chloroplasts." Plant Biol (Stuttg) **12 Suppl 1**: 42-55.

Pudelski, B., A. Schock, S. Hoth, R. Radchuk, H. Weber, J. Hofmann, U. Sonnewald, J. Soll and K. Philippar (2012). "The plastid outer envelope protein OEP16 affects metabolic fluxes during ABA-controlled seed development and germination." J Exp Bot **63**(5): 1919-1936.

Qiu, H., D. C. Price, A. P. Weber, F. Facchinelli, H. S. Yoon and D. Bhattacharya (2013). "Assessing the bacterial contribution to the plastid proteome." Trends Plant Sci **18**(12): 680-687.

Rassow, J., P. J. Dekker, S. van Wilpe, M. Meijer and J. Soll (1999). "The preprotein translocase of the mitochondrial inner membrane: function and evolution." J Mol Biol **286**(1): 105-120.

Röhl, T., M. Motzkus and J. Soll (1999). "The outer envelope protein OEP24 from pea chloroplasts can functionally replace the mitochondrial VDAC in yeast." FEBS Lett **460**(3): 491-494.

Rédei, G. P., Y. Hirono (1964). "Linkage studies." Arabidopsis Information Service **1:** 9-10.

Rosar, C., K. Kanonenberg, A. M. Nanda, M. Mielewczik, A. Bräutigam, O. Novak, M. Strnad, A. Walter and A. P. Weber (2012). "The leaf reticulate mutant dov1 is impaired in the first step of purine metabolism." Mol Plant **5**(6): 1227-1241.

Saiki, R. K., D. H. Gelfand, S. Stoffel, S. J. Scharf, R. Higuchi, G. T. Horn, K. B. Mullis and H. A. Erlich (1988). "Primer-directed enzymatic amplification of DNA with a thermostable DNA polymerase." Science **239**(4839): 487-491.

Saitou, N. and M. Nei (1987). "The neighbor-joining method: a new method for reconstructing phylogenetic trees." Mol Biol Evol **4**(4): 406-425.

Salome, P. A., K. Bomblies, R. A. Laitinen, L. Yant, R. Mott and D. Weigel (2011). "Genetic architecture of flowering-time variation in Arabidopsis thaliana." Genetics **188**(2): 421-433.

Samalova, M., B. Brzobohaty and I. Moore (2005). "pOp6/LhGR: a stringently regulated and highly responsive dexamethasone-inducible gene expression system for tobacco." Plant J **41**(6): 919-935.

Sambrook, J., E. F. Fritsch and T. Maniatis (1989). "Molecular Cloning. A Laboratory Manual." Cold Spring Harbor Laboratory, Cold Spring Harbor Press, New York.

Schleiff, E., L. A. Eichacker, K. Eckart, T. Becker, O. Mirus, T. Stahl and J. Soll (2003). "Prediction of the plant beta-barrel proteome: a case study of the chloroplast outer envelope." Protein Sci **12**(4): 748-759.

Schultz, J., C. P. Ponting, K. Hofmann and P. Bork (1997). "SAM as a protein interaction domain involved in developmental regulation." Protein Sci **6**(1): 249-253.

Schwacke, R., A. Schneider, E. van der Graaff, K. Fischer, E. Catoni, M. Desimone, W. B. Frommer, U. I. Flügge and R. Kunze (2003). "ARAMEMNON, a novel database for Arabidopsis integral membrane proteins." Plant Physiol **131**(1): 16-26.

Shepherd, M. and C. N. Hunter (2004). "Transient kinetics of the reaction catalysed by magnesium protoporphyrin IX methyltransferase." Biochem J **382**(Pt 3): 1009-1013.

Shepherd, M., J. D. Reid and C. N. Hunter (2003). "Purification and kinetic characterization of the magnesium protoporphyrin IX methyltransferase from Synechocystis PCC6803." Biochem J **371**(Pt 2): 351-360.

Slocum, R. D. (2005). "Genes, enzymes and regulation of arginine biosynthesis in plants." Plant Physiol Biochem **43**(8): 729-745.

Soll, J., G. Schultz, J. Joyard, R. Douce and M. A. Block (1985). "Localization and synthesis of prenylquinones in isolated outer and inner envelope membranes from spinach chloroplasts." Arch Biochem Biophys **238**(1): 290-299.

Srikanth, A. and M. Schmid (2011). "Regulation of flowering time: all roads lead to Rome." Cell Mol Life Sci **68**(12): 2013-2037.

Streatfield, S. J., A. Weber, E. A. Kinsman, R. E. Hausler, J. Li, D. Post-Beittenmiller, W. M. Kaiser, K. A. Pyke, U. I. Flugge and J. Chory (1999). "The phosphoenolpyruvate/phosphate translocator is required for phenolic metabolism, palisade cell development, and plastid-dependent nuclear gene expression." Plant Cell **11**(9): 1609-1622.

Su, Q., G. Frick, G. Armstrong and K. Apel (2001). "POR C of Arabidopsis thaliana: a third light- and NADPH-dependent protochlorophyllide oxidoreductase that is differentially regulated by light." Plant Mol Biol **47**(6): 805-813.

Szabados, L. and A. Savoure (2010). "Proline: a multifunctional amino acid." Trends Plant Sci **15**(2): 89-97.

Tamura, K., G. Stecher, D. Peterson, A. Filipski and S. Kumar (2013). "MEGA6: Molecular Evolutionary Genetics Analysis version 6.0." Mol Biol Evol **30**(12): 2725-2729.

Tanaka, R. and A. Tanaka (2007). "Tetrapyrrole biosynthesis in higher plants." Annu Rev Plant Biol **58**: 321-346.

Tyra, H. M., M. Linka, A. P. Weber and D. Bhattacharya (2007). "Host origin of plastid solute transporters in the first photosynthetic eukaryotes." Genome Biol **8**(10): R212.

Ulrich, T., L. E. Gross, M. S. Sommer, E. Schleiff and D. Rapaport (2012). "Chloroplast beta-barrel proteins are assembled into the mitochondrial outer membrane in a process that depends on the TOM and TOB complexes." J Biol Chem **287**(33): 27467-27479.

Vranova, E., D. Coman and W. Gruissem (2013). "Network analysis of the MVA and MEP pathways for isoprenoid synthesis." Annu Rev Plant Biol **64**: 665-700.

Waegemann, K., S. Eichacker and J. Soll (1992). "Outer envelope membranes from chloroplasts are isolated as right-side-out vesicles." Planta **187**(1): 89-94.

Wahl, V., J. Ponnu, A. Schlereth, S. Arrivault, T. Langenecker, A. Franke, R. Feil, J. E. Lunn, M. Stitt and M. Schmid (2013). "Regulation of flowering by trehalose-6-phosphate signaling in Arabidopsis thaliana." Science **339**(6120): 704-707.

Walker, C. J. and R. D. Willows (1997). "Mechanism and regulation of Mg-chelatase." Biochem J **327 (Pt 2)**: 321-333.

Weber, A. P. and K. Fischer (2007). "Making the connections--the crucial role of metabolite transporters at the interface between chloroplast and cytosol." FEBS Lett **581**(12): 2215-2222.

Wielopolska, A., H. Townley, I. Moore, P. Waterhouse and C. Helliwell (2005). "A high-throughput inducible RNAi vector for plants." Plant Biotechnol J **3**(6): 583-590.

Wigge, P. A., M. C. Kim, K. E. Jaeger, W. Busch, M. Schmid, J. U. Lohmann and D. Weigel (2005). "Integration of spatial and temporal information during floral induction in Arabidopsis." Science **309**(5737): 1056-1059.

Wingenter, K., O. Trentmann, I. Winschuh, Hormiller, II, A. G. Heyer, J. Reinders, A. Schulz, D. Geiger, R. Hedrich and H. E. Neuhaus (2011). "A member of the mitogen-activated protein 3-kinase family is involved in the regulation of plant vacuolar glucose uptake." Plant J **68**(5): 890-900.

Wirtz, M. and M. Droux (2005). "Synthesis of the sulfur amino acids: cysteine and methionine." Photosynth Res **86**(3): 345-362.

Xiao, Y., T. Savchenko, E. E. Baidoo, W. E. Chehab, D. M. Hayden, V. Tolstikov, J. A. Corwin, D. J. Kliebenstein, J. D. Keasling and K. Dehesh (2012). "Retrograde signaling by the plastidial metabolite MEcPP regulates expression of nuclear stress-response genes." Cell **149**(7): 1525-1535.

Zeth, K. and M. Thein (2010). "Porins in prokaryotes and eukaryotes: common themes and variations." Biochem J **431**(1): 13-22.

Zhou, C., Y. Yang and A. Y. Jong (1990). "Mini-prep in ten minutes." Biotechniques **8**(2): 172-173.

Zook, J. D., T. R. Molugu, N. E. Jacobsen, G. Lin, J. Soll, B. R. Cherry, M. F. Brown and P. Fromme (2013). "High-resolution NMR reveals secondary structure and folding of amino acid transporter from outer chloroplast membrane." PLoS One **8**(10): e78116.

Zuckerkandl, E. and L. Pauling (1965). "Molecules as documents of evolutionary history." J Theor Biol **8**(2): 357-366.

Figures

Figure 1: Solute transport across the chloroplast envelopes 5

Figure 2: Purification of At-OEP40 for antibody production and α-At-OEP40 antibody test 29

Figure 3: Mutation of the *PRAT2* genes in *Arabidopsis* 37

Figure 4: Phenotype of *prat2-dm* mutant plants under different light conditions 39

Figure 5: mRNA levels of *POR A*, *POR B* and *POR C* during greening 40

Figure 6: POR is reduced in *prat2-dm* mutant plants on the protein level 41

Figure 7: S-adenosylmethionine and methylthioadenosine levels in *prat2-dm* mutant plants 44

Figure 8: Levels of α-, δ- and γ-tocopherols in *prat2-dm* mutant plants 45

Figure 9: Changes in amino acid levels in *prat2-dm* mutant plants 47

Figure 10: Changes in carbohydrate levels in *prat2-dm* mutant plants 48

Figure 11: Changes in organic acid levels in *prat2-dm* mutant plants 49

Figure 12: Cysteine, glutathione and *O*-acetylserine levels in *prat2-dm* mutant plants 51

Figure 13: Transport activity of PRAT2 in yeast 52

Figure 14: Test of a new N-terminal against Ps-IEP57 and proteolysis experiments 55

Figure 15: Phylogenetic tree of the proteins of the *Arabidopsis* RER family 57

Figure 16: Alignment of the amino acid sequences of proteins of the *Arabidopsis* RER family 58

Figure 17: *At-IEP57*/popON inducible overexpressors display a chlorotic phenotype 60

Figure 18: Inducible *At-IEP57* RNAi plants display a chlorotic phenotype 62

Figure 19: Induction of RNAi in *At-IEP57*/popOFF plants grown in hydroponic culture 63

Figure 20: Feeding studies with the branched amino acid valine 64

Figure 21: Feeding studies with the aromaticAAs phenylalanine, tryptophan and tyrosine 66

Figure 22: Feeding studies with citrulline and ornithine 67

Figure 23: Feeding studies with the polyamines putrescine, spermidine and spermine 68

Figure 24: Feeding studies with the purines IMP, AMP and GMP 69

Figure 25: Feeding studies with IPP and MEcPP 70

Figure 26: Induction of hydroperoxide lyase (HPL) after wounding 72

Figure 27: OEP40 is an integral protein of the outer chloroplast envelope membrane 74

Figure 28: Purification of overexpressed Ps-OEP40 for electrophysiological measurements 75

Figure 29: *in vitro* translation of Ps-OEP40 for electrophysiological measurements..... 76

Figure 30: Single channel recording of Ps-OEP40 in planar lipid bilayer measurements 78

Figure 31: *oep40-1* is a knockdown and *oep40-3* a knockout line for *OEP40* in *Arabidopsis* 79

Figure 32: Phenotype of *oep40* mutant plants under low temperature conditions..... 81

Figure 33: Detailed phenotypic analysis of *oep40* mutant plants..... 82

Figure 34: Expression of flowering genes in *oep40* mutant plants 84

Figure 35: Floral transition occurs earlier in *OEP40* mutant lines compared to wild-type 86

Figure 36: Suggested compartmentation of isoprenoid precursor biosynthesis in higher plants..... 101

Figure 37: Temperature-dependent *FT* regulation 106

Figure 38: Trehalose-6-phosphate in the plant cell 108

Tables

Table 1: Oligonucleotides used in the work on PRAT2 in this study 10

Table 2: Oligonucleotides used in the work on IEP57 in this study 10

Table 3: Oligonucleotides used in the work on OEP40 in this study 11

Table 4: Plasmid vectors used in this study 12

Table 5: Contructs created in this study 12

Table 6: Light regimes used for the growth of *Arabidopsis thaliana* 15

Table 7: Detailed description of parameters recorded for phenotypic analysis 17

Table 8: Software, databases and algorithms used in this study 34

Table 9: Relative values of significantly changed amino acid levels in *prat2-dm* mutant plants 122

Table 10: Relative values of significantly changed organic acid levels in *prat2-dm* mutant plants 123

Table 11: Relative values of significantly changed carbohydrate levels in *prat2-dm* mutant plants 123

Table 12: Complete list of flowering genes analyzed by qRT-PCR using the flowering gene primer platform (available at the group of Prof. Dr. M Stitt, MPI of Molecular Plant Physiology) 124

Appendix

Table 9: Relative values of significantly changed amino acid levels in *prat2-dm* mutant plants

Name	**16h**			**16hd**			**24h**		
	Col-0	*dm#1*	*dm#3*	Col-0	*dm#1*	*dm#2*	Col-0	*dm#1*	*dm#3*
Asparagine	1,30 ±0,15	7,41 ±1,63	32,51 ±6,58	10,46 ±3,00	214,45 ±5,90	233,84 ±1,89	0,86 ±0,49	0,94 ±0,51	3,07 ±1,48
Aspartic acid	31,31 ±2,72	37,12 ±1,03	33,56 ±8,93	51,78 ±3,22	119,44 ±18,43	153,23 ±2,94	22,23 ±1,73	21,43 ±5,24	28,70 ±6,43
Cysteine	0,003 ±0,000	0,064 ±0,001	0,089 ±0,039	0,155 ±0,010	1,187 ±0,001	1,220 ±0,047	0,003 ±0,001	0,012 ±0,001	0,039 ±0,003
Glycine	4,57 ±033	1,66 ±0,58	1,28 ±0,35	39,81 ±0,99	14,91 ±2,88	16,65 ±1,07	2,58 ±0,44	3,46 ±0,83	5,72 ±3,87
Isoleucine	0,04 ±0,00	0,20 ±0,01	0,25 ±0,05	1,30 ±0,01	2,80 ±0,06	4,63 ±0,10	0,07 ±0,01	0,12 ±0,02	0,17 ±0,01
Leucine	0,03 ±0,00	0,16 ±0,01	0,20 ±0,04	1,58 ±0,10	3,45 ±0,07	6,26 ±0,24	0,09 ±0,02	0,10 ±0,02	0,14 ±0,02
Lysine	0,17 ±0,01	0,48 ±0,02	0,75 ±0,16	2,40 ±0,39	8,65 ±1,48	8,80 ±0,63	0,15 ±0,03	0,14 ±0,00	0,36 ±0,01
Methionine	0,16 ±0,00	0,46 ±0,01	1,13 ±0,08	0,8 ±0,50	4,62 ±0,14	5,31 ±0,22	0,12 ±0,04	0,10 ±0,02	0,29 ±0,06
Phenyl-alanine	0,46 ±0,00	0,47 ±0,05	0,48 ±0,01	4,32 ±0,03	6,47 ±0,17	8,33 ±0,52	0,39 ±0,01	0,20 ±0,03	0,53 ±0,01
Serine	21,49 ±5,74	76,86 ±10,30	74,51 ±14,16	59,49 ±3,84	149,76 ±45,88	256,30 ±7,52	40,00 ±12,66	22,24 ±1,94	78,38 ±0,27
Valine	0,26 ±0,02	0,82 ±0,03	1,26 ±0,38	12,65 ±1,83	24,00 ±3,16	34,19 ±2,32	0,39 ±0,11	0,64 ±0,07	1,05 ±0,06

Table 10: Relative values of significantly changed organic acid levels in *prat2-dm* mutant plants

Name	16h			16hd			24h		
	Col-0	*dm#1*	*dm#3*	Col-0	*dm#1*	*dm#2*	Col-0	*dm#1*	*dm#3*
Fumaric acid	225,48 ±15,19	4,06 ±0,14	2,59 ±0,08	1759,2 ±140,1	170,62 ±7,58	182,66 ±34,77	391,87 ±12,04	256,25 ±17,92	308,26 ±9,06
GABA	0,033 ±0,004	0,398 ±0,010	0,365 ±0,087	0,750 ±0,007	1,884 ±0,017	1,789 ±0,114	0,069 ±0,040	0,059 ±0,030	0,072 ±0,046
Glyceric acid	0,57 ±0,04	0,14 ±0,02	0,06 ±0,003	5,07 ±0,08	1,38 ±0,03	1,88 ±0,15	1,07 ±0,07	1,08 ±0,04	1,41 ±0,34
Isocitric acid	23,35 ±0,02	3,19 ±0,47	0,66 ±0,28	126,77 ±18,27	45,88 ±6,91	87,00 ±0,07	1,17 ±0,04	0,62 ±0,16	0,47 ±0,06
Maleic acid	0,274 ±0,05	0,1 ±0,02	0,15 ±0,04	8,99 ±1,53	5,84 ±0,47	6,54 ±1,71	0,44 ±0,08	0,27 ±0,05	0,24 ±0,01
Malic acid	59,66 ±2,25	4,63 ±0,59	1,38 ±0,24	132,35 ±13,10	24,34 ±0,18	49,21 ±0,99	85,58 ±16,05	55,25 ±0,75	38,13 ±2,03
Shikimate	1,62 ±0,06	0,60 ±0,02	0,44 ±0,07	30,39 ±4,08	10,11 ±0,81	10,48 ±1,10	2,61 ±0,14	1,39 ±0,12	2,14 ±0,12
Succinic acid	0,94 ±0,02	0,56 ±0,02	0,19 ±0,01	26,42 ±0,96	7,45 ±0,06	7,39 ±0,18	1,34 ±0,003	0,0,48 ±0,05	0,60 ±0,03
D-α-hydroxygl.	0,11 ±0,02	0,04 ±0,005	0,003 ±0,006	1,79 ±0,45	0,91 ±0,13	0,84 ±0,19	0,09 ±0,00	0,12 ±0,02	0,07 ±0,02

Table 11: Relative values of significantly changed carbohydrate levels in *prat2-dm* mutant plants

Name	16h			16hd			24h		
	Col-0	*dm#1*	*dm#3*	Col-0	*dm#1*	*dm#2*	Col-0	*dm#1*	*dm#3*
Fructose	23,43 ±3,81	1,76 ±0,26	1,70 ±0,12	15,31 ±0,10	5,41 ±2,0	9,40 ±0,16	4,28 ±1,04	2,37 ±0,37	1,11 ±0,16
Glucose	36,33 ±5,04	4,21 ±0,27	5,10 ±1,68	80,45 ±16,96	30,55 ±6,78	36,51 ±2,50	24,02 ±7,09	6,18 ±0,81	5,95 ±0,70
Maltose	3,25 ±0,1	1,53 ±0,17	1,25 ±0,09	141,85 ±5,52	58,83 ±0,97	67,91 ±2,30	3,19 ±0,24	1,45 ±0,25	1,95 ±0,16
Myo-inositol	57,80 ±0,47	5,34 ±0,73	4,26 ±0,19	239,67 ±6,91	97,88 ±4,22	123,52 ±8,69	37,03 ±5,64	24,87 ±1,89	25,21 ±0,32
Sucrose	452,19 ±16,05	335,57 ±5,56	138,70 ±8,93	3705,3 ±388,5	1104,4 ±6,01	992,0 ±45,25	530,75 ±24,29	465,58 ±4,62	622,13 ±45,52
Xylose	0,16 ±0,004	0,081 ±0,003	0,050 ±0,001	1,39 ±0,09	0,51 ±0,09	0,73 ±0,15	0,25 ±0,002	0,21 ±0,011	0,22 ±0,006

Table 12: Complete list of flowering genes analyzed by qRT-PCR using the flowering gene primer platform (available at the group of Prof. Dr. M Stitt, MPI of Molecular Plant Physiology)

#	Locus	Name	#	Locus	Name
1	At5g65080	At-AGL68/At-MAF5	46	At3g12810	At-CHR13/At-PIE1/At-SCRAP
2	At5g62430	At-CDF1	47	At3g11540	At-SPY
3	At5g61850	At-LFY/At-LFY3	48	At3g10390	At-FLD
4	At5g61380	At-APRR1/At-TOC1	49	At3g04610	At-FLK
5	At5g60910	At-AGL8/At-FUL	50	At3g02310	At-AGL4/At-SEP2
6	At5g60120	At-TOE2	51	At2g46830	At-CCA1
7	At5g57380	At-VIN3	52	At2g46340	At-SPA1
8	At5g55835	At-MIR156H	53	At2g45660	At-AGL20/At-SOC1
9	At5g51810	At-2353/At-GA20OX2	54	At2g42200	At-SPL9
10	At5g51230	At-EMF2/At-CYR1	55	At2g40080	At-ELF4
11	At5g37055	At-SWC6/At-SEF	56	At2g39250	At-SNZ
12	At5g26147	At-MIR156F	57	At2g33810	At-SPL3
13	At5g24860	At-FPF1	58	At2g32950	At-COP1/At-DET340/At-FUS1
14	At5g17690	At-LHP1/At-TFL2	59	At2g28550	At-RAP2.7/At-TOE1
15	At5g15840	At-BBX1/At-COFG	60	At2g28056	At.MIR172A
16	At5g11977	At-MIR156E	61	At2g27100	At-SE
17	At5g11530	At-EMF1	62	At2g25095	At-MIR156A
18	At5g10945	At-MIR156D	63	At2g23380	At-CLF/At-ICU1/At-SDG1/At-SET1
19	At5g10140	At-AGL25/At-FLC	64	At2g22540	At-AGL22/At-SVP
20	At5g04275	At-EAT/At-MIR172B	65	At2g19425	At-MIR156G
21	At5g03840	At-TFL1	66	At2g18790	At-HY3/At-OOP1/At-PHYB
22	At4g39100	At-SHL1	67	At2g17770	At-bZIP27/At-FDP
23	At4g36920	At-AP2/At-FLO2	68	At2g01570	At-RGA/At-RGA1
24	At4g35900	At-bZIP14/At-FD	69	At1g79730	At-ELF7
25	At4g31877	At-MIR156C	70	At1g78580	At-TPS1
26	At4g30972	At-MIR156B	71	At1g77300	At-ASH1/At-CCR1/At-EFS/At-TEM2
27	At4g25530	At-FWA/At-HDG6	72	At1g77080	At-AGL27/At-FLM/At-MAF1
28	At4g25420	At-2301/At-GA20OX1GA5	73	At1g69120	At-AGL7/At-AP1
29	At4g24540	At-AGL24	74	At1g68840	At-RAV2/At-EDF2/At-RAP2.8
30	At4g22950	At-AGL19	75	At1g68050	At-ADO3/At-FKF1
31	At4g22140	At-EBS	76	At1g65480	At-FT/At-RSB8
32	At4g20370	At-TSF	77	At1g53160	At-FTM6/At-SPL4
33	At4g16845	At-VRN2	78	At1g53090	At-SPA4
34	At4g16280	At-FCA	79	At1g30970	At-SUF4
35	At4g15880	At-ESD4	80	At1g30950	At-UFO
36	At4g08920	At-CRY1/At-BLU1/At-HY4	81	At1g27370	At-SPL10
37	At4g02780	At-ABC33/At-CPS1GA1	82	At1g26310	At-AGL10/At-CAL1
38	At4g02560	At-LD	83	At1g25560	At-TEM1/At-EDF1
39	At4g00650	At-FLA/At-FRI/At-RSB7	84	At1g22770	At-FB/At-GI
40	At3g57920	At-SPL15	85	At1g18100	At-E12A11/At-MFT
41	At3g54990	At-SMZ	86	At1g14920	At-GAI/At-RGA2
42	At3g54720	At-AMP1/At-COP2/At-HPT	87	At1g12610	At-DDF1
43	At3g18990	At-REM39/At-VRN1	88	At1g09570	At-FHY2/At-FRE1/At-HY8/At-PHYA
44	At3g15354	At-SPA3	89	At1g04400	At-PHH1/At-CRY2/At-FHA
45	At3g15270	At-SPL5	90	At1g01060	At-LHY/At-LHY1

Curriculum vitae

Personal details

Name	Annette Constanze Schock
Date of Birth	July 26th, 1984
Birthplace	Göppingen, Germany
Nationality	German

Education and Research Experience

May, 2010 – present	PhD student in the lab of Prof. Dr. J. Soll Ludwig-Maximilians-University, Munich, Germany Research topic: Transport of metabolites in chloroplasts
April 2009 – March 2010	Diploma thesis in the lab of Prof. Dr. A. Kuhn University of Hohenheim, Stuttgart, Germany Research topic: Studies on the assembly of the light harvesting complex I in *Rhodospirillum rubrum*
Sept 2006 – March 2009	Graduate studies of Biology University of Hohenheim, Stuttgart, Germany Major subject: microbiology Minor subjects: plant physiology, genetics
Oct 2004 – Aug 2006	Basic studies of Biology University of Hohenheim, Stuttgart, Germany
1995 – 2004	Freihof Gymnasium, Göppingen, Germany general university entrance qualification

Publication	Pudelski, B., A. Schock, S. Hoth, R. Radchuk, H. Weber, J. Hofmann, U. Sonnewald, J. Soll and K. Philippar (2012). "The plastid outer envelope protein OEP16 affects metabolic fluxes during ABA-controlled seed development and germination." J Exp Bot 63(5): 1919-1936.

Eidesstattliche Erklärung

Ich versichere hiermit an Eides statt, dass die vorgelegte Dissertation von mir selbstständig und ohne unerlaubte Hilfe angefertigt ist.

München, den ……. ……

(Unterschrift)

Erklärung

Hiermit erkläre ich, *

☐ dass die Dissertation nicht ganz oder in wesentlichen Teilen einer anderen Prüfungskommission vorgelegt worden ist.

☐ dass ich mich anderweitig einer Doktorprüfung ohne Erfolg **nicht** unterzogen habe.

☐ dass ich mich mit Erfolg der Doktorprüfung im Hauptfach ……

und in den Nebenfächern……

bei der Fakultät für …… der ……

(Hochschule/Universität)

unterzogen habe.

☐ dass ich ohne Erfolg versucht habe, eine Dissertation einzureichen oder mich einer Doktorprüfung zu unterziehen.

München, den …… ……

(Unterschrift)

*) Nichtzutreffendes streichen

Danksagung

Mein erster und besonderer Dank geht an Prof. Dr. Soll für die Möglichkeit, meine Arbeit zu diesem interessanten Forschungsthema in seiner Arbeitsgruppe anfertigen zu können. Vielen Dank für die Unterstützung und die Herausforderung in den letzten vier Jahren!

Ein ganz herzliches Dankeschön geht an meine Betreuerin PD Dr. Katrin Philippar. Danke für deine Unterstützung und Hilfe im Laboralltag, deinen Rat und für deine ausführlichen Korrekturen und deine Tipps zu meiner Arbeit. Außerdem Danke für die vielen schönen Treffen mit der Gruppe Philippar außerhalb des Labors!

Bei allen Kooperationspartnern möchte ich mich für die Hilfe und die Beiträge zu meiner Arbeit herzlich bedanken: Dr. Armin Schlereth und Dr. Vanessa Wahl (Gruppe Stitt, MPI Golm), PD Dr. Markus Geisler (Université de Fribourg), Prof. Dr. Andreas Weber (Universität Düsseldorf) und Prof. Dr. Richard Wagner (Universität Osnabrück).

Allen aktuellen und ehemaligen Kollegen aus der AG Soll möchte ich für ihre Hilfsbereitschaft und Unterstützung ganz herzlich danken! Danke für die tolle Arbeitsatmosphäre und die schönen Zeiten inner- und außerhalb des Labors! Ein ganz großer Dank ans Labor003: Sabrina, Dani, Ingrid, Ceci, Nannan, Roland, Angela, Julia B., Kathi W. und an Karl – eure Erfahrung und eure Unterstützung haben mir den Laboralltag sehr erleichtert und die Arbeit mit euch hat jede Menge Spaß gemacht!
Ein besonderer Dank geht an mein fleißiges Bienchen Kathi Schöngruber – mit welchem Eifer und welcher Fröhlichkeit du mich unterstützt hast, ist unglaublich!
Besonders danken möchte ich dem besten Kollegen der Welt – Roland, ohne dein Wissen, deine Erfahrung und deine Computerkenntnisse wäre ich verloren gewesen! Danke für all deine Hilfe und Unterstützung und unsere Keks-Gespräche! ☺

Ein ganz besonderer Dank gilt meiner Familie und meinen Freunden:
Daniela – fürs ablenken! Und Thomas – für den Ansporn! ☺
Ein ganz herzliches Dankeschön geht an Hans, Gudrun, Chrissi und Alex für euer stetes Interesse und eure Unterstützung.
Meiner „Leidensgenossin“ Franzi danke ich für die bisherige tolle Zeit in München! Danke für dein Verständnis und die vielen geteilten Kilometer!
Ein besonderer Dank geht an Lars Sören Becker, der dafür gesorgt hat, dass ich mich doch noch mit der bayrischen Landeshauptstadt angefreundet habe! ☺

Meinen beiden Geschwistern Christine und David danke ich von ganzem Herzen –
ihr zwei seid unersetzlich! Christine, without you, my thesis literally would not exist! ☺

Von ganzem Herzen danke ich meinen Eltern, die mich immer bedingungslos bei allem unterstützen. Danke dafür, dass ihr euch immer für meine Arbeit interessiert und euch um mich gesorgt habt und dass ich zu Hause immer ein sicheres Plätzchen in all dem Trubel habe! Danke, dass ihr mir das verrückte Leben in den letzten Jahren ermöglicht habt!

Der größte Dank geht an Tobias – einfach für alles!